

## Sensitizer-controlled photochemical reactivity *via* upconversion of red light

Felix Glaser and Oliver S. Wenger \*

Department of Chemistry, University of Basel, St. Johannis-Ring 19, 4056 Basel, Switzerland

### Table of Contents

1.	General experimental details	3
2.	Synthetic procedures and photocatalysis experiments	5
2.1.	Synthetic procedures for substrates and catalysts	5
2.2.	Photoredox catalysis and isolated products	6
2.2.1.	Photocatalytic reaction – general procedure for NMR scale reactions	6
2.2.2.	Isolated yield for [2+2]-cycloaddition of substrate 2	6
2.2.3.	Isolated yield for ether-to-ester rearrangement of substrate 4	6
2.3.	Reaction optimisation and control experiments	7
2.3.1.	Isomerisation of <i>cis</i> -stilbene (1)	8
2.3.2.	[2+2]-Cycloaddition of vinylcarbazole (2)	9
2.3.3.	Newman-Kwart rearrangement	11
2.3.4.	Ether-to-ester rearrangement	13
2.3.5.	Reaction progress over time	14
3.	Irradiation setup	18
4.	Optical spectroscopic measurements	20
4.1.1.	Photophysical characterisation in different solvents	20
4.1.2.	Cyclic voltammetry of catalysts	22
4.1.3.	Spectro-electrochemical study of oxidized and reduced species	23
4.1.4.	Cyclic voltammetry of substrates	24
4.2.	Mechanistic investigation of sTTA-UC	26

4.2.1.	Overview	26
4.2.2.	Triplet-triplet energy transfer from $^3[\text{Os}(\text{bpy})_3]^{2+}$ to DCA	27
4.3.	Triplet-triplet annihilation upconversion	34
4.3.1.	Triplet-triplet annihilation rate constants	34
4.3.2.	Power dependence and upconversion quantum yield estimation	37
4.3.3.	Limiting factors of upconversion quantum yield	44
4.4.	Mechanistic investigations of <i>cis-trans</i> isomerisation of stilbene	46
4.4.1.	Quenching of DCA by stilbene	47
4.4.2.	Quenching of $[\text{Os}(\text{bpy})_3](\text{PF}_6)_2$ by stilbene	50
4.5.	Mechanistic investigations of [2+2]-cycloaddition	52
4.5.1.	Quenching of DCA by vinylcarbazole (2)	53
4.5.2.	Quenching of $[\text{Os}(\text{bpy})_3](\text{PF}_6)_2$ by vinylcarbazole (2)	54
4.6.	Mechanistic investigations of Newman-Kwart rearrangement	55
4.6.1.	Quenching of DCA by substrate 3 or redox mediator	56
4.6.2.	Quenching of $[\text{Os}(\text{bpy})_3](\text{PF}_6)_2$ by substrate 3 or redox mediator	59
4.7.	Mechanistic investigations of ether-to-ester rearrangement	60
4.7.1.	Quenching of DCA by substrate 4 or $4^-$	61
4.7.2.	Quenching of triplet-excited $[\text{Os}(\text{bpy})_3](\text{PF}_6)_2$ by substrate 4 or $4^-$	62
4.8.	Radical chain mechanism, salt effect and deactivation pathways	64
4.8.1.	Exciplex formation	64
4.8.2.	Salt effect of $\text{TBAPF}_6$	65
4.8.3.	Photochemical quantum yield estimation and radical chain mechanism	68
4.8.4.	Deactivation <i>via</i> electron transfer cascade pathway	71
4.8.5.	Catalyst stability under long-term irradiation	74
5.	NMR data	76
6.	References	78

## 1. General experimental details

All deuterated solvents were purchased from Cambridge Isotope Laboratories Inc or Apollo Scientific. All reagents and substrates without synthetic procedure given below (section 2.1) were purchased from Fluorochem, Alfar Aesar, Acros Organics or Sigma-Aldrich/Merck in “reagent grade” purity or better and were used as received. 9,10-Dicyanoanthracene (DCA) was purchased from Sigma-Aldrich/Merck.  $[\text{Os}(\text{bpy})_3](\text{PF}_6)_2$  was synthesized following a reported procedure.<sup>1</sup> Solvents for spectroscopic measurements were purchased “extra dry” in 99.8% purity from Acros Organics.

NMR spectra were recorded on a Bruker Avance III instrument operating at 400 MHz proton frequency. All samples were recorded at 295 K in 5 mm diameter tubes. Chemical shifts were referenced internally to residual solvent peaks using  $\delta$  values as reported previously.<sup>2</sup> Starting material consumption and product formation were determined from  $^1\text{H}$ -NMR measurements ( $^1\text{H}$ : 400 MHz, 16 scans) in NMR tubes against dioxane as internal standard.

Sample preparation for spectrophotometric measurements were performed in screw cap quartz cuvettes. Solutions with DCA in acetone and acetonitrile were sonicated in an ultrasonic bath prior to spectroscopic measurements. All solutions were purged with argon to remove oxygen and sealed under argon with septum caps. Sample preparation for photoredox reactions was done in a LabStar Eco glove box from MBrown with an argon atmosphere. Alternatively, samples were deoxygenated with three cycles of freeze-pump-thaw and then transferred to a screw cap NMR tube and sealed.

Absorption spectra were recorded on a Cary 5000 UV-Vis-NIR spectrometer from Varian. Photoluminescence spectra were recorded on a Fluorolog-322 instrument from Horiba Jobin-Yvon. For laser flash photolysis, a LP920-KS apparatus from Edinburgh Instruments was used. A frequency-tripled Nd:YAG laser (Quantel Brilliant, ca. 10 ns pulse width) equipped with an OPO from Opotek and a beam expander (GBE02-A from Thorlabs) in the beam path were used for excitation with visible light. The direct output of another frequency-doubled Nd:YAG laser (Quantel Q-smart 450 mJ, ca. 10 ns pulse width) with a beam expander (GBE02-A from Thorlabs) in the beam path was used for excitation at 532 nm. The excitation energies were varied by the Q-switch delays and measured with a pyroelectric detector. Typically, pulse energies of ~50 mJ were used for the measurements with 532 nm. Detection of transient absorption and time-resolved emission spectra was performed with an iCCD camera (Andor). Kinetics at single wavelengths were recorded using a photomultiplier tube.

Cyclic voltammetry was performed using a Versastat3-200 potentiostat from Princeton Applied Research. A saturated calomel electrode (SCE) served as reference electrode, a glassy carbon disk electrode was employed as working electrode, and a silver wire was used as counter electrode. Measurements were performed with potential sweep rates of 100 mV/s in dry de-aerated solvent with 0.1 M TBAPF<sub>6</sub> (tetra-*n*-butylammonium hexafluorophosphate) as supporting electrolyte. Sample concentrations were adjusted to values between 1 mM and 5 mM of analyte.

Spectro-electrochemical measurements were performed in a quartz cuvette with 1 mm path length using the abovementioned potentiostat and the UV-Vis-NIR spectrometer. A platinum grid electrode served as

working electrode, a platinum wire was used as counter electrode and an SCE was employed as reference electrode.

As light source for cw-laser experiments in photocatalysis, a 635 nm (optical output up to 500 mW) continuous wave (cw) laser (Roithner Lasertechnik) with precisely adjustable radiative power was used. For measurements with a 623 nm LED, a high power LED (Thorlabs Solis-623C, min. 3.8 W) was used, collimated with a biconvex lens (Thorlabs, LB4592), and a 590 nm long-pass filter (Thorlabs) was installed between the lamp and the sample. Output spectra of the LED and cw laser have recently been reported.<sup>3</sup> For measurements with a 440 nm LED, a Kessil PR160 LED (40 W) was used, and a 400 nm long-pass filter (coloured glass 400 nm cut-off filter, Reichmann Feinoptik GmbH) was installed between the lamp and the sample. An output spectrum of the LED has been reported previously.<sup>4</sup> For excitation with 705 nm light a Lambda Beam 705 (optical output up to 45 mW) cw laser (RGB lasersystems) was used. An output spectrum is reported in Figure S7.

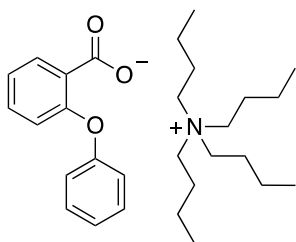
For the measurements of the triplet-triplet annihilation upconversion power dependencies, the Fluorolog-3-22 was equipped with the abovementioned cw laser (Roithner Lasertechnik) as light source and a beam expander (GBE02-A from Thorlabs) was installed backwards in the beam path to obtain a compressed laser beam. The beam size was measured with a SP932U high resolution from Ophir and for the combination with a beam expander an average beam area of 0.007 cm<sup>2</sup> was measured. For excitation with 705 nm laser light no additional collimation was performed and a beam area of 0.001 cm<sup>2</sup> was used for calculations.

In some cases, acetonitrile and dichloromethane are abbreviated with the known short forms MeCN and DCM.

## 2. Synthetic procedures and photocatalysis experiments

### 2.1. Synthetic procedures for substrates and catalysts

#### *N*-tetrabutylammonium 2-phenoxybenzoate (TBA<sup>+</sup> 4<sup>-</sup>)



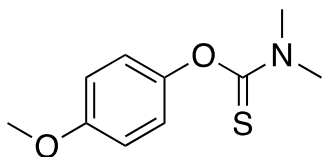
Following a literature procedure,<sup>5</sup> 2-phenoxybenzoic acid (428 mg, 2.0 mmol, 1 eq.) was dissolved in tetrabutylammonium hydroxide (40% in MeOH, 2.0 mL, 2.0 mmol, 1 eq.) and the reaction mixture was stirred over night at room temperature. The solvent was removed under reduced pressure and the crude product was dried under high vacuum to obtain *N*-tetrabutylammonium 2-phenoxybenzoate (TBA<sup>+</sup> 4<sup>-</sup>, 899 mg, 1.97 mmol, 98%) as a viscous oil.

<sup>1</sup>H-NMR (400 MHz, CD<sub>2</sub>Cl<sub>2</sub>): δ 7.56 (dd, *J* = 7.5, 1.9 Hz, 1H), 7.27 (dd, *J*<sub>H,H</sub> = 8.6 Hz, *J*<sub>H,H</sub> = 7.2 Hz, 2H), 7.16 (td, *J*<sub>H,H</sub> = 7.7 Hz, *J*<sub>H,H</sub> = 1.9 Hz, 1H), 7.05 (td, *J*<sub>H,H</sub> = 7.4 Hz, *J*<sub>H,H</sub> = 1.2 Hz, 1H), 6.98 (m, 3H), 6.81 (dd, *J*<sub>H,H</sub> = 8.1, *J*<sub>H,H</sub> = 1.2 Hz, 1H), 3.15 (m, 8H), 1.55 (m, 8H), 1.36 (h, <sup>3</sup>*J*<sub>H,H</sub> = 7.4 Hz, 8H), 0.96 (t, <sup>3</sup>*J*<sub>H,H</sub> = 7.3 Hz, 12H) ppm.

<sup>13</sup>C-NMR (101 MHz, CD<sub>2</sub>Cl<sub>2</sub>): δ 171.6, 159.3, 153.5, 136.7, 130.0, 129.8, 128.5, 123.7, 122.5, 120.5, 118.7, 59.2, 24.4, 20.2, 13.9 ppm.

These analytical data are in agreement with previously reported characterization data for this compound.<sup>6</sup>

#### *O*-(4-Methoxyphenyl) dimethylcarbamothioate (**3**)



Following a literature procedure,<sup>5</sup> 4-methoxyphenol (500 mg, 4.03 mmol, 1 eq.) was dissolved in DMF (5 mL), cooled to 0 °C, and sodium hydride (60% in mineral oil, 177 mg, 4.43 mmol, 1.1 eq.) was added in small portions. The reaction mixture was stirred for 1 h at 0 °C followed by the addition of *N,N*-dimethylthiocarbonyl chloride (650 mg, 5.24 mmol, 1.3 eq.) and further stirring at room temperature for 1 hour. The reaction mixture was poured into 25 mL of deuterated water and the formed precipitate was filtered off. The crude product was purified by recrystallization from cyclohexane to obtain the desired *O*-(4-methoxyphenyl) dimethylcarbamothioate (**3**, 472 mg, 2.23 mmol, 55%) as a white solid.

<sup>1</sup>H-NMR (400 MHz, CDCl<sub>3</sub>): δ 6.98 (m, 2H), 6.90 (m, 2H), 3.81 (s, 3H), 3.45 (s, 3H), 3.33 (s, 3H) ppm.

<sup>13</sup>C-NMR (101 MHz, CDCl<sub>3</sub>): δ 188.5, 157.4, 147.8, 123.6, 114.3, 55.7, 43.4, 38.8 ppm.

These analytical data are in agreement with previously reported characterization data for this compound.<sup>5</sup>

## 2.2. Photoredox catalysis and isolated products

### 2.2.1. Photocatalytic reaction – general procedure for NMR scale reactions

An oven-dried screw-cap glass container was charged with [Os(bpy)<sub>3</sub>](PF<sub>6</sub>)<sub>2</sub>, DCA and solid reagents (e.g. solid substrates or naphthalene). The tube was transferred to a glovebox and deuterated solvent (normally 1 mL, substrate concentration 50-200 mM) as well as liquid reagents (e.g. *cis*-stilbene), additives (e.g. tMePy) and dioxane as internal standard were added. The reaction components were mixed and 0.6 mL were transferred to a screw-capped NMR tube and sealed under an Argon atmosphere. Product formation was monitored by <sup>1</sup>H-NMR spectroscopy. The solutions were irradiated for specified durations with a 635 nm diode laser (Roithner Lasertechnik, 250 to 500 mW) using a beam expander (Thorlabs, GBE05-A used backwards) to compress the beam. The conversion and the yield were determined against the internal standard.

The exact conditions for the individual reactions are provided in the captions of the reaction optimisation tables and in the captions of the relevant figures in the ESI.

### 2.2.2. Isolated yield for [2+2]-cycloaddition of substrate 2

In a Schlenk tube, 9-vinyl-9H-carbazole (**2**, 77.2 mg, 399 μmol, 1 eq.) was dissolved in acetone (2 mL) and [Os(bpy)<sub>3</sub>](PF<sub>6</sub>)<sub>2</sub> (1.90 mg, 1.98 μmol, 0.5 mol%) and DCA (2.21 mg, 9.68 μmol, 2.4 mol%) were added. The mixture was degassed by three freeze-pump-thaw cycles and irradiated for 90 h at room temperature with a red LED (623 nm) collimated with a converging glass. A 590 nm long-pass filter (Thorlabs) was installed between the lamp. The solvent was evaporated and the crude mixture was purified by flash column chromatography (SiO<sub>2</sub>, cyclohexane/dichloromethane 1/0 → 5/1) to obtain the desired cyclized product (**2-P**, 50.1 mg, 130 μmol, 65%) as white solid.

<sup>1</sup>H-NMR (400 MHz, CDCl<sub>3</sub>): δ 8.06 (d, *J*<sub>H,H</sub> = 7.7 Hz, 4H), 7.56 (d, *J*<sub>H,H</sub> = 8.3 Hz, 4H), 7.39 (t, *J*<sub>H,H</sub> = 8.4 Hz, *J*<sub>H,H</sub> = 7.5 Hz, 4H), 7.21 (t, *J*<sub>H,H</sub> = 7.5 Hz, 4H), 6.30 (m, 2H), 3.11 (m, 2H), 2.75 (m, 2H) ppm.

<sup>13</sup>C-NMR (101 MHz, CDCl<sub>3</sub>): δ 140.1, 125.9, 123.7, 120.7, 119.5, 109.8, 54.6, 21.1 ppm.

These analytical data are in agreement with previously reported characterization data for this compound.<sup>7,8</sup>

### 2.2.3. Isolated yield for ether-to-ester rearrangement of substrate 4

In microwave tube, 2-phenoxybenzoic acid (**4**, 54.5 mg, 254 μmol, 1 eq.) was dissolved in dichloromethane (2.5 mL) and [Os(bpy)<sub>3</sub>](PF<sub>6</sub>)<sub>2</sub> (1.15 mg, 1.20 μmol, 0.5 mol%), DCA (2.80 mg, 9.68 μmol, 4.8 mol%), tetra-*n*-butylammonium hexafluorophosphate (98.5 mg, 254 μmol, 1.0 mol) and 2,4,6-trimethylpyridine (33.6 μL, 254 μmol, 1.0 eq.) were added. The mixture was purged with argon for 10 minutes and sealed. The reaction was irradiated with a red LED (623 nm), collimated with a converging glass and a 590 nm long-pass filter (Thorlabs) installed between the lamp and the sample, for 140 h at room temperature. The solvent was

evaporated and the crude mixture was purified by flash column chromatography (SiO<sub>2</sub>, cyclohexane/ethyl acetate 100/0 → 97/3) to obtain the desired product (**4-P**, 40.9 mg, 191 μmol, 75%).

<sup>1</sup>H-NMR (400 MHz, CDCl<sub>3</sub>): δ 10.51 (s, 1H), 8.09 (dd,  $J_{\text{H,H}} = 8.0$  Hz,  $J_{\text{H,H}} = 1.8$  Hz, 1H), 7.55 (ddd,  $J_{\text{H,H}} = 8.8$  Hz,  $J_{\text{H,H}} = 7.2$  Hz,  $J_{\text{H,H}} = 1.8$  Hz, 1H), 7.46 (t,  $J_{\text{H,H}} = 8.0$  Hz, 2H), 7.32 (t,  $J_{\text{H,H}} = 7.5$  Hz, 1H), 7.22 (d,  $J_{\text{H,H}} = 8.6$  Hz, 2H), 7.05 (d,  $J_{\text{H,H}} = 8.5$  Hz, 1H), 6.98 (dd,  $J_{\text{H,H}} = 8.2$  Hz,  $J_{\text{H,H}} = 7.2$  Hz, 1H) ppm.

<sup>13</sup>C-NMR (101 MHz, CDCl<sub>3</sub>): δ 169.1, 162.4, 150.3, 136.6, 130.5, 129.8, 126.5, 121.8, 119.6, 118.0, 112.0 ppm.

These analytical data are in agreement with previously reported characterization data for this compound.<sup>6</sup>

### 2.3. Reaction optimisation and control experiments

For all photocatalytic reactions that have not been reported with DCA as photocatalyst up to now,<sup>9</sup> a preliminary screening with blue light (440 nm LED) has been performed to investigate whether the reaction occurs at all (following direct monophotonic excitation), typically starting from conditions (solvent, substrate concentration) that have been reported in earlier studies with other catalysts. In a second step, suitable reactions were then tested with different solvents to find conditions that are best for our investigated upconversion system (based on red biphotonic excitation).

For the measurements of reaction progress over time, fit curves were sometimes included as guidance for the eye. For irreversible reactions (substrates **3** and **4**) an exponential fit curve was used (assuming first order kinetics,  $y = A \cdot \exp(k \cdot x)$ ), while for reactions that are expected to have significant contributions of backward reaction (substrates **1** and **2**), a biexponential fit curve was used (assuming second order kinetics,  $y = A_1 \cdot \exp(k_1 \cdot x) + A_2 \cdot \exp(k_2 \cdot x)$ ).

#### Comparison of irradiation setups

For photoredox catalysis *via* triplet-triplet annihilation upconversion, the power density and the light intensity emitted by the lamp are more curical factors than for mono-photonic mechanisms. Therefore typically (cw) laser irradiation is used for triplet-triplet annihilation upconversion in photoredox catalysis,<sup>10,11</sup> and only in recent publications (collimated) LED irradiation was taken into account.<sup>10,12,13</sup> Herein, a 635 nm cw laser with an output power of up to 500 mW and a collimated high power 623 nm LED providing at least 3.8 W were used. Both light sources are significantly weaker than the blue LEDs (440 nm, 40 W) used for the reaction optimisation (Table S1, Table S3, Table S5, Table S7). In the case of the cw laser, the irradiation beam spot size was between 0.005 cm<sup>2</sup> and 0.01 cm<sup>2</sup> after collimation, and thus the light beam passed essentially completely through the middle of the NMR sample tube (inner diameter 0.4 cm), thereby maximizing the amount of light absorbed by the osmium complex. For the collimated LED, a squared beam shape with a side length of ~1.25 cm was formed, consequently leading to a quadratic area with ~1.56 cm<sup>2</sup>. Given the limited size of the NMR tube (~1.25 cm · 0.4 cm = ~0.5 cm<sup>2</sup>), this implies that about ~1.22 W of photons pass indeed through the reaction solution. However, given the curvature of the NMR tube (causing

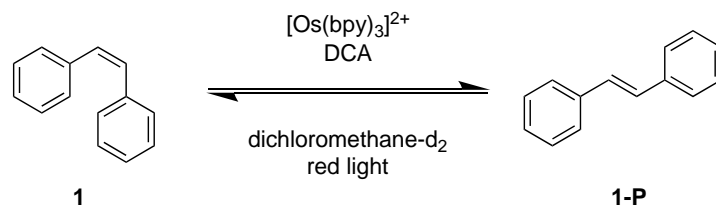
shorter beam paths at the edges than in the middle), the number of absorbed photons is most likely considerably lower than this estimated value. Furthermore, the estimated power density for the collimated LED is  $\sim 2.43 \text{ W}\cdot\text{cm}^{-2}$  and this value is only slightly above the determined threshold value of  $\sim 1.65 \text{ W}\cdot\text{cm}^{-2}$ . At the threshold intensity determined herein, one fourth of the maximum upconversion quantum yield is reached, and it seems likely that with the power density of the LED our system is not yet operating in the fully linear regime.<sup>14-16</sup> Overall, a direct comparison between both setups is not readily possible, but even with the high overall output power of the LED, the cw laser is most likely equally good or even slightly better due to the comparably low power density of the LED and the smaller overlap between the NMR tube and the LED beam size. Notably, when upscaling the reaction, the irradiated area significantly increases and essentially the full beam penetrates the solution and the full output from the LED with a power of at least 3.8 W can be absorbed. Consequently, better performance might be possible under these conditions. Irradiation with the employed 705 nm cw laser is expected to be less efficient, especially due to its low output power of only 45 mW. Due to the highly collimated nature of the laser beam it is assumed that the linear regime is more easily accessible with this setup. In comparison to the almost constant absorbance between 550 nm and 650 nm (indicating similar photon absorption by the 623 m LED and the 635 nm cw laser for the same concentration of  $[\text{Os}(\text{bpy})_3](\text{PF}_6)_2$ ), the absorbance above 700 nm is significantly weaker (Figure S8). Consequently, the amount of absorbed photons is lower with this setup. Evidently, the exact catalyst loading and the effective concentrations in solution are relevant for the respective measurements, and a direct comparison (especially between different reactions) is therefore not easily possible.

### 2.3.1. Isomerisation of *cis*-stilbene (**1**)

**Table S1.** Optimization for isomerisation of *cis*-stilbene (**1**) with blue light.<sup>a</sup>

entry	DCA / mol%	solvent	time / h	conversion / % <sup>b</sup>
1	5	acetonitrile	1	97
2	5	dichloromethane	1	79

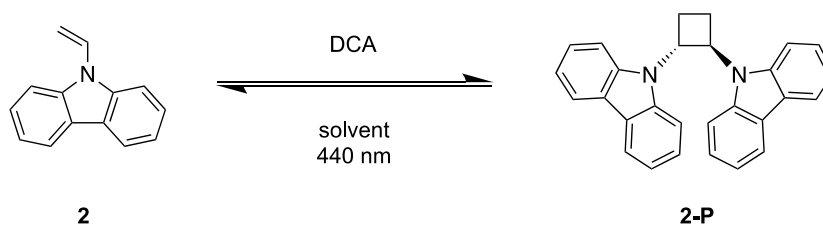
a) Reaction conditions: 100 mM *cis*-stilbene in 1 mL non-deuterated de-aerated solvent. Sample de-aerated by three freeze-pump-thaw cycles, irradiated with a 440 nm Kessil PR160 LED (40 W) and a 400 nm long-pass filter between the lamp and the reaction flask under an inert atmosphere at room temperature. b) After removal of the solvent the crude product mixture was analysed by <sup>1</sup>H-NMR spectroscopy and the ratio between remaining starting material and product determined as relative conversion.

**Table S2.** Optimization and control experiments for isomerisation of *cis*-stilbene (**1**) with red light.<sup>a</sup>

entry	[Os(bpy) <sub>3</sub> ](PF <sub>6</sub> ) <sub>2</sub> / mol%	DCA / mol%	light source	time / h	yield (conv.) / % <sup>b</sup>
1	1	5	623 nm LED <sup>c</sup>	2	60 (61)
				4	82 (83)
2	1	5	635 nm laser	2	78 (78)
3	1	5	635 nm laser	3	80 (80)
4	0.1	5	635 nm laser	16	82 (82)
5	-	5	635 nm laser	16	0 (1)
6	0.1	-	635 nm laser	16	0 (0)
7	0.1	5	dark	20	0 (0)

a) Reaction conditions: 100 mM *cis*-stilbene in 1 mL de-aerated dichloromethane-d<sub>2</sub>. Sample irradiated in a sealed NMR tube under an inert atmosphere at room temperature. b) Yields and conversions (in parentheses) were determined by quantitative <sup>1</sup>H-NMR analysis using dioxane as internal standard. c) LED collimated with a lens.

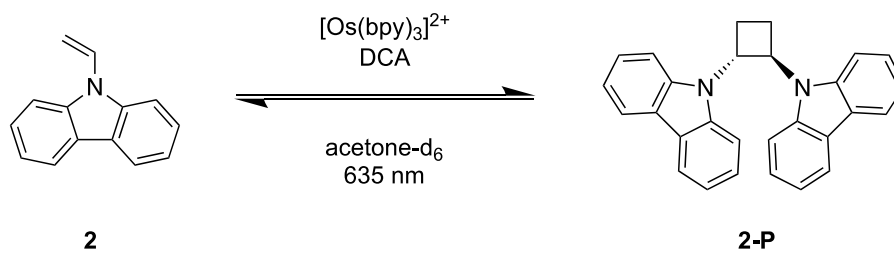
### 2.3.2. [2+2]-Cycloaddition of vinylcarbazole (**2**)

**Table S3.** Optimization for isomerisation of [2+2]-cycloaddition of substrate **2** with blue light.<sup>a</sup>

entry	DCA / mol%	solvent	time / h	conversion / % <sup>b</sup>
1 <sup>c</sup>	-	acetone	0.5	18
2	-	acetone	0.5	2
3	2.5	acetone	0.5	80
4	2.5	dichloromethane	0.5	19

a) Reaction conditions: 200 mM substrate **2** in 1 mL non-deuterated de-aerated solvent. Sample de-aerated by three freeze-pump-thaw cycles, and irradiated with a 440 nm Kessil PR160 LED (40 W) and a 425 nm long-pass filter between the lamp and the reaction flask under an inert atmosphere at room temperature. b) After removal of the solvent the crude product mixture was analysed by <sup>1</sup>H-NMR spectroscopy and the ratio between remaining starting material and product determined as conversion. c) 400 nm long-pass filter instead of 425 nm long-pass filter.

**Table S4.** Optimization and control experiments of [2+2]-cycloaddition of **2** with red light.<sup>a</sup>

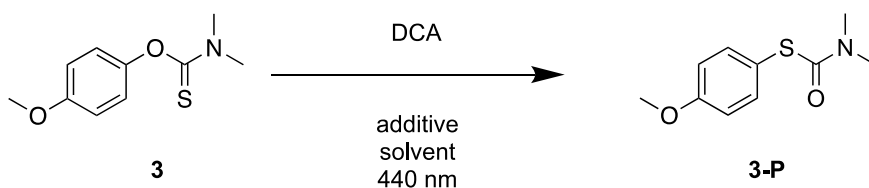


entry	$[\text{Os}(\text{bpy})_3](\text{PF}_6)_2$ / mol%	DCA / mol%	solvent	time / h	yield (conv.) / % <sup>b</sup>
1	0.5	2.5	acetone-d <sub>6</sub>	2.5	15 (15)
2	0.5	2.5	acetone-d <sub>6</sub>	7	34 (35)
3	0.5	2.5	acetone-d <sub>6</sub>	90	71 (71)
3	-	2.5	acetone-d <sub>6</sub>	65	1 (2)
4	0.5	-	acetone-d <sub>6</sub>	40	0 (0)
5 <sup>c</sup>	0.5	2.5	acetone-d <sub>6</sub>	65	0 (0)

a) Reaction conditions: 200 mM substrate **2** in 1 mL de-aerated acetone-d<sub>6</sub>. Sample irradiated in a sealed NMR tube under an inert atmosphere at room temperature. b) Yields and conversions (in parentheses) were determined by quantitative <sup>1</sup>H-NMR analysis using dioxane as internal standard. c) No irradiation.

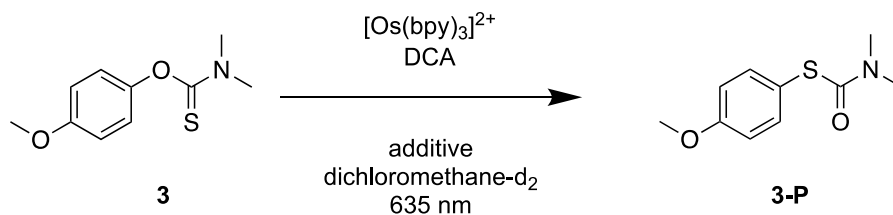
### 2.3.3. Newman-Kwart rearrangement

**Table S5.** Optimization for Newman-Kwart rearrangement of substrate **3** with blue light.<sup>a</sup>



entry	DCA / mol%	solvent	additive	time / h	conversion / % <sup>b</sup>
1	5	acetonitrile	-	2	0
2	5	acetonitrile	biphenyl (1 eq.)	2	8
3	5	acetonitrile	naphthalene (1 eq.)	2	15
				8	56
4	5	dichloromethane	biphenyl (1 eq.)	1	0
5	5	dichloromethane	biphenyl (1 eq.), TBAPF <sub>6</sub> (1 eq.)	1	~5 <sup>c</sup>
6	5	dichloromethane	naphthalene (1 eq.)	2	0
7	5	dichloromethane	naphthalene (1 eq.) TBAPF <sub>6</sub> (1 eq.)	2	58
8	5	dichloromethane	TBAPF <sub>6</sub> (1 eq.)	1	4

a) Reaction conditions: 50 mM substrate **3** in 1 mL non-deuterated de-aerated solvent. Sample de-aerated by three freeze-pump-thaw cycles, irradiated with a 440 nm Kessil PR160 LED (40 W) and a 400 nm long-pass filter between the lamp and the reaction flask under an inert atmosphere at room temperature. b) After removal of the solvent the crude product mixture was analysed by <sup>1</sup>H-NMR spectroscopy and the ratio between remaining starting material and product determined as relative conversion. c) Overlap between resonances of biphenyl and the product complicate the integration of product signals.

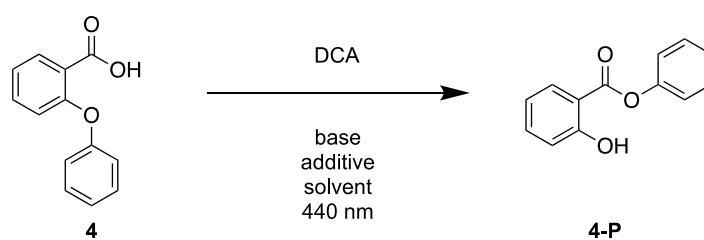
**Table S6.** Optimization and control experiments for the Newman-Kwart rearrangement of **3** with red light.<sup>a</sup>

entry	$[\text{Os}(\text{bpy})_3](\text{PF}_6)_2$ / mol%	DCA / mol%	additive	time / h	yield (conv.) / % <sup>b</sup>
1	1	10	naphthalene (2 eq.), TBAPF <sub>6</sub> (1 eq.)	20	10 (10)
2	1	10	naphthalene (2 eq.)	40	0 (0)
3	1	10	TBAPF <sub>6</sub> (1 eq.)	60	0 (0)
4	-	10	naphthalene (2 eq.), TBAPF <sub>6</sub> (1 eq.)	40	0 (0)
5	1	-	naphthalene (2 eq.), TBAPF <sub>6</sub> (1 eq.)	40	0 (0)
6 <sup>c</sup>	1	10	naphthalene (2 eq.), TBAPF <sub>6</sub> (1 eq.)	65	0 (0)

a) Reaction conditions: 50 mM substrate in 1 mL de-aerated dichloromethane- $\text{d}_2$ . Sample irradiated in a sealed NMR tube under an inert atmosphere at room temperature. b) Yields and conversions (in parentheses) were determined by quantitative  $^1\text{H}$ -NMR analysis using dioxane as internal standard. c) No irradiation.

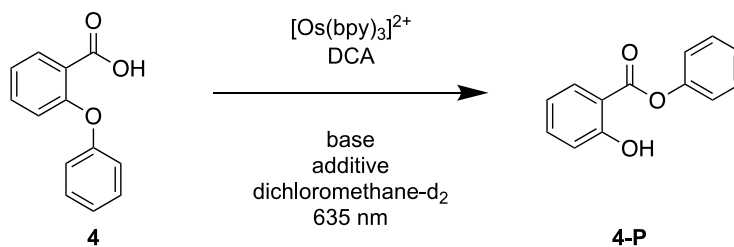
### 2.3.4. Ether-to-ester rearrangement

Table S7. Optimization for rearrangement of substrate **4** with blue light.<sup>a</sup>



entry	DCA / mol%	solvent	base, additive	time / h	conversion / % <sup>b</sup>
1	5	acetonitrile	Cs <sub>2</sub> CO <sub>3</sub> (0.1 eq.)	1	98
2	5	acetonitrile	Et <sub>3</sub> N (0.1 eq.)	1	61
3	5	dichloromethane	Et <sub>3</sub> N (0.1 eq.)	1	11
4	5	dichloromethane	Et <sub>3</sub> N (0.1 eq.), TBAPF <sub>6</sub> (1 eq.)	1	73
5	5	dichloromethane	DBU (0.1 eq.), TBAPF <sub>6</sub> (1 eq.)	1	65
6	5	dichloromethane	CsOAc (0.1 eq.), TBAPF <sub>6</sub> (1 eq.)	1	98
7	5	dichloromethane	tMePy (0.1 eq.), TBAPF <sub>6</sub> (1 eq.)	1	39
8	5	dichloromethane	tMePy (1 eq.), TBAPF <sub>6</sub> (1 eq.)	0.5	72
				1	98
9	5	dichloromethane	tMePy (1 eq.)	0.5	59
				1	97

a) Reaction conditions: 100 mM substrate **4** in 1 mL non-deuterated de-aerated solvent. Sample de-aerated by three freeze-pump-thaw cycles, irradiated with a 440 nm Kessil PR160 LED (40 W) and a 400 nm long-pass filter between the lamp and the reaction flask under an inert atmosphere at room temperature. b) After removal of the solvent the crude product mixture was analysed by <sup>1</sup>H-NMR spectroscopy and the ratio between remaining starting material and product determined as relative conversion.

**Table S8.** Optimization and control experiments for rearrangement of substrate **4** with red light.<sup>a</sup>

entry	$[\text{Os}(\text{bpy})_3](\text{PF}_6)_2$ / mol%	DCA / mol%	base, additive	time / h	yield (conv.) / % <sup>b</sup>
1	0.5	5	tMePy (1 eq.), TBAPF <sub>6</sub> (1 eq.)	20	24 (35)
2	0.5	5	tMePy (1 eq.)	20	5 (8)
3	0.5	5	TBAPF <sub>6</sub> (1 eq.)	20	0 (2)
4	-	5	tMePy (1 eq.), TBAPF <sub>6</sub> (1 eq.)	65	0 (0)
5	0.5	-	tMePy (1 eq.), TBAPF <sub>6</sub> (1 eq.)	65	0 (0)
6 <sup>c</sup>	0.5	5	tMePy (1 eq.), TBAPF <sub>6</sub> (1 eq.)	65	0 (0)

a) Reaction conditions: 100 mM substrate **4** in 1 mL de-aerated solvent. Sample irradiated in a sealed NMR tube under an inert atmosphere at room temperature. b) Yields and conversions (in parentheses) were determined by quantitative <sup>1</sup>H-NMR analysis using dioxane as internal standard. c) No irradiation.

### 2.3.5. Reaction progress over time

#### Isomerisation of *cis*-stilbene (**1**) over time

The reaction progress for the isomerisation of *cis*-stilbene by direct excitation of DCA with 440 nm reveals a fast reaction in acetonitrile and dichloromethane that is finished within one to three hours (Figure S1a and b). In acetonitrile, essentially complete isomerisation is observed while in dichloromethane an equilibrium state with ~85% *trans*-stilbene (**1-P**) and ~15% *cis*-stilbene (**1**) is found.<sup>17</sup> With  $[\text{Os}(\text{bpy})_3](\text{PF}_6)_2$  as sensitizer in the presence of DCA under 623 nm LED irradiation the reaction progress is much faster in dichloromethane than in acetonitrile (Figure S1c), most likely due to the higher upconversion quantum yield in the more apolar solvent (see section 4.3.2). As expected, the reaction is faster with higher concentrations of sensitizer under 635 nm cw laser irradiation (Figure S1d) and the change to the weaker 705 nm cw laser as light source (see above for technical details) results in a comparably slow reaction progress (Figure S1e).

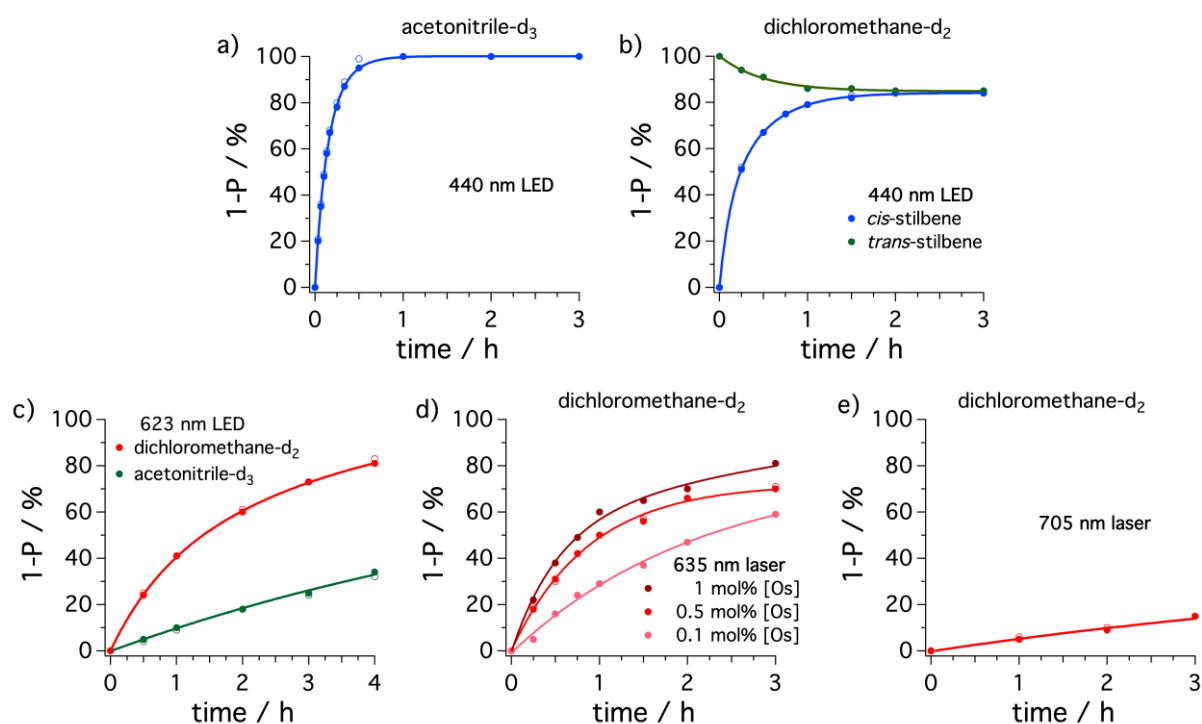


**Figure S1.** Isomerisation of *cis*-stilbene (**1**) over time. Following the general procedure for NMR scale reactions, the isomerisation of *cis*-stilbene (**1**, 100 mM) was investigated by direct excitation of DCA (5 mol%) with 440 nm LED (40 W) in (a) acetonitrile-d<sub>3</sub> and (b) dichloromethane-d<sub>2</sub> (blue traces). For the reaction starting with *trans*-stilbene (100% **1-P**) and otherwise identical conditions the same equilibrium state is found in dichloromethane-d<sub>2</sub> (green trace in b) as with *cis*-stilbene **1** (blue trace). The reaction progress for the isomerisation in acetonitrile-d<sub>3</sub> and dichloromethane-d<sub>2</sub> for a solution containing [Os(bpy)<sub>3</sub>](PF<sub>6</sub>)<sub>2</sub> (1 mol%) and DCA (5 mol%) under collimated 623 nm LED light irradiation (min. 3.8 W) with a 590 nm long-pass filter (Thorlabs) in the beam path is provided in (c). The influence of the concentration of [Os(bpy)<sub>3</sub>](PF<sub>6</sub>)<sub>2</sub> under 635 nm cw laser irradiation (~450 mW) in dichloromethane-d<sub>2</sub> is illustrated in (d). The reaction progress over the first 3 hours under 705 nm cw laser irradiation (~45 mW) for a solution containing [Os(bpy)<sub>3</sub>](PF<sub>6</sub>)<sub>2</sub> (1 mol%) and DCA (5 mol%) is presented in (e). The amount of *trans*-stilbene (**1-P**, determined by quantitative <sup>1</sup>H-NMR spectroscopy against dioxane as internal standard) in the reaction mixture is reported as filled circles while the substrate conversion is given as empty circles in the same colour (often overlapping with the filled circles).

### [2+2] Cycloaddition of vinylcarbazole (2) over time

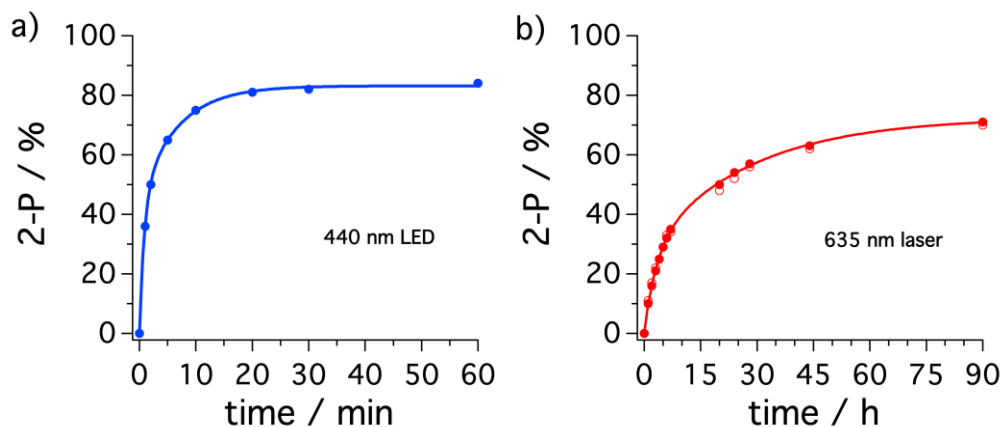


**Figure S2.** [2+2]-Cycloaddition over time. a) Following the general procedure for NMR scale reactions, the isomerisation of vinylcarbazole (**2**, 200 mM) was investigated by direct excitation of DCA (2.5 mol%) in acetone- $d_6$  under 440 nm LED irradiation. A 425 nm long-pass filter was placed between the lamp and the sample. b) Reaction progress for the [2+2]-cycloaddition under collimated 635 nm cw-laser irradiation of a solution containing  $[\text{Os}(\text{bpy})_3](\text{PF}_6)_2$  (0.5 mol%) and DCA (2.5 mol%) in acetone- $d_6$  as a function of time. In all graphs the product yield (**2-P**, determined by quantitative  $^1\text{H-NMR}$  spectroscopy against dioxane as internal standard) in the reaction mixture is represented by filled circles while the conversion of substrate **2** is given as empty circles in the same colour as the yield (often overlapping with the filled circles).

### Newman-Kwart rearrangement over time

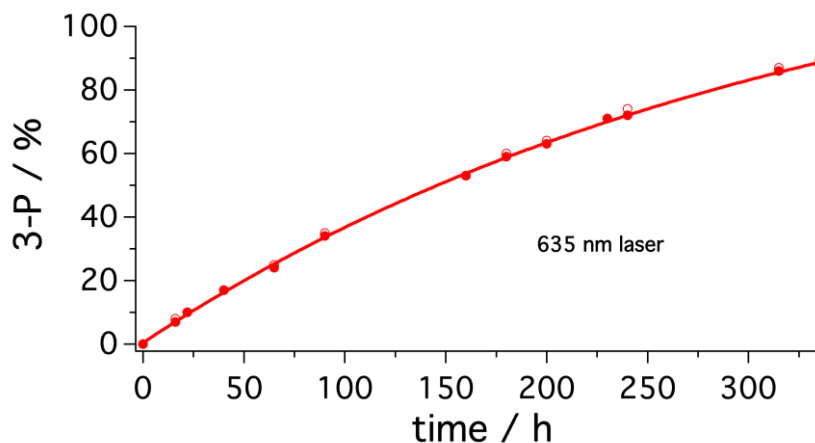


**Figure S3.** Newman-Kwart rearrangement over time. Following the general procedure for NMR scale reactions, a solution containing substrate **3** (50 mM),  $[\text{Os}(\text{bpy})_3](\text{PF}_6)_2$  (1 mol%), DCA (10 mol%), naphthalene (100 mM) and  $\text{TBAPF}_6$  (50 mM) in dichloromethane- $d_2$  has been prepared and the product formation under collimated 635 nm laser irradiation has been monitored over time. The product yield (**3-P**, determined by quantitative  $^1\text{H-NMR}$  spectroscopy against dioxane as internal standard) in the reaction mixture is reported as filled circles while the conversion of substrate **3** is given as empty circles in the same colour as the yield (often overlapping with the filled cycles of the yield).

### Ether-to-ester rearrangement over time

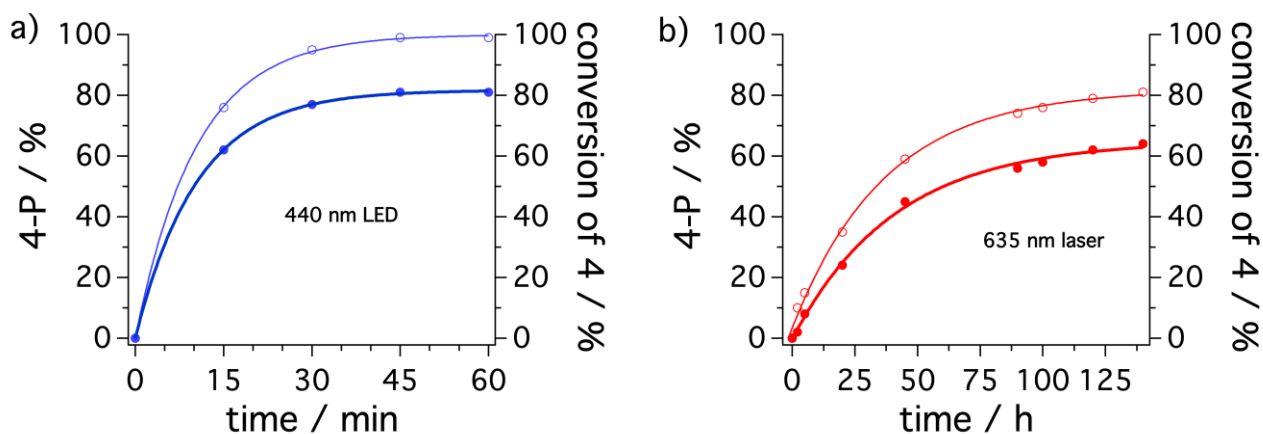


**Figure S4.** Ether-to-ester rearrangement over time. a) Following the general procedure for NMR scale reactions, the isomerisation of substrate **4** (100 mM) was investigated by direct excitation of DCA (5 mol%) in the presence of tMePy (100 mM) and TBAPF<sub>6</sub> (100 mM) in dichloromethane-d<sub>2</sub> under 440 nm LED irradiation. b) The reaction progress for an identical solution as in (a), but with [Os(bpy)<sub>3</sub>](PF<sub>6</sub>)<sub>2</sub> (0.5 mol%) irradiated with a collimated 635 nm cw-laser has been monitored over time. The product yield (**4-P**, determined by quantitative <sup>1</sup>H-NMR spectroscopy against dioxane as internal standard) in the reaction mixture is given as filled circles while the conversion of substrate **4** is given as empty circles.

### 3. Irradiation setup

The laser output of the red cw laser (635 nm),<sup>3</sup> the high-power red LED (623 nm)<sup>3</sup> and the blue LED (440 nm)<sup>10</sup> have been reported recently. The setup with the red cw laser (635 nm) is given as Figure S5 and the collimated red LED setup is given in Figure S6.

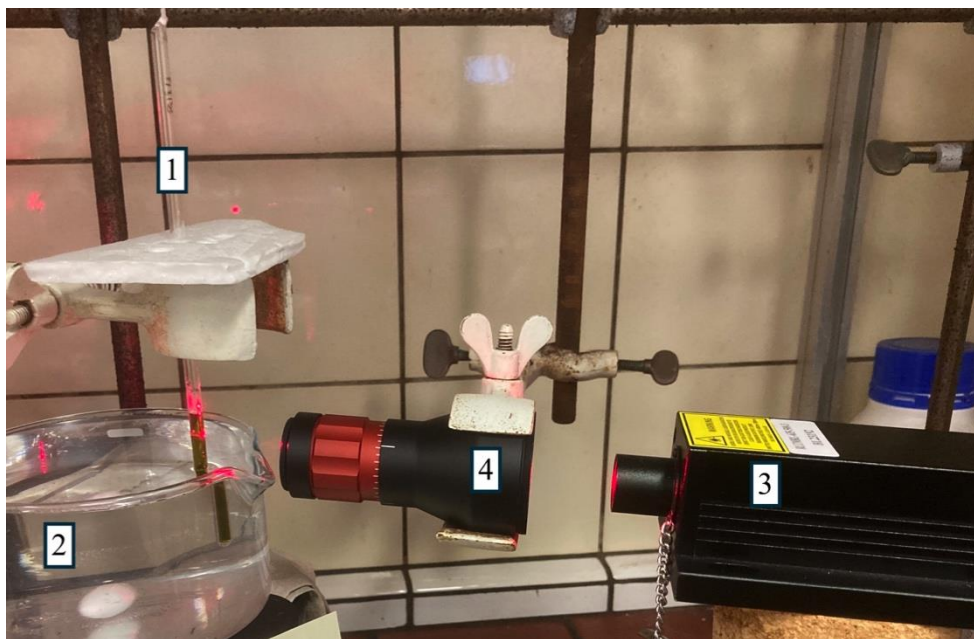


**Figure S5.** Irradiation setup for photoredox reactions with laser irradiation. 1: screw-capped or flame-sealed NMR tube with reaction mixture under Argon; 2: stirred water bath for cooling of irradiated solution; 3: cw laser (635 nm, up to 500 mW); 4: beam expander (used backwards) to reduce the size the laser beam.

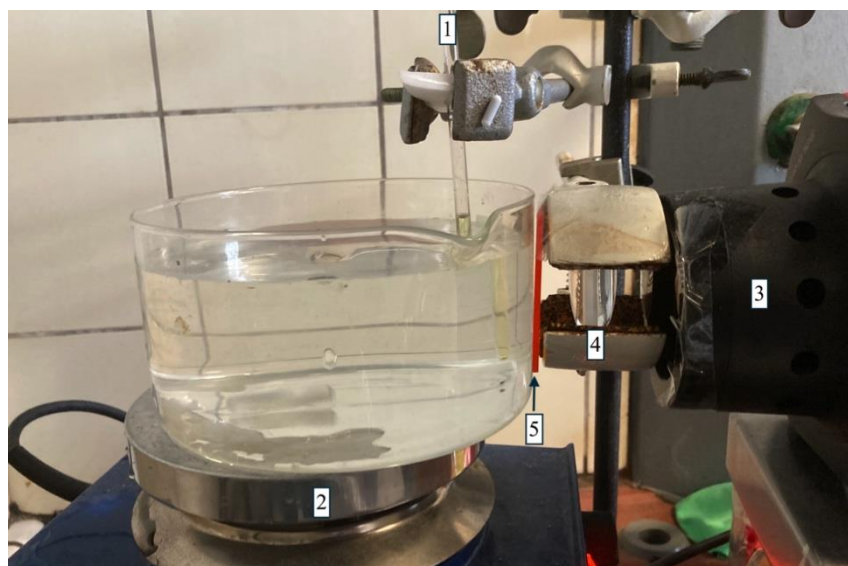


**Figure S6.** Irradiation setup for photoredox reactions with collimated LED irradiation. 1: screw-capped or flame-sealed NMR tube with reaction mixture under Argon; 2: stirred water bath for cooling of irradiated solution; 3: high-power LED (623 nm, min. 3.8 W); 4: lens (Thorlabs, LB4592); 5: 590 nm long-pass filter (Thorlabs).

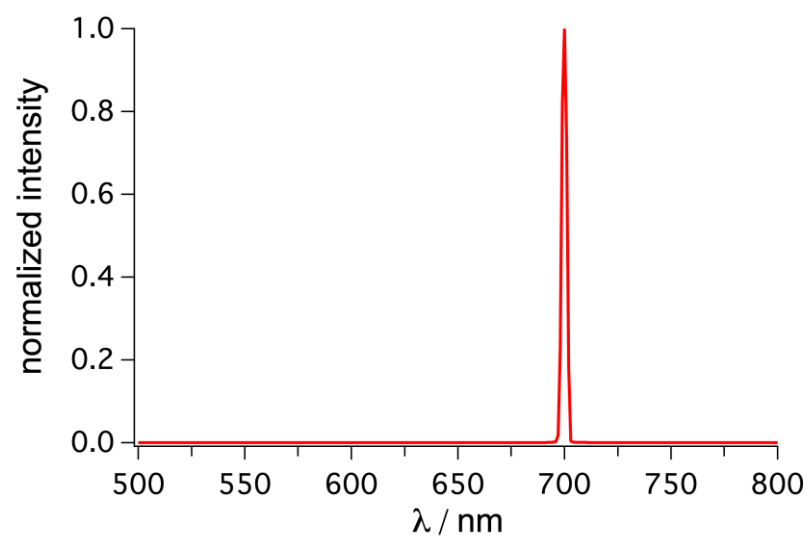


**Figure S7.** Emission spectrum of the 705 nm cw-laser used in this study.

## 4. Optical spectroscopic measurements

### 4.1. Spectroscopic properties of $[\text{Os}(\text{bpy})_3](\text{PF}_6)_2$ and DCA

#### 4.1.1. Photophysical characterisation in different solvents

All measurements were performed in de-aerated solvents at room temperature.

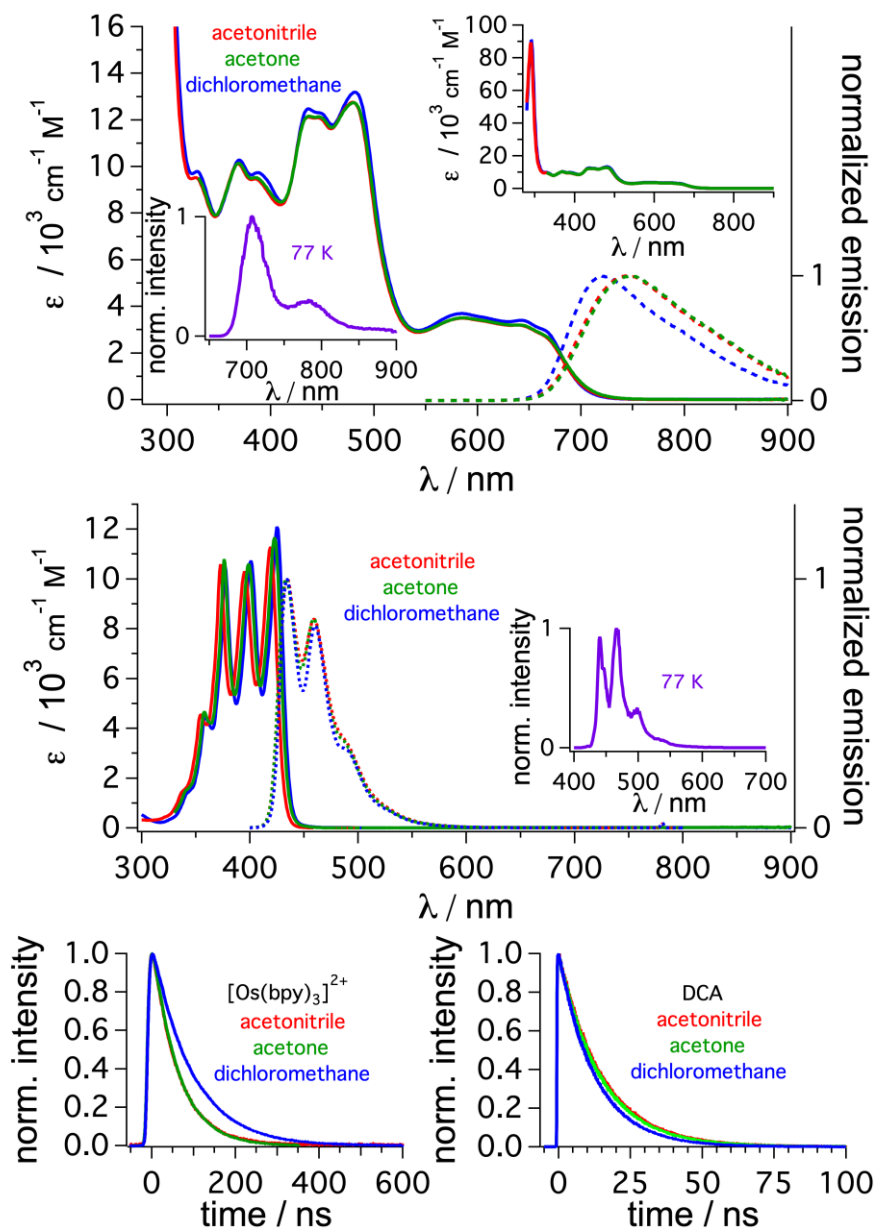


**Figure S8.** UV-vis absorption and emission spectra of  $[\text{Os}(\text{bpy})_3](\text{PF}_6)_2$  (top) and DCA (middle) in de-aerated solvents (colour codes indicated in the respective figure parts). The emission lifetimes measured at the respective emission band maximum for both compounds are presented in the bottom part. Low temperature emission in frozen matrix ( $[\text{Os}(\text{bpy})_3](\text{PF}_6)_2$  in butyronitrile, DCA in 2-methyl-tetrahydrofuran) is presented as insets. The main data is also summarized in Table S9.

**Table S9.** Overview of photophysical properties of [Os(bpy)<sub>3</sub>](PF<sub>6</sub>)<sub>2</sub> and DCA at 20 °C in different solvents.

catalyst	solvent	$\lambda_{\text{abs}} (\epsilon) / \text{nm}$ ( $10^3 \text{ M}^{-1} \text{ s}^{-1}$ )	$\lambda_{\text{em}} /$ nm	$\phi / \% ^a$	$\phi_{\text{air}} / \% ^a$	$\tau_0 / \text{ns}$	$E^{0,0} /$ eV <sup>b</sup>
DCA	acetonitrile	419 (11.2)	434	93 ± 1	-	14.9	2.91
	acetone	423 (11.7)	434	95 ± 1	-	14.4	2.90
	dichloromethane	425 (12.1)	434	97 ± 1	-	12.6	2.89
[Os(bpy) <sub>3</sub> ](PF <sub>6</sub> ) <sub>2</sub>	acetonitrile	480 (12.7)	741	1.1 ± 0.1	0.75 ± 0.03	60.5	1.80
		635 (3.19)					
	acetone	480 (12.7)	749	1.0 ± 0.1	0.74 ± 0.01	61.5	1.80
		635 (3.20)					
	dichloromethane	481 (13.2)	720	2.7 ± 0.1	2.2 ± 0.1	94.1	1.81
		635 (3.23)					

a) Photoluminescence quantum yields of [Os(bpy)<sub>3</sub>](PF<sub>6</sub>)<sub>2</sub> were determined relative to an aerated solution of [Ru(bpy)<sub>3</sub>](PF<sub>6</sub>)<sub>2</sub> in acetonitrile ( $\phi = 0.018$ )<sup>18</sup>. Photoluminescence quantum yields of DCA were determined relative to a de-aerated solution of 9,10-diphenylanthracene in cyclohexane ( $\phi = 0.90$ )<sup>19</sup>. b) The energies of first singlet excited state (for DCA) and triplet excited state (for [Os(bpy)<sub>3</sub>]<sup>2+</sup>) ( $E^{0,0}$ ) were estimated based on the energy at the intersection of the normalized emission and absorption spectra.

Absorption spectra, emission spectra, luminescence quantum yields, excited-state lifetimes and the energy of the lowest excited singlet state of DCA are in agreement with prior studies.<sup>3,20–22</sup>

For [Os(bpy)<sub>3</sub>](PF<sub>6</sub>)<sub>2</sub>, the absorption spectra, excited-state lifetimes and the energy of the lowest triplet excited state were similar to prior studies.<sup>1,23–28</sup> Surprisingly, our detected emission shape does not perfectly resemble the data known from literature, where no emission was detectable at 900 nm.<sup>26</sup> As a consequence, our measured quantum yields are somewhat higher than the values reported in literature (literature values listed later in this paragraph). Two reasonable explanations for this behaviour are plausible. First of all, literature-known quantum yields of [Os(bpy)<sub>3</sub>]<sup>2+</sup> are typically reported from emission spectra that do not return to the baseline in the near-infrared region similar to our data.<sup>25,26,29</sup> Therefore it is unsurprising that our reported emission quantum yields differ from the (inconsistent) literature values (1.19 % in acetonitrile;<sup>26</sup> 1.0 % in acetonitrile;<sup>30</sup> 0.8 % in acetonitrile;<sup>25</sup> 0.8 % in acetonitrile;<sup>27</sup> 0.49 % in acetonitrile;<sup>29</sup> 0.5 % in acetonitrile;<sup>31</sup> 0.35 % in acetonitrile;<sup>32</sup> 1.4 % in dichloromethane;<sup>25</sup> 0.58 % in dichloromethane;<sup>33</sup> 0.9 % in dichloroethane<sup>1</sup>; in many cases it is unclear whether aerated or deaerated solvents). Secondly, our steady state emission setup seems to have a poor instrument response towards the detector limit,<sup>34,35</sup> and the emission intensity is likely overestimated in this part of the spectrum. This hypothesis is in line with a slightly different shape of the emission observed in the time-resolved spectra with pulsed lasers on our nanosecond laser setup (see Figure S16a, blue trace) where the emission indeed returns to the baseline towards 850 nm.

#### 4.1.2. Cyclic voltammetry of catalysts

Cyclic voltammetry was performed with a saturated calomel electrode (SCE) as reference electrode, a glassy carbon disk electrode as working electrode, and a silver wire as counter electrode. Measurements were performed in dry de-aerated solvents with 0.1 M TBAPF<sub>6</sub> as an electrolyte. For oxidations or reductions with irreversible peaks, a peak potential (at maximum current) is given instead of a half-wave potential.

**Table S10.** Oxidation and reduction potentials in different solvents vs SCE.

catalyst	$E_{1/2,ox} / V$ vs SCE		$E_{1/2,red} / V$ vs SCE	
	acetonitrile	dichloromethane	acetonitrile	dichloromethane
[Os(bpy) <sub>3</sub> ](PF <sub>6</sub> ) <sub>2</sub>	0.84	0.96	-1.27	-1.19
	1.20 <sup>a</sup>		-1.46	-1.48
			-1.78	
DCA <sup>b</sup>	1.09 <sup>a</sup>	-	-0.93 <sup>a</sup>	-1.01
			-1.62	

Conditions: Measurements in de-aerated solvent vs SCE in the presence of 0.1 M TBAPF<sub>6</sub>. a) Irreversible oxidation/reduction peak. b) These values have recently been published.<sup>3</sup> All measurements are in line with previous reports.<sup>28</sup>

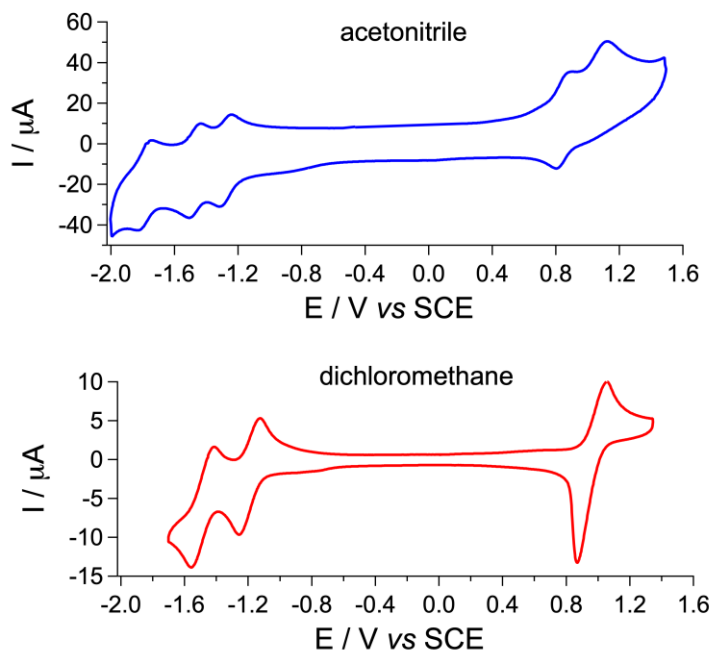


**Figure S9.** Cyclic voltammetry measurements of [Os(bpy)<sub>3</sub>](PF<sub>6</sub>)<sub>2</sub> with TBAPF<sub>6</sub> (0.1 M) as supporting electrolyte in de-aerated acetonitrile (blue) and dichloromethane (red) vs SCE. Voltammograms recorded with scan rate of 500 mV s<sup>-1</sup> in acetonitrile and 100 mV s<sup>-1</sup> in dichloromethane.

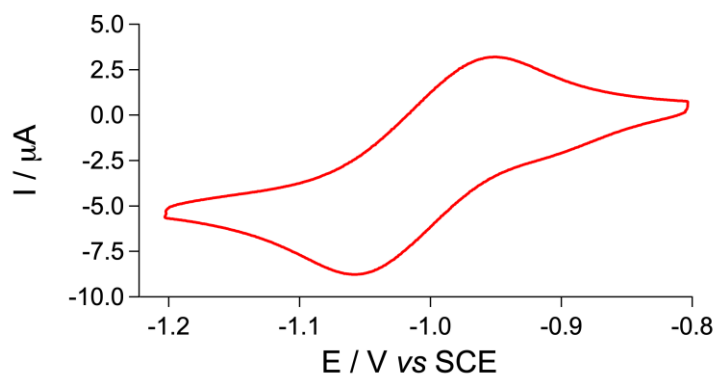


**Figure S10.** Cyclic voltammetry measurement of DCA with TBAPF<sub>6</sub> (0.1 M) as supporting electrolyte in de-aerated and dichloromethane vs SCE. Voltammogram recorded with scan rate of 100 mV s<sup>-1</sup>.

#### 4.1.3. Spectro-electrochemical study of oxidized and reduced species

Data for the spectro-electrochemical reduction DCA to DCA<sup>•-</sup> in de-aerated acetonitrile has been published recently.<sup>3</sup> The electrochemical oxidation of [Os(bpy)<sub>3</sub>]<sup>2+</sup> indicates that all absorption bands in the visible range are occurring as negative signal in the difference spectrum (Figure S11) and only between 300 and 350 nm a new positive band is detected.

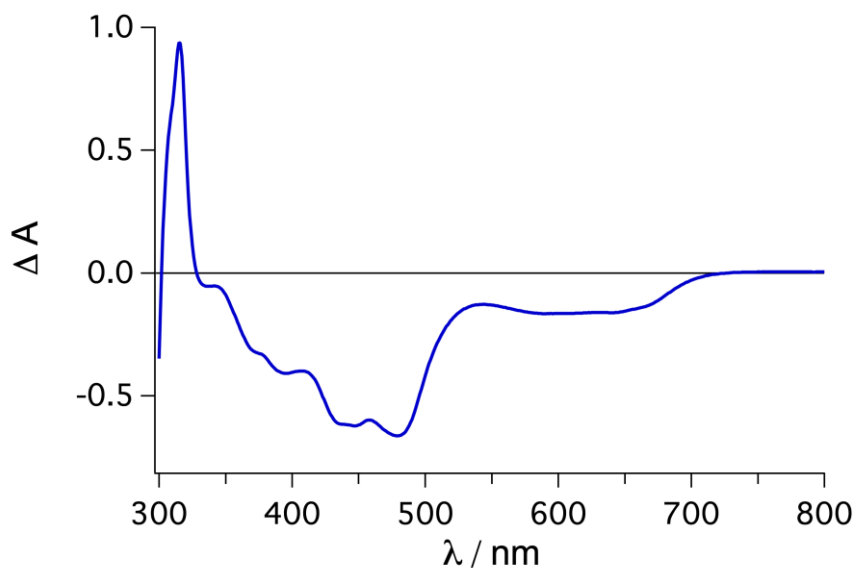


**Figure S11.** UV-Vis difference spectrum obtained upon electrochemical oxidation of [Os(bpy)<sub>3</sub>](PF<sub>6</sub>)<sub>2</sub> in de-aerated acetonitrile with an applied potential of 1.0 V vs SCE in the presence of TBAPF<sub>6</sub> (0.1 M) as supporting electrolyte. The UV-Vis spectrum without a potential applied served as baseline.

#### 4.1.4. Cyclic voltammetry of substrates

**Table S11.** Oxidation potentials of substrates and additives in acetonitrile vs SCE.

substrate / additive	$E_{1/2, \text{ox}} / \text{V vs SCE}^{\text{a}}$
<i>cis</i> -stilbene ( <b>1</b> )	1.64
<i>trans</i> -stilbene ( <b>1-P</b> )	1.50
vinylcarbazole ( <b>2</b> )	1.30
<i>O</i> -(4-methoxyphenyl)dimethylcarbamothioate ( <b>3</b> )	~1.05
2-phenoxybenzoic acid ( <b>4</b> )	1.92
2-phenoxybenzoate ( <b>4</b> <sup>-</sup> )	1.11
2,4,6-trimethylpyridine (tMePy)	2.25
1,8-diazabicyclo(5.4.0)undec-7-ene (DBU)	1.24
naphthalene	1.72
biphenyl	1.95

Conditions: Measurements in de-aerated acetonitrile vs SCE with 0.1 M TBAPF<sub>6</sub> and a scan rate of 0.1 V s<sup>-1</sup>.

a) Irreversible oxidation peak.

The measured values for stilbenes (**1** and **1-P**)<sup>9,36</sup> substrates **3**<sup>5</sup> and **4**<sup>37</sup> as well as the additives DBU,<sup>38</sup> naphthalene,<sup>39</sup> and biphenyl<sup>40</sup> are in line with previously reported values. The oxidation potentials of **4**<sup>-</sup> (literature: 1.77 V vs SCE, here 1.11 V vs SCE) and **2** (literature: 0.94 V vs SCE, here 1.30 V vs SCE) are different, and we tentatively attribute this to the different conditions (electrolyte, reference electrode) in the respective measurements.

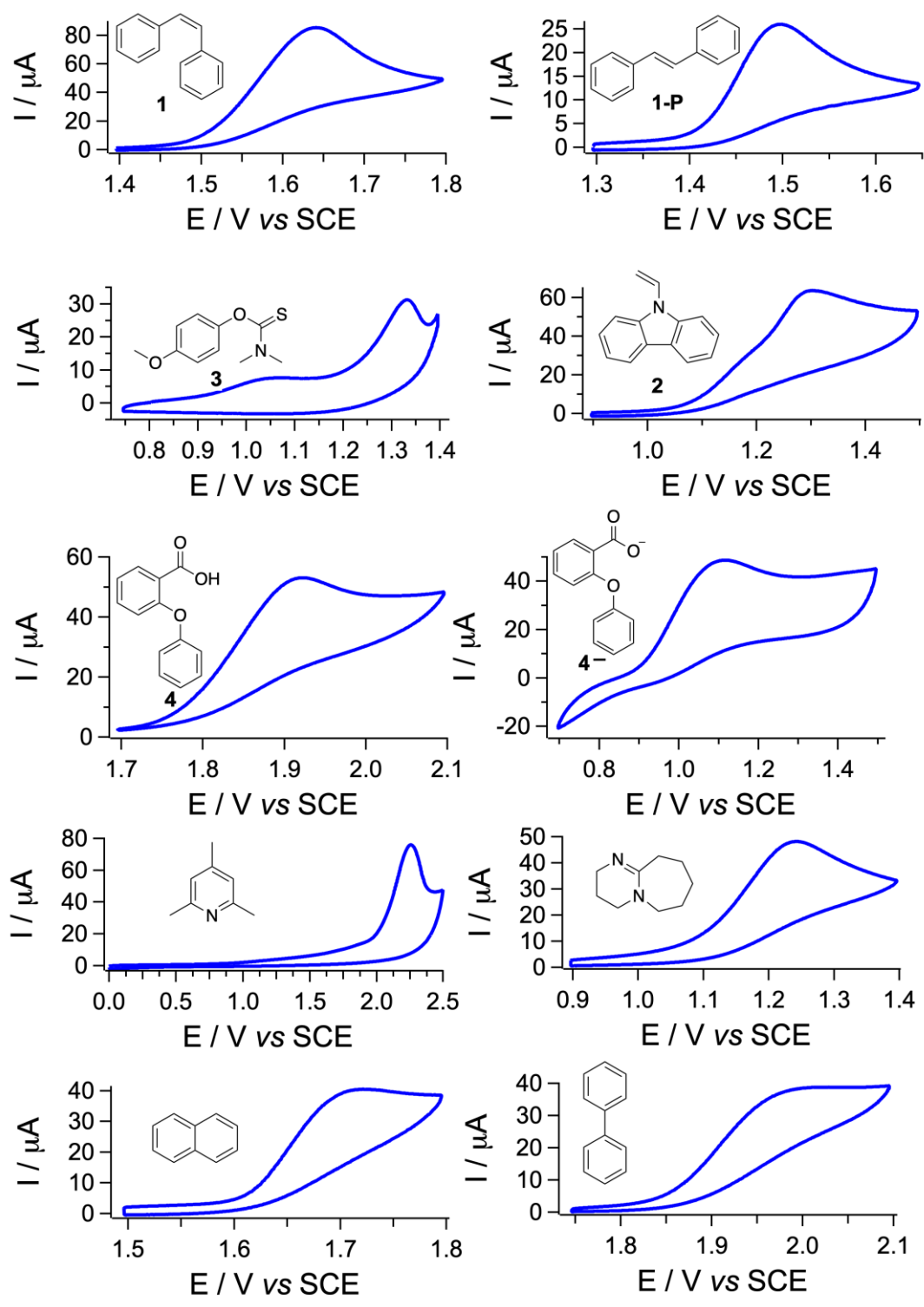


**Figure S12.** Cyclic voltammety measurements of substrates and additives determined with  $\text{TBAPF}_6$  (0.1 M) as supporting electrolyte in de-aerated acetonitrile vs SCE. Voltammogram recorded with scan rate of  $100 \text{ mV s}^{-1}$ .

## 4.2. Mechanistic investigation of sTTA-UC

The solubility of DCA is very limited in polar solvents such as acetonitrile or acetone (~0.5 mM), and this limits the obtainable data quality and complicates the spectroscopic analysis. Therefore, the variation between different datasets is typically high and a good reproducibility of the datasets is less easily achieved in polar solvents. For acetonitrile and acetone we assume an error of 10-20% on the spectroscopic measurements (e.g. upconversion quantum yields, triplet-triplet annihilation constant and triplet state lifetime), while for the investigations in dichloromethane the higher solubility (and consequent higher signal intensity) provides a better quality of the datasets. Spectroscopic measurements are therefore expected to be more accurate in this apolar solvent.

### 4.2.1. Overview

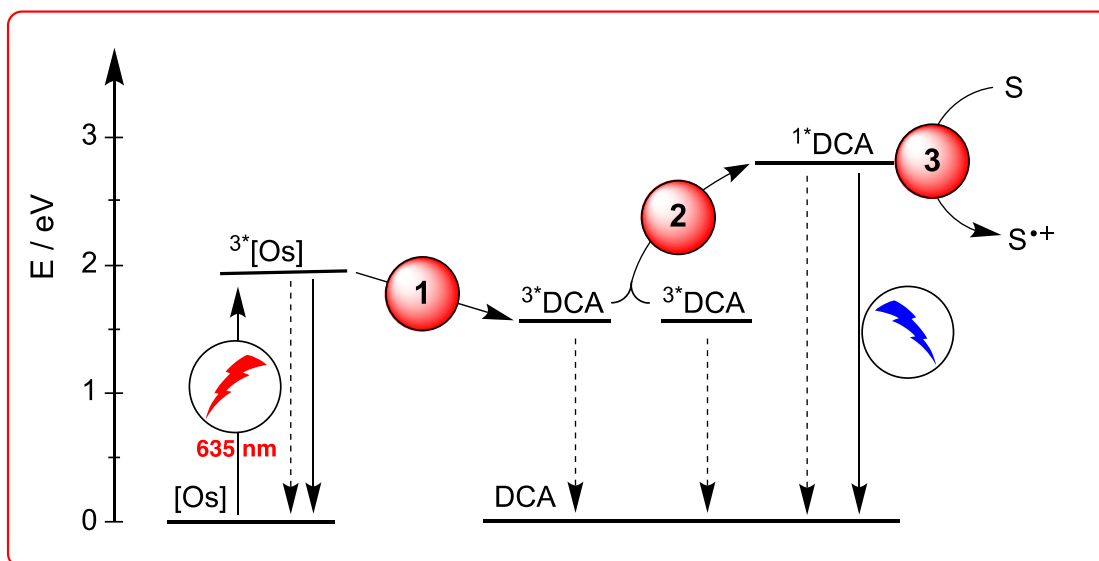


**Figure S13.** Possible mechanistic pathway for red light driven photoredox catalysis *via* sensitized triplet-triplet annihilation upconversion (sTTA-UC) with  $[\text{Os}(\text{bpy})_3](\text{PF}_6)_2$  (abbreviated as  $[\text{Os}]$ ) and DCA followed by reductive quenching of  $^1\text{DCA}$  by the substrate. A description of the different elementary steps is provided in Table S12.

**Table S12.** Summary of relevant data for sTTA-UC in different solvents.<sup>a</sup>

step no.	general description	symbol	acetonitrile	acetone	DCM
1	TTET from $[\text{Os}(\text{bpy})_3]^{2+}$ to DCA	$k_{\text{TTET}}$	$4 \cdot 10^9 \text{ M}^{-1} \text{ s}^{-1}$	$4 \cdot 10^9 \text{ M}^{-1} \text{ s}^{-1}$	$3 \cdot 10^9 \text{ M}^{-1} \text{ s}^{-1}$
2	triplet-triplet annihilation	$k_{\text{TTA}}$	$6.9 \cdot 10^9 \text{ M}^{-1} \text{ s}^{-1}$	$6.4 \cdot 10^9 \text{ M}^{-1} \text{ s}^{-1}$	$6.7 \cdot 10^9 \text{ M}^{-1} \text{ s}^{-1}$
1+2	sensitized TTA-UC quantum yield	$\phi_{\text{sTTA-UC}}^{\text{c}}$	0.22 %	0.13 %	1.5 %
		$\phi_{\text{sTTA-UC}}^{\text{d}}$	0.10 %	0.15 %	1.4 %
3	electron transfer from a suitable substrate S to $^1\text{DCA}$	$k_{\text{ET}}$	- <sup>b</sup>	- <sup>b</sup>	- <sup>b</sup>

a) The same data is presented in the main manuscript as Table 1. b) The respective values for the investigated reactions are presented in section 4.4-4.7. c) Excitation wavelength of 635 nm. d) Excitation wavelength of 705 nm. Further details are provided in the individual subsections of this chapter.

#### 4.2.2. Triplet-triplet energy transfer from $^3[\text{Os}(\text{bpy})_3]^{2+}$ to DCA

Further information concerning step 1 (TTET) in Figure S13 is given here together with possible alternative reaction pathways.

##### Oxidative quenching or energy transfer between $^3[\text{Os}(\text{bpy})_3]^{2+}$ and DCA

A comparison of the UV-vis absorption spectra of both catalysts (see in section 4.1) reveals that only the metal complex has an absorption band in the red spectral range. After selective excitation of  $[\text{Os}(\text{bpy})_3]^{2+}$ , two different possibilities for a thermodynamically feasible (exothermic) quenching of excited  $[\text{Os}(\text{bpy})_3](\text{PF}_6)_2$  by DCA are in principle conceivable. The first possibility is triplet-triplet energy transfer (TTET) from  $^3[\text{Os}(\text{bpy})_3]^{2+}$  ( $\sim 1.8$  eV, see Table S9) to populate the lowest triplet excited state of dicyanonanthracene ( $^3\text{DCA}$ ) with an energy of  $\sim 1.8$  eV.<sup>31</sup> The second possibility is photoinduced electron transfer (PET) to form the oxidized metal complex and dicyanoanthracene radical anion ( $\text{DCA}^{\bullet-}$ ). The excited state oxidation potential for  $^3[\text{Os}(\text{bpy})_3]^{2+}$  can be estimated by  $^*E_{\text{ox}}(^3[\text{Os}]^{2+}/[\text{Os}]^{3+}) \approx E_{\text{ox}}([\text{Os}]^{2+}/[\text{Os}]^{3+}) - E_{0,0}(^3[\text{Os}]^{2+}) = 0.84 \text{ V vs SCE} - 1.8 \text{ eV} \approx -0.96 \text{ V vs SCE}$ , and this is similar to the ground state reduction potential of DCA ( $-0.93 \text{ V vs SCE}$  in acetonitrile, section 4.1.2). Hence, both elementary steps (TTET and PET) do not have a large driving force but are both in principle thermodynamically viable. The respective two reaction types (TTET and PET) can be distinguished by transient absorption spectroscopy.

##### Triplet-triplet energy transfer from $^3[\text{Os}(\text{bpy})_3]^{2+}$ to DCA

Transient absorption spectroscopy of  $50 \mu\text{M}$   $[\text{Os}(\text{bpy})_3](\text{PF}_6)_2$  excited at  $532 \text{ nm}$  in the presence of  $500 \mu\text{M}$  DCA in de-aerated solvents (Figure S14 a: acetonitrile, b: acetone, c: dichloromethane) indicates a ground state bleach caused by population of excited  $^3[\text{Os}(\text{bpy})_3]^{2+}$  for a measurement with  $10 \text{ ns}$  delay after the laser pulse (light traces in Figure S14, time integrated over  $200 \text{ ns}$ ). The typical spectroscopic features of  $^3\text{DCA}$  are visible with longer delay times of  $10 \mu\text{s}$  (dark traces in Figure S14, time integrated over  $200 \text{ ns}$ ). Furthermore, no spectroscopic signals of  $\text{DCA}^{\bullet-}$  (with a maximum expected around  $705 \text{ nm}$ )<sup>3</sup> or any prolonged bleach caused by oxidized osmium complex (reference spectrum in Figure S11) are visible in any of the investigated solvents. These measurements reveal that only triplet-triplet energy transfer and no electron transfer is occurring between  $^3[\text{Os}(\text{bpy})_3]^{2+}$  and DCA. Detecting the change of transient absorption traces with different time delays after the laser pulse, a deactivation of  $^3[\text{Os}(\text{bpy})_3]^{2+}$  (bleach in Figure S15a) and a simultaneous formation of  $^3\text{DCA}$  (new positive spectroscopic features in Figure S15a) are detectable. While this is visible on a timescale of several hundred nanoseconds and can be confirmed by the corresponding kinetic traces (Figure S15c) the formed  $^3\text{DCA}$  decays on a microsecond timescale (Figure S15b and d). This analysis of transient spectra with different time delays after the laser pulse further confirms that no  $\text{DCA}^{\bullet-}$  is formed and no oxidative excited state quenching of the metal complex is occurring.

Even within these measurements at comparably low concentrations of DCA (500  $\mu\text{M}$ ) a clear filter effect from the ground state absorption of DCA between 360 nm and ca 430 nm is detectable (marked in Figure S15 a + b by vertical dotted lines). While at these concentrations of DCA its triplet state can clearly be detected in all three investigated solvents (see Figure S14), this blocking of the light from the flash lamp of the transient absorption setup is of course even more prominent at higher concentrations of DCA. While the solubility in acetonitrile and acetone is limited, in more apolar solvents such as dichloromethane higher concentrations of DCA are soluble.

Therefore, in dichloromethane changes upon different concentrations of DCA can more easily be investigated than in acetone or acetonitrile. In fact, integration of the emission spectra over 200  $\mu\text{s}$  of a solution containing  $[\text{Os}(\text{bpy})_3](\text{PF}_6)_2$  (50  $\mu\text{M}$ ) excited at 532 nm clearly provides an increasingly intense emission of  $^1\text{DCA}$  between 400 nm to 600 nm upon higher concentrations of DCA in dichloromethane (Figure S16a). In line with more efficient quenching  $^3[\text{Os}(\text{bpy})_3]^{2+}$  by DCA, for higher concentrations of DCA the intensity of the prompt  $^3[\text{Os}(\text{bpy})_3]^{2+}$  emission is furthermore decreasing (around 700 nm in Figure S16a). Upon increasing concentration of DCA at concentrations in the millimolar range, the upconverted emission of  $^1\text{DCA}$  is detectable below  $\sim 440$  nm as a negative signal in the transient absorption spectra (in Figure S16b). DCA absorbs essentially all light of the flash lamp and therefore the very prominent negative emission signal appears. Furthermore, upon increasing concentration of DCA this filter effect and emission complicates the proper detection of  $^3\text{DCA}$  at its maximum around 440 nm.<sup>41,42</sup> In fact, while the transient absorption maxima around 735 nm and 810 nm increase upon increasing concentrations of DCA (exact conditions given in Figure S16b) the maximum around 440 nm shifts towards 450 nm and decreases at the same time, indicating a significant filter effect at these concentrations. This is also observable when the kinetic traces at 450 nm and 810 nm are compared for a solution containing  $[\text{Os}(\text{bpy})_3]^{2+}$  excited at 532 nm in the 2 mM DCA; while at 450 nm hardly any positive signal of  $^3\text{DCA}$  is detectable, this is indeed the case at 810 nm (Figure S16c). A detection of the emission at 707 nm on a sub-microsecond timescale reveals that the emission at 707 nm (corresponding to prompt emission by  $^3[\text{Os}(\text{bpy})_3]^{2+}$ ) decreases over time while the emission around 450 nm is growing over time. This is in line with a sensitized triplet-triplet annihilation upconversion mechanism. Focusing on the kinetic traces on longer timescales of a few hundred microseconds, the  $^3\text{DCA}$  signal (detected at 810 nm, Figure S16d) and the upconversion luminescence intensity of  $^1\text{DCA}$  (detected at 450 nm, Figure S16d), both increase in intensity with concentrations of DCA.

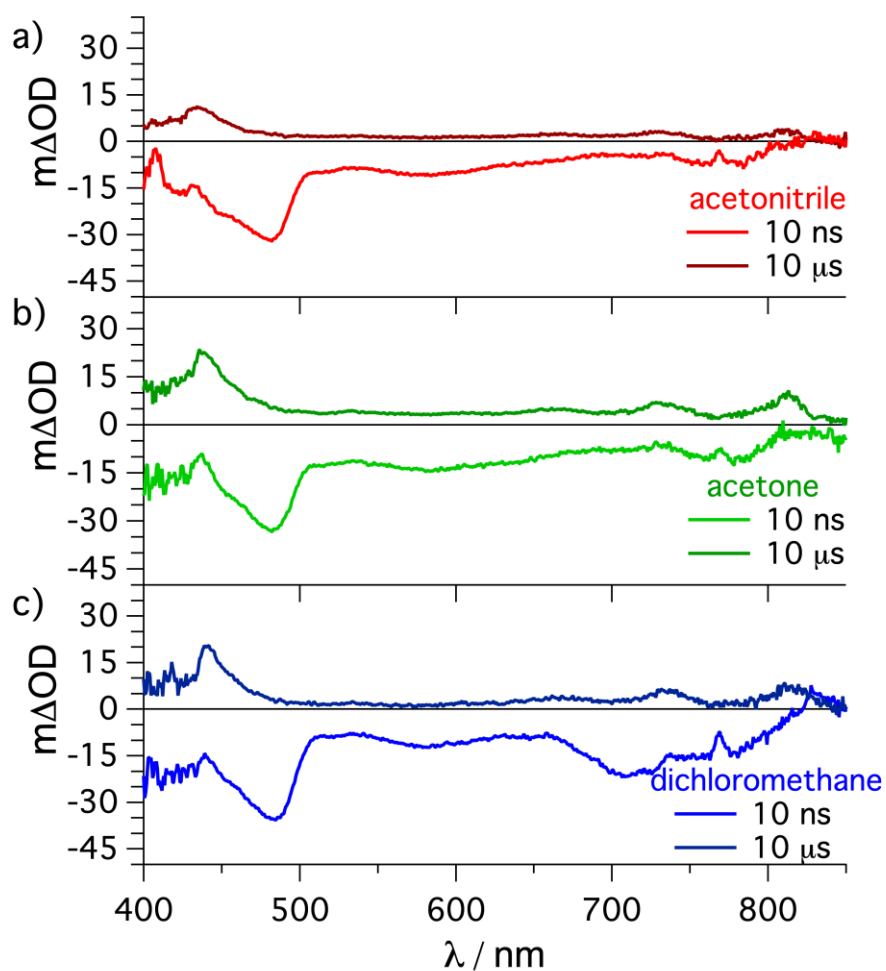


**Figure S14.** Sensitized formation of  $^3\text{DCA}$ .  $[\text{Os}(\text{bpy})_3](\text{PF}_6)_2$  ( $50 \mu\text{M}$ ) in de-aerated solvent was excited at 532 nm and the transient absorption spectra recorded in the presence of DCA ( $500 \mu\text{M}$ ) with time delays of 10 ns and 10  $\mu\text{s}$  (both time-integrated over 200 ns). The individual spectra were recorded in acetonitrile (red), acetone (green) and dichloromethane (blue), and in all cases mainly the ground state bleach of  $[\text{Os}(\text{bpy})_3](\text{PF}_6)_2$  is present when recording with a time delay of 10 ns after the laser pulse (along with the emission signal around 650-850 nm). When using a delay time of 10  $\mu\text{s}$ , the spectroscopic characteristics of  $^3\text{DCA}$  are detected.<sup>3</sup>

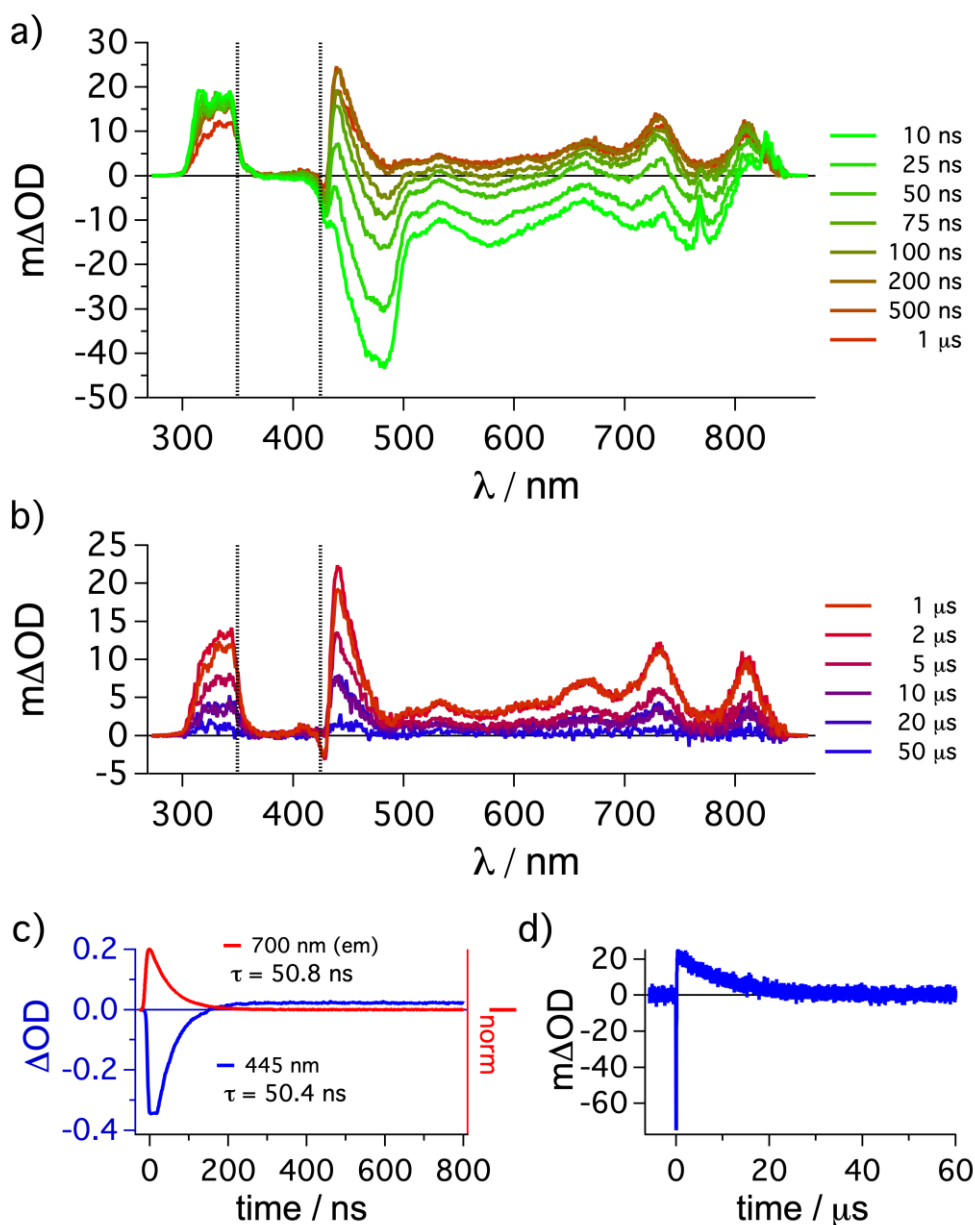


**Figure S15.** Triplet state formation and decay of  ${}^3\text{DCA}$ .  $[\text{Os}(\text{bpy})_3](\text{PF}_6)_2$  (50  $\mu\text{M}$ ) in de-aerated acetonitrile was excited at 532 nm and the transient absorption spectra were recorded in the presence of DCA (500  $\mu\text{M}$ ) with different time delays, time-integrated over 200 ns.  ${}^3\text{DCA}$  formation visible in the transient absorption traces over time (a) correlate to the signal growth monitored at 445 nm within the first 800 ns after the laser pulse in comparison to the emission of  $[\text{Os}(\text{bpy})_3]^{2+}$  of the same solution (c). Decay of  ${}^3\text{DCA}$  on a longer time scale (d). In the transient absorption spectra the ground state absorption blocking the flashlight between 360 nm and ca. 430 nm is clearly visible in (a) and (b), as marked by dotted vertical lines.

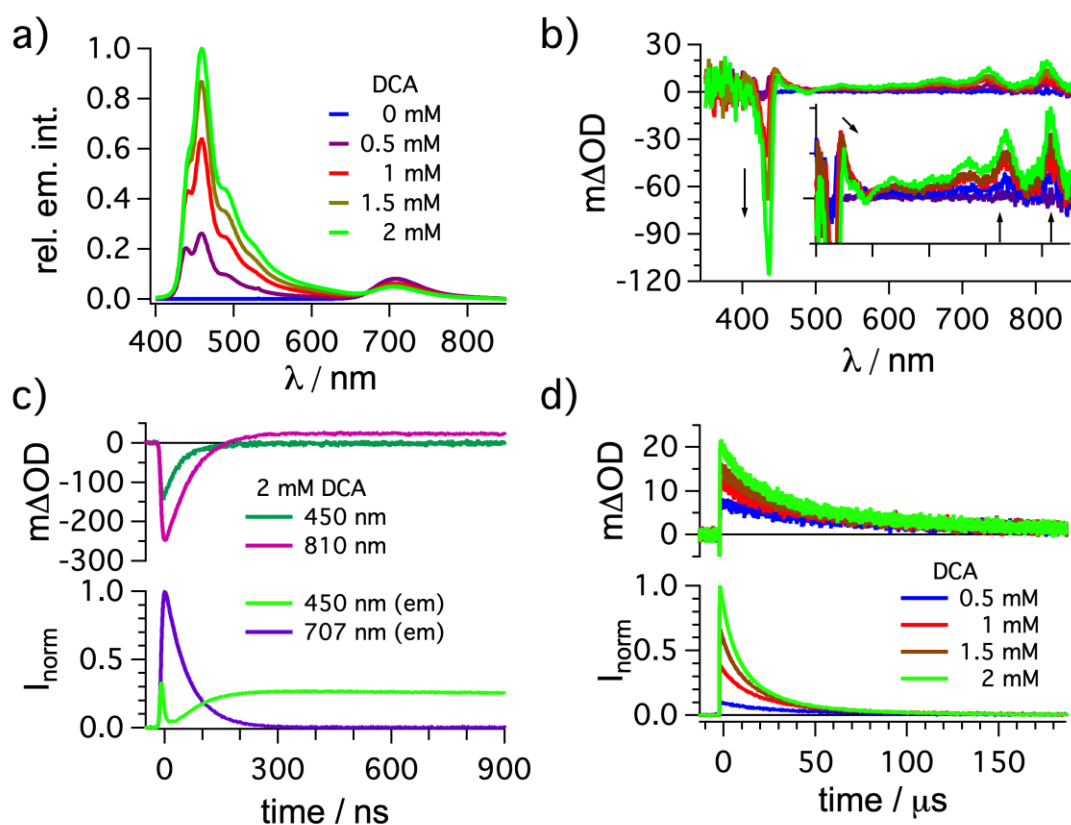


**Figure S16.** Upconverted emission, transient absorption spectra and kinetics with different concentrations of DCA.  $[\text{Os}(\text{bpy})_3](\text{PF}_6)_2$  ( $50 \mu\text{M}$ ) in de-aerated dichloromethane was excited at  $532 \text{ nm}$  and the emission spectra recorded in the absence and in the presence of different concentrations of DCA (colour code as indicated in the figure) with no time delay after the laser pulses, time-integrated over  $200 \mu\text{s}$  (a). Transient absorption spectra of the same solutions as described under (a) were measured with a delay of  $1 \mu\text{s}$  after the laser pulses, time-integrated for  $200 \text{ ns}$  (b). The inset presents a zoom of the spectral region featuring positive signals, and the arrows indicate the change of the signals upon increasing concentration of DCA (color code identical to (a)). The kinetics of the transient absorption (top) and emission traces (bottom) for the solution containing  $2 \text{ mM}$  DCA were measured at different wavelengths (c). The decay of  $^3\text{DCA}$  at  $810 \text{ nm}$  (top) as well as the emission intensity at  $450 \text{ nm}$  for the solutions described under (a) are presented in (d).

### Triplet-triplet energy transfer rate constants ( $k_{\text{TTET}}$ )

Further information concerning the rate constant of step 1 in Figure S13 is given here.

In acetone and acetonitrile as solvents, Stern-Volmer quenching experiments (Figure S17 and Figure S18) of the emission of  $[\text{Os}(\text{bpy})_3](\text{PF}_6)_2$  after excitation with a 532 nm laser resulted in quenching constants of  $4 \cdot 10^4 \text{ M}^{-1} \text{ s}^{-1}$  (acetonitrile) and  $4 \cdot 10^4 \text{ M}^{-1} \text{ s}^{-1}$  (acetone). These bimolecular rate constants are about five times lower than the diffusion limit in these solvents ( $1.9 \cdot 10^{10} \text{ M}^{-1} \text{ s}^{-1}$  in acetonitrile and  $2.1 \cdot 10^{10} \text{ M}^{-1} \text{ s}^{-1}$  in acetone).<sup>31</sup> As already mentioned before, the low solubility of DCA in acetonitrile and acetone complicates our optical spectroscopic measurements, and the  $k_{\text{TTET}}$  values might be not fully accurate. In both cases, at higher concentrations DCA is not soluble anymore (0.5 - 1 mM) and the ratio of  $\tau$  to  $\tau_0$  does not change with increasing amounts of DCA added. Therefore, these datapoints were omitted for the respective Stern-Volmer analyses.

For dichloromethane, a Stern-Volmer analysis with higher concentrations of DCA is possible (Figure S19) and a quenching constant of  $3 \cdot 10^9 \text{ M}^{-1} \text{ s}^{-1}$  is measured, but with much narrower distribution of individual data points. Overall, a comparison of all investigated solvents indicates that the rate constant for the energy transfer is not strongly dependent on the solvent in this case.

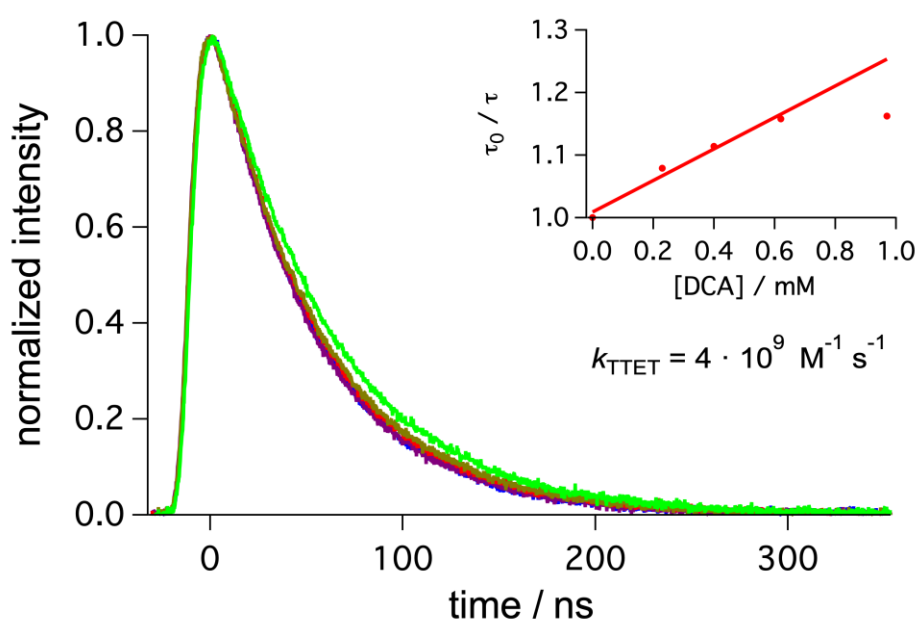


**Figure S17.** Emission lifetime quenching of  $^3[\text{Os}(\text{bpy})_3](\text{PF}_6)_2$  by DCA.  $[\text{Os}(\text{bpy})_3](\text{PF}_6)_2$  (50  $\mu\text{M}$ ) in de-aerated acetonitrile was excited at 532 nm and the emission decay was monitored at 720 nm in the absence (green) and in the presence of different concentrations of DCA (0.23, 0.40, 0.62, 0.97 mM). The Stern-Volmer plot obtained from this data set and the resulting quenching rate constant for a fit of all datapoints up to 0.6 mM are given in the inset.

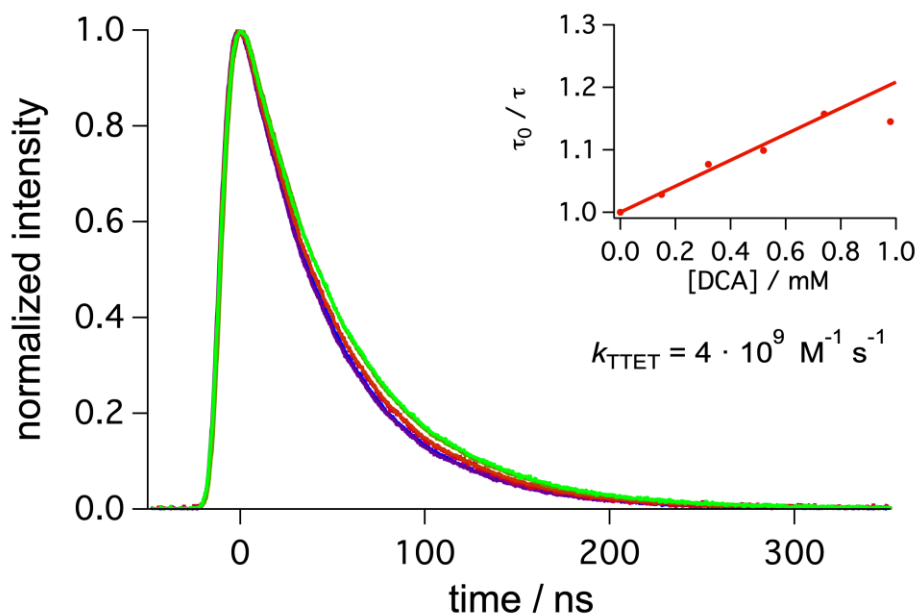


**Figure S18.** Emission lifetime quenching of  $^3[\text{Os}(\text{bpy})_3](\text{PF}_6)_2$  by DCA.  $[\text{Os}(\text{bpy})_3](\text{PF}_6)_2$  (50  $\mu\text{M}$ ) in de-aerated acetone was excited at 532 nm and the emission decay was monitored at 720 nm in the absence (green) and in the presence of different concentrations of DCA (0.15, 0.32, 0.52, 0.74, 0.98 mM). The Stern-Volmer plot obtained from this data set and the resulting quenching rate constant for a fit of all datapoints up to 0.74 mM are given in the inset.

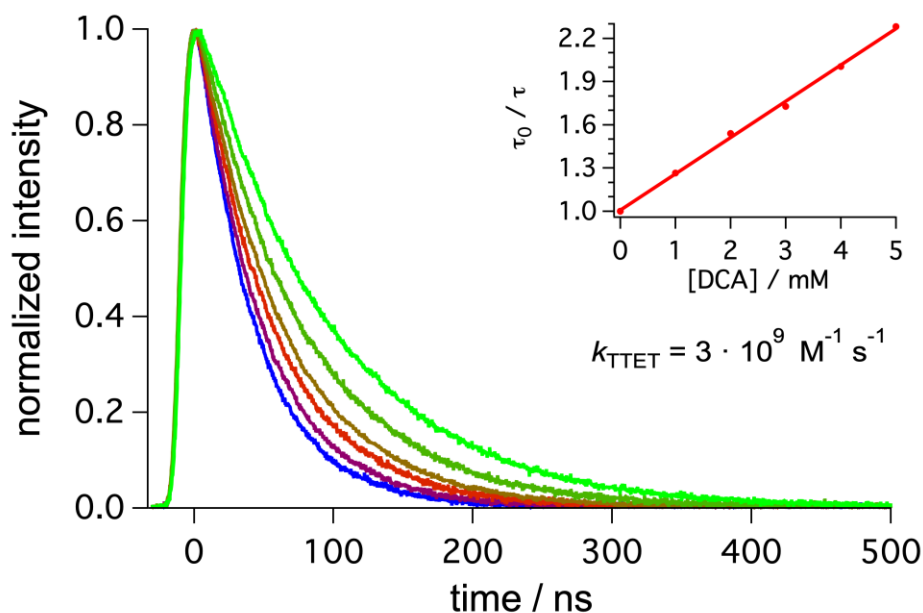


**Figure S19.** Emission lifetime quenching of  $^3[\text{Os}(\text{bpy})_3](\text{PF}_6)_2$  by DCA.  $[\text{Os}(\text{bpy})_3](\text{PF}_6)_2$  (50  $\mu\text{M}$ ) in de-aerated dichloromethane was excited at 532 nm and the emission decay was monitored at 707 nm in the absence (green) and in the presence of different concentrations of DCA (1, 2, 3, 4, 5 mM). The Stern-Volmer plot obtained from this data set and the resulting quenching rate constant are given in the inset.

### 4.3. Triplet-triplet annihilation upconversion

#### 4.3.1. Triplet-triplet annihilation rate constants

For the triplet state deactivation of DCA two concurrent pathways are possible.<sup>43</sup> Triplet-triplet annihilation upconversion as a second-order decay pathway between two <sup>3</sup>DCA molecules as well as the natural decay to the ground state as a first order reaction pathway are viable and both dependent on the concentration of <sup>3</sup>DCA. Using equations S1 and S2,<sup>10,12,43,44</sup> the triplet-triplet annihilation constant ( $k_{TTA}$ ) and the natural lifetime  $\tau_0$  ( $= 1/k_T$ ) can be calculated when the initial triplet concentration ( $[^3A]_0$ ) is known. For DCA the extinction coefficient is known at 440 nm ( $9000 \text{ M}^{-1} \text{ cm}^{-1}$ ),<sup>42</sup> and the corresponding concentration can be calculated from the initial intensity at a delay time of 0  $\mu\text{s}$  at this wavelength. The measurements were repeated with different laser excitation intensities and the obtained values were averaged.

$$\Delta A = \frac{\Delta A_0 \cdot (1 - \beta)}{\exp(k_T \cdot t) - \beta} \quad (\text{S1})$$

$$\beta = \frac{k_{TTA} \cdot [^3A]_0}{k_{TTA} \cdot [^3A]_0 + k_T} \quad (\text{S2})$$

In our measurements the excitation wavelength is 532 nm for these experiments (due to the limited light intensity available at 635 nm on our setup). With more sophisticated setups also a determination by emission measurements would be possible (yielding potentially more precise triplet-triplet annihilation rate constants),<sup>14,15</sup> nevertheless the method herein likely provides a reasonable estimation for the triplet-triplet annihilation constant and the rate constant and natural lifetime of <sup>3</sup>DCA in different solvents. While the solubility limits the concentration of DCA in acetone and acetonitrile (as mentioned above), the achievable ratio in these measurements is comparably high, and detection at the maximum of the <sup>3</sup>DCA absorption (440 nm) is possible.<sup>42</sup> For the measurements in dichloromethane higher concentrations of DCA are dissolvable, but filter effects (see Figure S22) prevent reliable detection at 440 nm. Consequently, the extinction coefficient for the <sup>3</sup>DCA absorption signals at 735 nm and 810 nm were determined based on a comparison between a sample containing  $[\text{Os}(\text{bpy})_3](\text{PF}_6)_2$  and either 0.5 mM or 2 mM of DCA. A normalisation to  $9000 \text{ M}^{-1} \text{ cm}^{-1}$  at 440 nm and overlay between both spectra above 500 nm yielded approximate values for the extinction coefficients at 735 nm ( $\sim 3500 \text{ M}^{-1} \text{ cm}^{-1}$ ) and 810 nm ( $\sim 4500 \text{ M}^{-1} \text{ cm}^{-1}$ ). While the lower concentrated sample clearly has its maximum around 440 nm, with a higher concentration of DCA a significant decrease of the signal intensity around 440 nm is visible (Figure S22). On the other hand, the higher concentration of DCA results in a more efficient quenching of the osmium complex and higher concentrations of <sup>3</sup>DCA are detectable, resulting in an increased signal intensity and better data quality above 500 nm. Consequently, the determination of the natural lifetime and the triplet-triplet annihilation rate constant in dichloromethane is feasible using 735 nm or 810 nm as detection wavelengths (Figure S23).

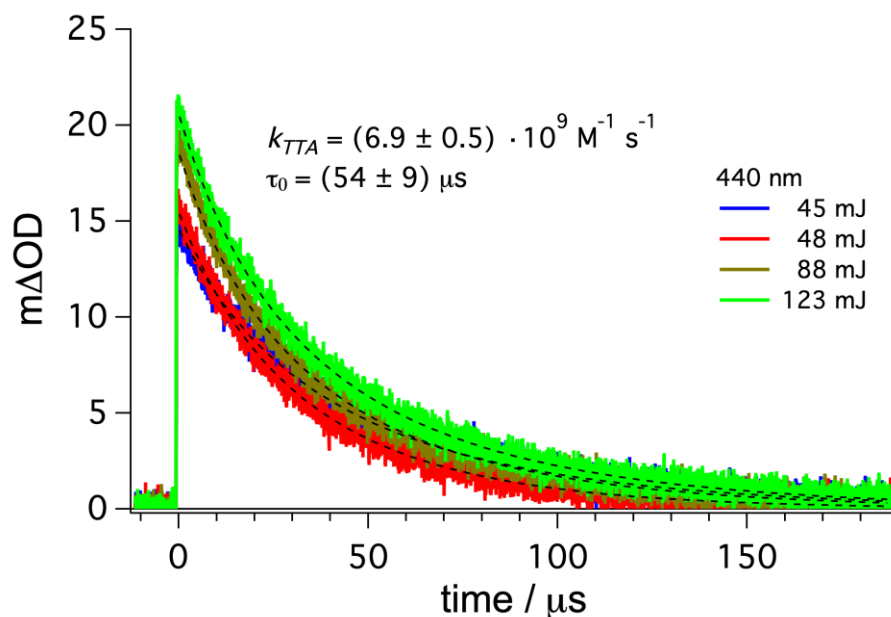


**Figure S20.** Power-dependent decay of  $^3\text{DCA}$  in acetonitrile.  $[\text{Os}(\text{bpy})_3](\text{PF}_6)_2$  ( $50 \mu\text{M}$ ) in de-aerated acetonitrile was excited at 532 nm in the presence of DCA ( $500 \mu\text{M}$ ). Decay of transient absorption signals corresponding to  $^3\text{DCA}$  were monitored at 440 nm with different excitation pulse energies (as indicated in inset) and the corresponding fitting curves are displayed as dashed black traces. The individual values for all traces were averaged to obtain  $k_{\text{TTA}}$  and  $\tau_0$ .

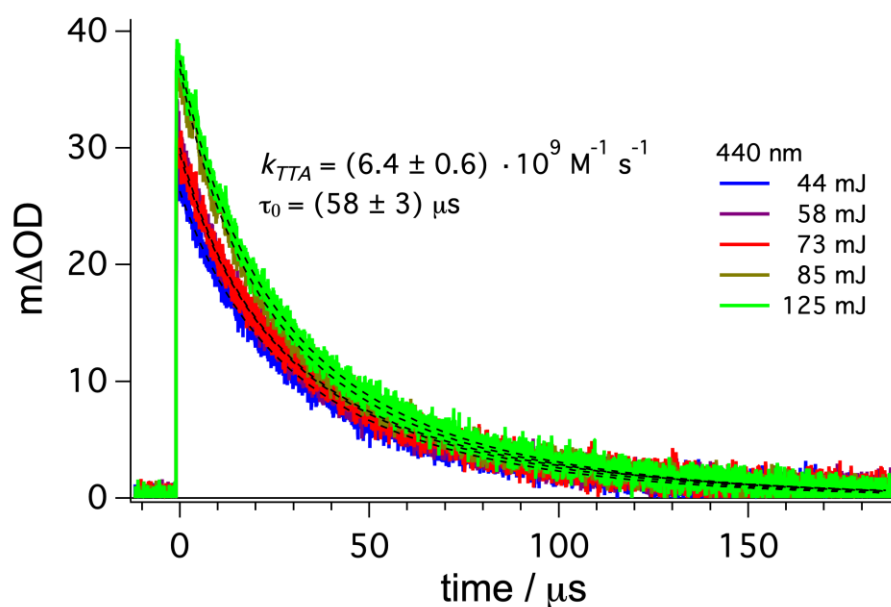


**Figure S21.** Power-dependent decay of  $^3\text{DCA}$  in acetone.  $[\text{Os}(\text{bpy})_3](\text{PF}_6)_2$  ( $50 \mu\text{M}$ ) in de-aerated acetone was excited at 532 nm in the presence of DCA ( $500 \mu\text{M}$ ). Decay of transient absorption signals of  $^3\text{DCA}$  were monitored at 440 nm with different excitation pulse energies (as indicated in inset) and the corresponding fitting curves are displayed as dashed black traces. The individual values for all traces were averaged to obtain  $k_{\text{TTA}}$  and  $\tau_0$ .

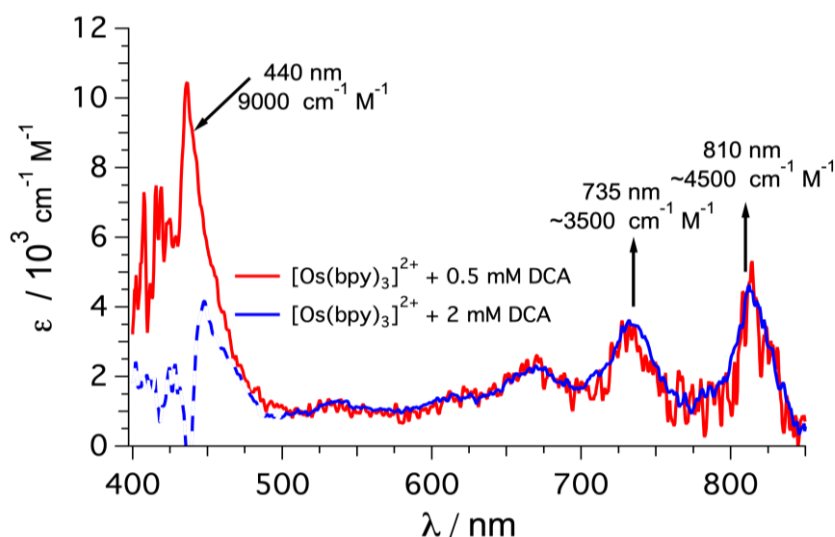


**Figure S22.** Molar absorption coefficients of  $^3\text{DCA}$  at different wavelengths.  $[\text{Os}(\text{bpy})_3](\text{PF}_6)_2$  ( $50 \mu\text{M}$ ) was excited at  $532 \text{ nm}$  in the presence of  $0.5 \text{ mM}$  (red) and  $2 \text{ mM}$  (blue) DCA and transient absorption spectra were measured  $1 \mu\text{s}$  after the laser pulse (time-integrated for  $200 \text{ ns}$ ). After that time delay only spectroscopic signals corresponding to the  $^3\text{DCA}$  are expectable. The trace recorded at a lower concentration of DCA (red) was normalized to the known extinction coefficient ( $9000 \text{ M}^{-1} \text{ cm}^{-1}$  at  $440 \text{ nm}$ )<sup>42</sup> and the trace recorded at a higher concentration of DCA (blue) was scaled to the transient bands above  $500 \text{ nm}$ . Below  $500 \text{ nm}$  (dotted blue trace) a filter effect (and contributions from emission of  $^1\text{DCA}$ ) is clearly visible for a DCA concentration of  $2 \text{ mM}$  (blue), while the spectral resolution is better above  $500 \text{ nm}$  compared to the sample containing  $0.5 \text{ mM}$  DCA (red).

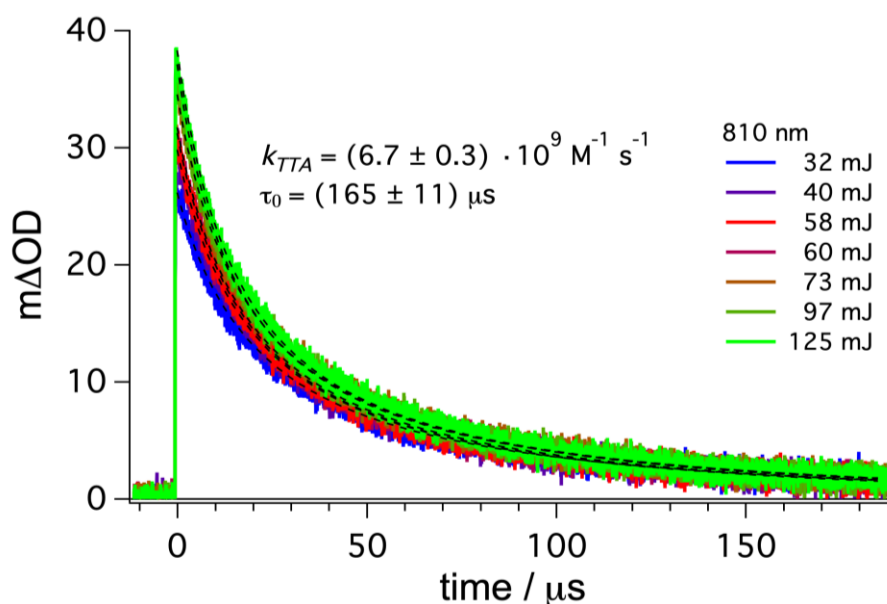


**Figure S23.** Power-dependent decay of  $^3\text{DCA}$  in dichloromethane.  $[\text{Os}(\text{bpy})_3](\text{PF}_6)_2$  ( $50 \mu\text{M}$ ) in de-aerated dichloromethane was excited at  $532 \text{ nm}$  in the presence of DCA ( $3 \text{ mM}$ ). Decay of transient signals of  $^3\text{DCA}$  were monitored at  $810 \text{ nm}$  with different excitation pulse energies (as indicated in inset) and the corresponding fitting curves are displayed as dashed black traces. The individual values for all traces were averaged to obtain  $k_{\text{TTA}}$  and  $\tau_0$ .

### 4.3.2. Power dependence and upconversion quantum yield estimation

#### Upconversion quantum yield estimation

The upconversion quantum yield ( $\phi_{sTAA-UC}$ ) for our system in different solvents was measured as relative value in comparison to the prompt emission of  $[\text{Os}(\text{bpy})_3]^{2+}$  in the respective solvent. Equation S3 is used to calculate the relative quantum yield. The absorbance at the excitation wavelength ( $A$ ), the integrated emission ( $I$ ) and the refractive index of the solvent  $\eta$  are needed for the upconversion system (denoted with subscript UC) and the reference system (denoted with subscript Ref) under identical conditions. In our case a sample of  $[\text{Os}(\text{bpy})_3]^{2+}$  in the respective solvent without annihilator served as reference.

$$\phi_{sTTA-UC} = \phi_{Ref} \cdot \frac{A_{Ref}}{A_{UC}} \cdot \frac{I_{UC}}{I_{Ref}} \cdot \frac{\eta_{UC}^2}{\eta_{Ref}^2} \quad (\text{S3})$$

The general experimental setup used for these measurements has been described earlier, incorporating a blue (rather than red) cw laser.<sup>44</sup> The necessary attenuation of the prompt emission intensity by neutral density filters (to avoid detector over-saturation) has been accounted for in our analysis. As it evident from the spectroscopic datasets (Figure S24-Figure S29), the prompt emission of  $[\text{Os}(\text{bpy})_3]^{2+}$  tails into the near-infrared spectral range and at the detector limit at 900 nm, the emission has not fully returned to the baseline. To avoid a systematic error in our reference system caused by this detector limit, the photoluminescence quantum yield of  $[\text{Os}(\text{bpy})_3]^{2+}$  was determined on the same instrument in all three solvents relative to  $[\text{Ru}(\text{bpy})_3]^{2+}$  (Table S9). These photoluminescence quantum yield values were then used as references for our upconversion quantum yield determinations. This method minimizes errors caused by the incomplete emission detection caused by the detector cut-off around 900 nm.

In dichloromethane the lifetime and quantum yield of  $[\text{Os}(\text{bpy})_3]^{2+}$  (see Table S9) as well as the solubility of DCA is much higher than in acetonitrile and acetone, hence it is unsurprising that the upconversion quantum yield ( $\phi_{sTAA-UC}$ ) is significantly higher in dichloromethane (see also next paragraph). Nevertheless, a direct comparison might be misleading due to the different concentrations of DCA used in the different solvents.

For the measurements with a 705 nm cw-laser light source, the prompt emission of  $^3[\text{Os}(\text{bpy})_3]^{2+}$  is not fully detectable because it spectrally overlaps with the excitation wavelength. The integration of the reference emission was therefore performed using a scaled emission trace of the full emission spectrum obtained by excitation at a shorter wavelength (see Figure S8). In these datasets, the lowest excitation power density ( $2.5 \text{ W} \cdot \text{cm}^{-2}$ ) is close to the determined threshold intensity ( $\sim 1.65 \text{ W} \cdot \text{cm}^{-2}$ ) and therefore a comparatively high upconversion quantum yield is detectable even for the datapoints acquired at the lowest power densities (Figure S25, Figure S27, Figure S29).

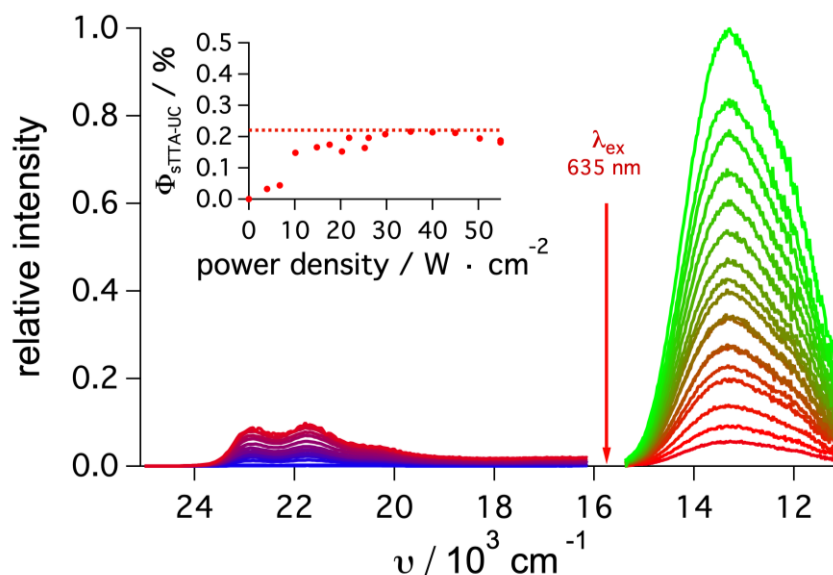


**Figure S24.** Emission and upconversion quantum yield ( $\Phi_{\text{STTA-UC}}$ ) of the  $[\text{Os}(\text{bpy})_3](\text{PF}_6)_2$  (20  $\mu\text{M}$ ) and DCA (500  $\mu\text{M}$ ) combination in de-aerated **acetonitrile**. The excitation power-dependent steady-state emission of upconverted  $^1\text{DCA}$  fluorescence (blue spectral range) as well as the prompt emission of a solution of  $[\text{Os}(\text{bpy})_3](\text{PF}_6)_2$  in the absence of annihilator as reference system (red spectral range) upon excitation at 705 nm with a continuous-wave laser are displayed. The inset contains the calculated upconversion quantum yield with respect to the power density of the excitation light source (see text for details).

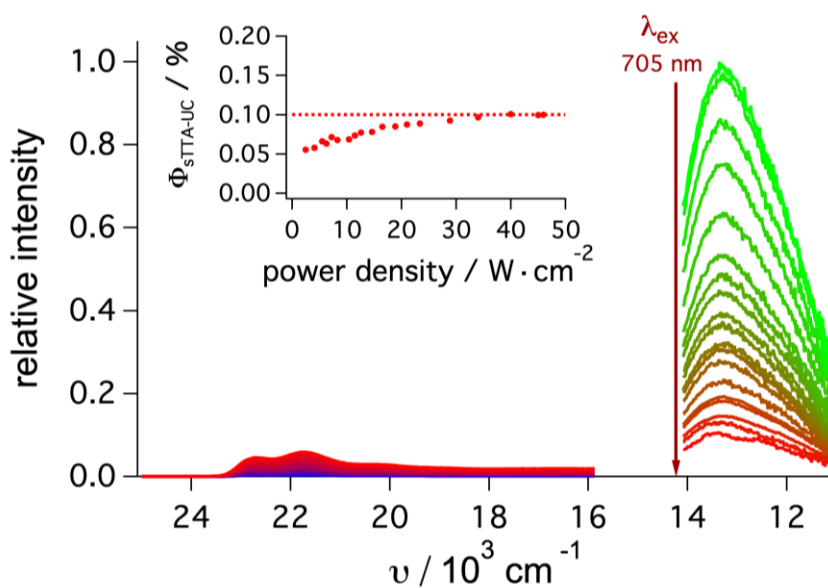


**Figure S25.** Emission and upconversion quantum yield ( $\Phi_{\text{STTA-UC}}$ ) of  $[\text{Os}(\text{bpy})_3](\text{PF}_6)_2$  (50  $\mu\text{M}$ ) and DCA (500  $\mu\text{M}$ ) in de-aerated **acetonitrile**. The excitation power-dependent steady-state emission of upconverted  $^1\text{DCA}$  fluorescence (blue spectral range) as well as the prompt emission of a solution of  $[\text{Os}(\text{bpy})_3](\text{PF}_6)_2$  in the absence of annihilator as reference system (red spectral range) upon excitation at 705 nm with a continuous-wave laser are displayed. The inset contains the calculated upconversion quantum yield with respect to the power density of the excitation light source (see text for details).

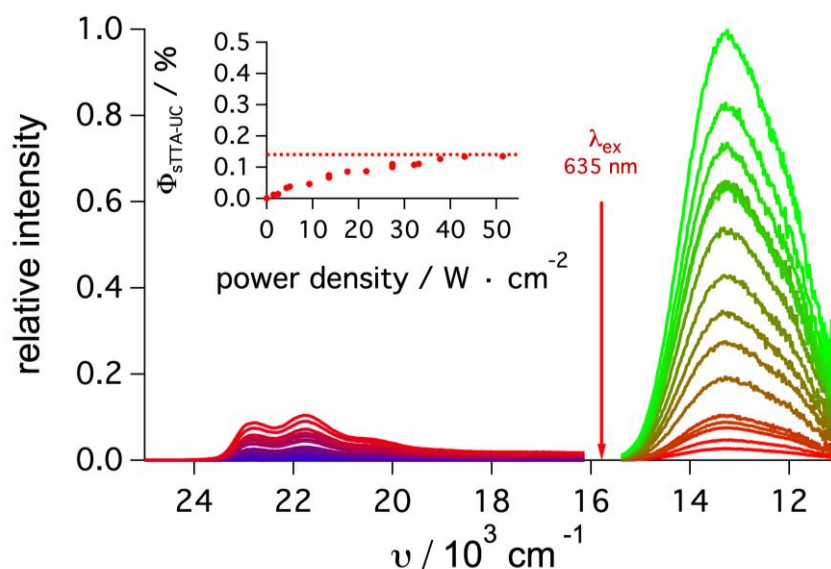


**Figure S26.** Emission and upconversion quantum yield ( $\Phi_{\text{STTA-UC}}$ ) of  $[\text{Os}(\text{bpy})_3](\text{PF}_6)_2$  (20  $\mu\text{M}$ ) and DCA (500  $\mu\text{M}$ ) in de-aerated **acetone**. The steady-state emission of upconverted  $^1\text{DCA}$  fluorescence (blue spectral range) as well as the prompt emission of a solution of  $[\text{Os}(\text{bpy})_3](\text{PF}_6)_2$  in the absence of annihilator as reference system (red spectral range) upon excitation at 635 nm with a continuous-wave laser are displayed. The inset contains the calculated upconversion quantum yield with respect to the power density of the excitation light source (see text for details).

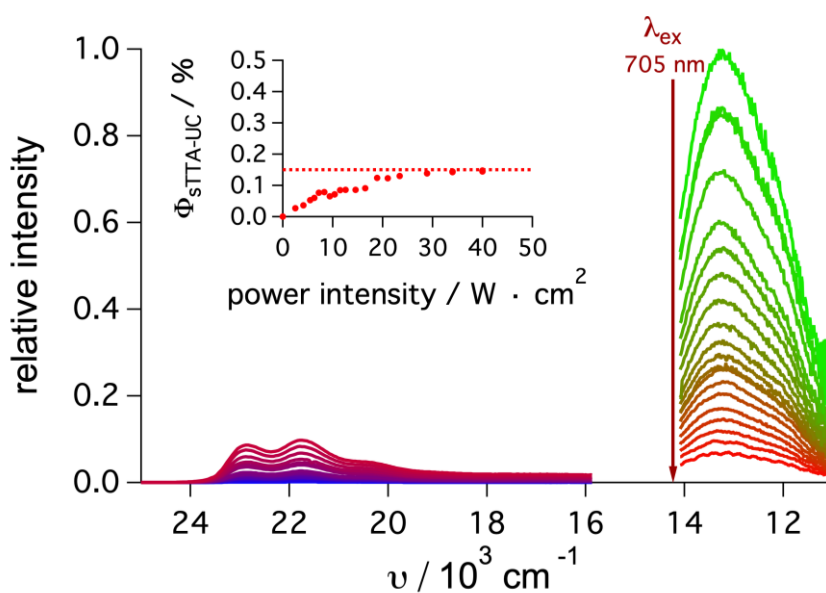


**Figure S27.** Emission and upconversion quantum yield ( $\Phi_{\text{STTA-UC}}$ ) of  $[\text{Os}(\text{bpy})_3](\text{PF}_6)_2$  (50  $\mu\text{M}$ ) and DCA (500  $\mu\text{M}$ ) in de-aerated **acetone**. The excitation power-dependent steady-state emission of upconverted  $^1\text{DCA}$  fluorescence (blue spectral range) as well as the prompt emission of a solution of  $[\text{Os}(\text{bpy})_3](\text{PF}_6)_2$  in the absence of annihilator as reference system (red spectral range) upon excitation at 705 nm with a continuous-wave laser are displayed. The inset contains the calculated upconversion quantum yield with respect to the power density of the excitation light source (see text for details).

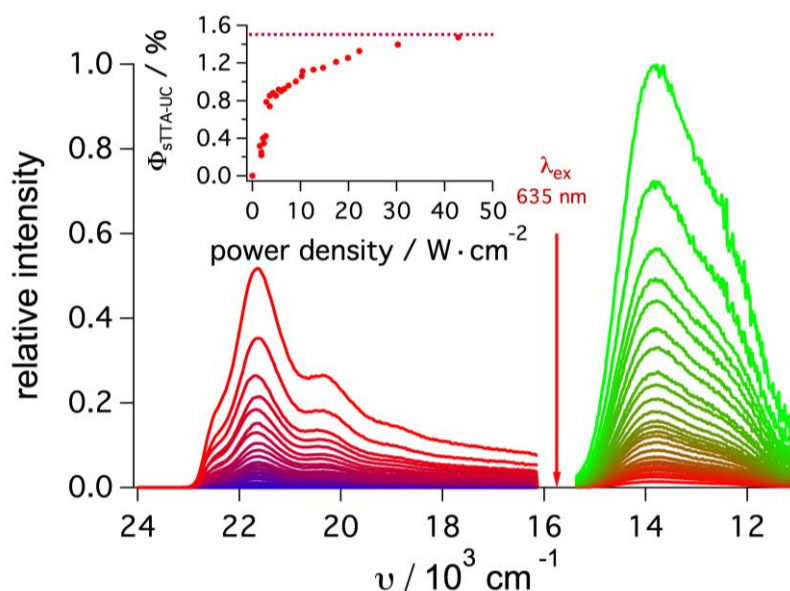


**Figure S28.** Emission and upconversion quantum yield ( $\Phi_{\text{STTA-UC}}$ ) of  $[\text{Os}(\text{bpy})_3](\text{PF}_6)_2$  (20  $\mu\text{M}$ ) and DCA (3 mM) in de-aerated **dichloromethane**. The excitation power-dependent steady-state emission of upconverted  $^1\text{DCA}$  fluorescence (blue spectral range) as well as the prompt emission of a solution of  $[\text{Os}(\text{bpy})_3](\text{PF}_6)_2$  in the absence of annihilator as reference system (red spectral range) upon excitation at 635 nm with a continuous-wave laser are displayed. The inset contains the calculated upconversion quantum yield with respect to the power density of the excitation light source (see text for details). The same dataset is also presented in the main manuscript in Figure 2c.

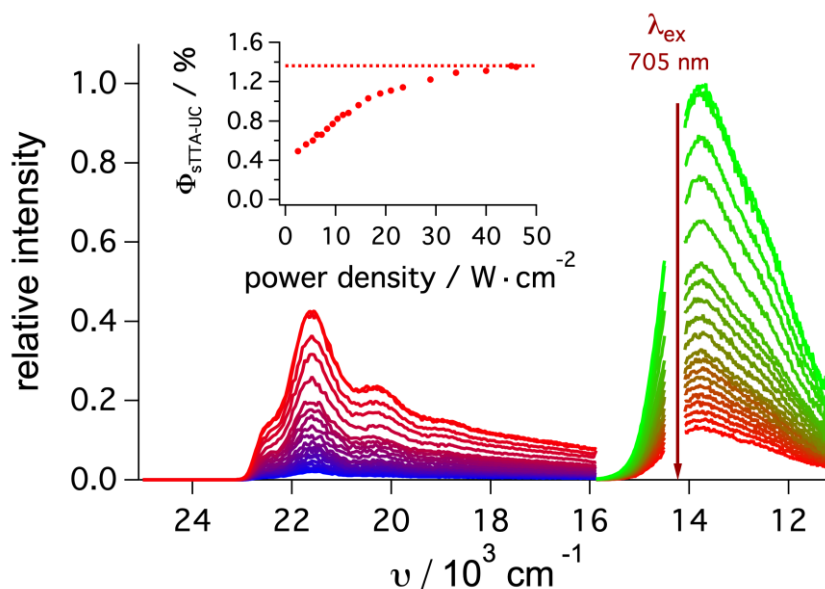


**Figure S29.** Emission and upconversion quantum yield ( $\Phi_{\text{STTA-UC}}$ ) of  $[\text{Os}(\text{bpy})_3](\text{PF}_6)_2$  (20  $\mu\text{M}$ ) and DCA (3 mM) in de-aerated **dichloromethane**. The excitation power-dependent steady-state emission of upconverted  $^1\text{DCA}$  fluorescence (blue spectral range) as well as the prompt emission of a solution of  $[\text{Os}(\text{bpy})_3](\text{PF}_6)_2$  in the absence of annihilator as reference system (red spectral range) upon excitation at 705 nm with a continuous-wave laser are displayed. The inset contains the calculated upconversion quantum yield with respect to the power density of the excitation light source (see text for details).

### Quadratic power dependence

For small excitation power densities, a quadratic dependence of the upconverted emission of  $^1\text{DCA}$  relative to the excitation power density can be expected.<sup>45,46</sup> Since the measurements of the upconversion luminescence quantum yields in the previous paragraphs do not contain enough datapoints with sufficiently low excitation power densities, additional measurements in dichloromethane were performed to analyse this aspect in more detail.

In Figure S30 different laser intensities between 0 and 60 mW were used to analyse the power dependence, and the laser intensity was attenuated by neutral density filters. For the emission of  $[\text{Os}(\text{bpy})_3]^{2+}$  in the absence of DCA (b), an essentially linear dependence on the excitation power is obtained (d, slope  $\sim 0.97$ ), while for the upconverted emission (a) indeed a quadratic dependence is found at low power densities (c, slope  $\sim 2.06$ ). The dataset in Figure S30c is a non-logarithmic representation of the data presented in Figure 2c of the main manuscript, with a focus on low excitation densities. The emission spectra in Figure S30a represent the original data for the respective figure in the main paper.

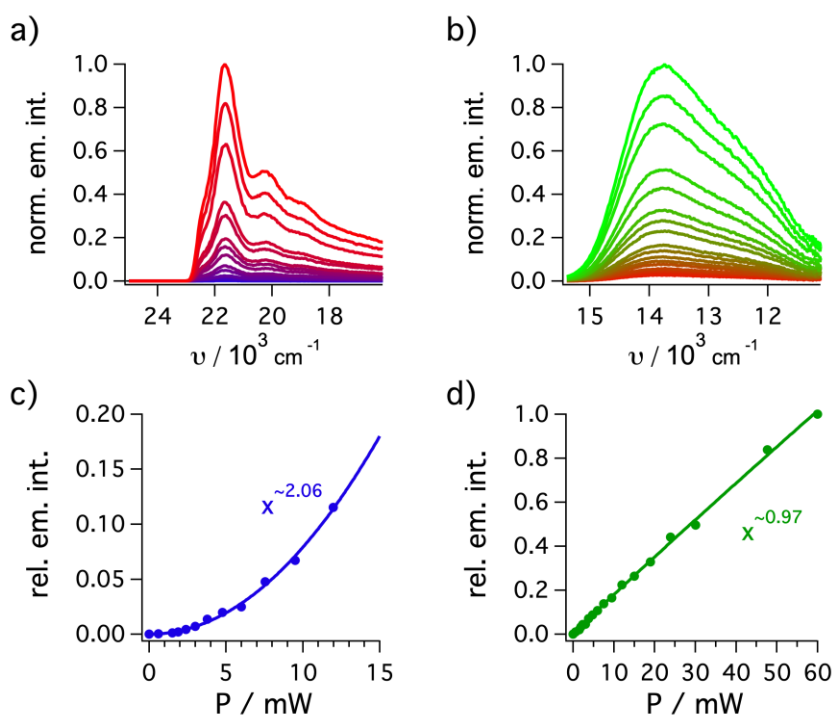


**Figure S30.** Power dependence of emission intensities. Steady state emission spectra of DCA (3 mM) upon excitation of  $[\text{Os}(\text{bpy})_3](\text{PF}_6)_2$  (50  $\mu\text{M}$ ) in de-aerated dichloromethane with variation of the irradiation power of a 635 nm cw laser (a) and of an identical solution in the absence of DCA (b, as reference system, monitoring the prompt emission of the osmium complex) were measured. The relation between the excitation power of the laser and the integrated relative emission intensity of the upconverted emission of  $^1\text{DCA}$  (c) and the prompt emission of the osmium sensitizer (d) for the data from (a) and (b) is shown together with the corresponding best power function fit results (fit function  $y(x) = a \cdot x^b$ ; fit curves in green and blue). In (c), a focus to the powers up to 15 mW with a quadratic dependence is shown, while the full dataset is presented in the main manuscript as Figure 2c (in a double logarithmic representation).

### Anti-Stokes shift, excimer emission and inner filter effects

For upconversion systems several different approaches to calculate the anti-Stokes shift have been used in the literature.<sup>1,34,47,48</sup> Especially differences in the emission band maximum for the upconverted delayed emission and the prompt annihilator emission obtained by direct excitation of a diluted solution can make a difference for the actual value of the anti-Stokes shift. This effect becomes evident in the calculated anti-Stokes shifts for different solvents (Table S13) based on the datasets presented in the previous section. In the case of acetonitrile and acetone the solubility of DCA is low and the inner filter effect affects the emission bandshape. Consequently, the emission maximum of the upconverted emission is at lower energy and the calculated anti-Stokes shift is smaller for dichloromethane compared to the more polar solvents (e.g. 0.73 eV vs 0.88 eV for excitation with a 635 nm cw laser, Table S13).

**Table S13.** Summary of anti-Stokes shift calculation with different light sources.

solvent	$\lambda_{\text{ex}} (E) / \text{nm (eV)}$	$\lambda_{\text{em,max}} (E) / \text{nm (eV)}$	$\Delta E / \text{eV}^{\text{a}}$
acetonitrile	635 (1.95)	438 (2.83)	0.88
	705 (1.76)	440 (2.82)	1.06
acetone	635 (1.95)	438 (2.83)	0.88
	705 (1.76)	437 (2.84)	1.08
dichloromethane	635 (1.95)	462 (2.68)	0.73
	705 (1.76)	462 (2.68)	0.92

Anti-Stokes shift estimates for the upconversion measurements presented earlier (Figure S24 – Figure S29).

a) The apparent pseudo anti-Stokes shift is calculated here as the difference between the excitation wavelength and the band emission band maximum of the delayed upconverted fluorescence. Further discussion is provided in the text.

Hanson, Castellano and co-workers recently distinguished between two different ways to define the upconversion quantum yield. On the one hand, they considered the measured upconversion quantum yield ( $\Phi_{\text{sTTA-UC}}$ , for the upconverted delayed fluorescence) and on the other hand they considered the so-called generated upconversion quantum yield, which takes filter effects into account ( $\Phi_{\text{sTTA-UC,g}}$ ).<sup>49</sup>

In our case, the actual photo-generated quantum yield for <sup>1</sup>\*DCA formation *via* upconversion would furthermore be of interest, because this is in fact more relevant for the photoredox catalysis than the actual upconversion luminescence quantum yield. A normalization of the upconverted emission spectrum obtained with 635 nm cw-laser excitation (Figure S31, green trace, bottom) at 460 nm and a normalization of the emission of <sup>1</sup>\*DCA generated by direct excitation of a diluted solution of DCA (red trace) at the same wavelength clearly shows the inner filter effect in the upconversion system. This is unsurprising due to the increasing absorption below ~460 nm (especially caused by the ground state absorption of DCA, Figure S31,

top), and under these conditions in dichloromethane ~35% of the generated emission below 460 nm cannot be detected (value calculated based on emission traces normalized to their maximum around 460 nm, see figure caption). Unfortunately a (weak) excimer emission is also detectable under upconversion conditions (in line with a literature report)<sup>50,51</sup> and the emission above ~500 nm has also contributions from excimer emission.<sup>14,49</sup> Based on the normalized emission at 460 nm, this additional excimer emission increases the overall measured emission intensity by about ~25%. Due to the unknown contribution of the inner filter effect and the excimer emission, the normalization at 460 nm at the peak maximum represents only a proxy, and therefore a more accurate calculation of the generated upconversion quantum yield is not possible. In our system, the overestimation of the upconversion quantum yield by integrating part of the excimer emission and the neglect of the emission reabsorbed by the inner filter effect seem to have similar absolute contributions.

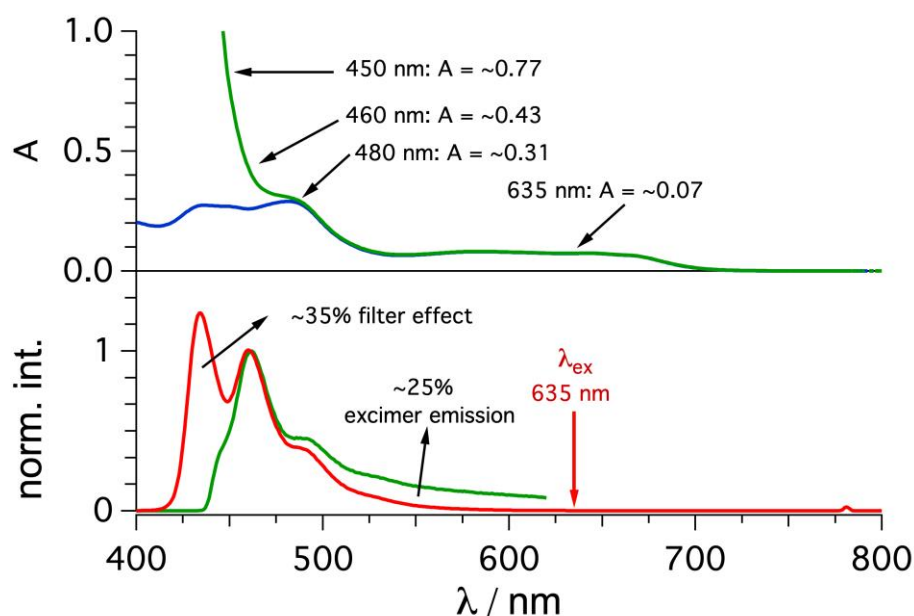


**Figure S31.** Excimer emission and inner filter effect. Bottom: <sup>1\*</sup>DCA emission following direct excitation of DCA (15 μM) at 385 nm and generated *via* sensitized triplet-triplet annihilation upconversion (20 μM [Os(bpy)<sub>3</sub>](PF<sub>6</sub>)<sub>2</sub>, 3mM DCA) under cw laser excitation at 635 nm. For both measurements the solvent is dichloromethane and the spectra are normalized to the (local) peak maximum around ~460 nm. Top: UV-vis absorption spectrum of [Os(bpy)<sub>3</sub>](PF<sub>6</sub>)<sub>2</sub> (20 μM) in the absence (blue) and in the presence of DCA (3 mM) in dichloromethane (green). For the measurement with annihilator present, the absorbance values at different wavelengths are indicated.

### 4.3.3. Limiting factors of upconversion quantum yield

**Table S14.** Summary of quantum yields of each step of sTTA-UC in different solvents.<sup>a</sup>

symbol	general description	abbreviation	acetonitrile	acetone	dichloro- methane
$\phi_{\text{sTTA-UC}}$	measured upconversion quantum yield <sup>a</sup>	sTTA-UC	0.22 %	0.13 %	1.5 %
$\phi_{\text{TTET}}$	quantum yield of triplet-triplet energy transfer <sup>b</sup>	TTET	11 %	11 %	46 %
$\phi_{\text{TAA}}$	triplet-triplet annihilation quantum yield <sup>b</sup>	TTA	- <sup>c</sup>	- <sup>c</sup>	- <sup>c</sup>
$\phi_{\text{FL}}$	fluorescence quantum yield of <sup>1</sup> *DCA <sup>d</sup>	FL	93 %	95 %	97 %

a) Details provided in section 4.3.2. b) Details provided in the text below. c) These values were not determined. d) Details provided in section 4.1.1.

In principle, the triplet-triplet annihilation upconversion quantum yield ( $\phi_{\text{UC,g}}$ ) should be the product of all individual steps involved (equation S4). It has to be emphasized that the abovementioned quantum yield of  $\phi_{\text{TAA-UC}}$  corresponds to experimentally determined values, while  $\phi_{\text{UC,g}}$  represents the internal (generated) quantum yield based on the calculated values for all individual steps (and without taking inner-filter effects of the upconversion measurements into account, as discussed in the previous section).<sup>14,49</sup>

$$\phi_{\text{UC,g}} = f \cdot \phi_{\text{TTET}} \cdot \phi_{\text{TTA}} \cdot \phi_{\text{FL}} \quad (\text{S4})$$

In equation S4,  $f$  is the spin-statistical factor,  $\phi_{\text{TTET}}$  is the quantum yield for triplet-triplet energy transfer,  $\phi_{\text{TAA}}$  is the triplet-triplet annihilation quantum yield, and  $\phi_{\text{FL}}$  is the fluorescence quantum yield of the annihilator. While the fluorescence quantum yield of <sup>1</sup>\*DCA is almost equal in all three solvents (see Table S9), differences in  $\phi_{\text{TTET}}$  and  $\phi_{\text{TAA}}$  depending on the solvent can result in a change of the overall upconversion quantum yield.

$$\phi_{\text{TTET}} = \phi_{\text{ISC,Os}} \frac{k_{\text{TTET}} \cdot [Q]}{k_{\text{TTET}} \cdot [Q] + k_{\text{T}}} \quad (\text{S5})$$

For the determination of  $\phi_{\text{TTET}}$ , the contribution of energy transfer ( $k_{\text{TTET}} \cdot [Q]$ ) to the overall deactivation of the excited <sup>3</sup>\*[Os(bpy)<sub>3</sub>]<sup>2+</sup> is relevant (equation S5).<sup>14</sup> This quantity can be calculated by taking into account the quantum yield for the formation of the lowest triplet excited state of [Os(bpy)<sub>3</sub>]<sup>2+</sup> via intersystem crossing

( $\phi_{ISC, Os}$ , which is essentially unity for this compound).<sup>52</sup> The triplet-triplet energy transfer rate constants determined in 4.3.1 and the natural lifetime (using  $k_T = 1/\tau_0$ ) provided in Table S9 are furthermore needed to obtain  $\phi_{TTET}$ .<sup>14</sup>

For the determination of the triplet-triplet annihilation quantum yield  $\phi_{TTA}$  a new method was developed recently by Albinsson and co-workers.<sup>14,15</sup> In principle equation S6 with the triplet-triplet annihilation constant and the natural lifetime of  $^3DCA$  can be used to calculate the respective quantum yield.

$$\phi_{TTA} = \frac{k_{TTA} \cdot [^3A]_S}{2 \cdot k_{TTA} \cdot [^3A]_S + k_T} \quad (S6)$$

However, this equation requires knowledge of the steady-state concentration of  $^3DCA$  (abbreviated as  $[^3A]_S$  in equation S6), and with our spectroscopic setup this value is not readily available. While the triplet-triplet annihilation rate constant is determined by time-resolved transient absorption kinetic measurements with a pulsed 532-nm laser, a determination of the steady-state triplet concentration would require a modulated cw laser setup with the 635 nm laser used for all other upconversion measurements.<sup>14,15</sup> Consequently, the absolute  $^3DCA$  concentration is not accessible to us.

Our rather simple analysis of different steps contributing to the overall quantum yield clearly indicates that the limited solubility of DCA is a key factor. While possible small differences between acetone and acetonitrile are not readily distinguishable (and the limiting solubility might introduce larger overall errors to the determined absolute values), the higher solubility in dichloromethane clearly increases the quantum yield of the triplet-triplet energy transfer as a main factor for the higher observable sensitized triplet-triplet annihilation upconversion quantum yield.

#### 4.4. Mechanistic investigations of *cis-trans* isomerisation of stilbene

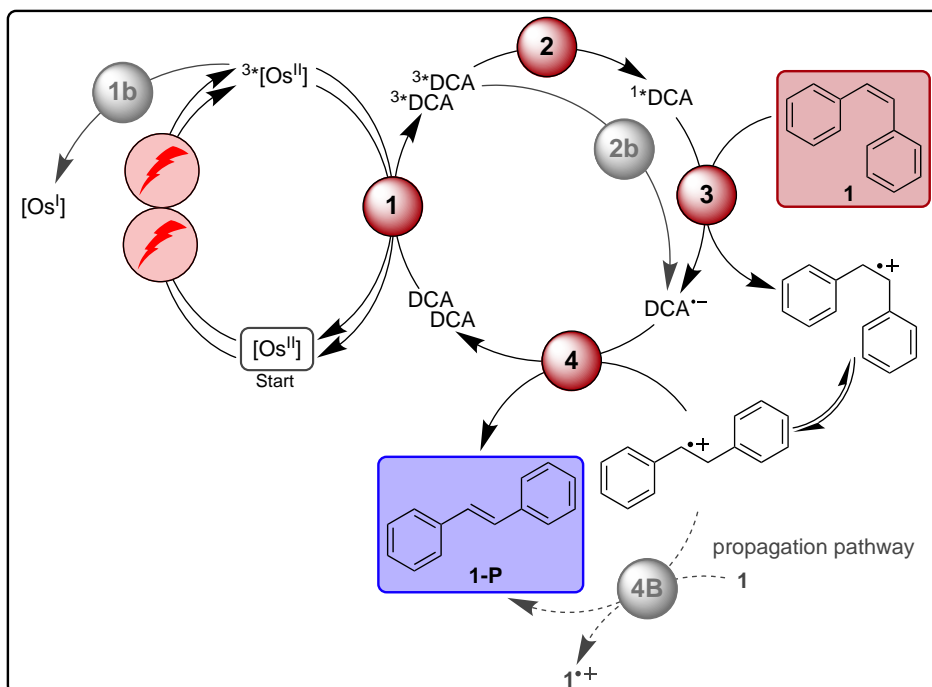


**Figure S32.** Possible mechanism for red light driven photoredox catalysis with  $[\text{Os}(\text{bpy})_3](\text{PF}_6)_2$  and DCA, as in Figure 3 of the main manuscript, but here including the additional side reaction steps 1b, 2b and 4B.

**Table S15.** Summary of relevant data for sTTA-UC for the isomerisation of *cis-* to *trans*-stilbene.<sup>a</sup>

step no.	description of step	$k_Q / \text{M}^{-1} \cdot \text{s}^{-1}$		Figure
		MeCN	DCM	
1	TTET from $[\text{Os}(\text{bpy})_3]^{2+}$ to DCA	$4 \cdot 10^9$	$3 \cdot 10^9$	Figure S17 Figure S19
1b	reductive quenching of $[\text{Os}(\text{bpy})_3]^{2+}$ by <b>1</b>	$<10^7$	-	Figure S39
1b	reductive quenching of $[\text{Os}(\text{bpy})_3]^{2+}$ by <b>1-P</b>	$<10^7$	-	Figure S40
2	triplet-triplet annihilation between $^3\text{DCA}$	$6.9 \cdot 10^9$	$6.8 \cdot 10^9$	Figure S20 Figure S23
2b	reductive quenching of $^1\text{DCA}$ by <b>1</b>	N/A <sup>b</sup>	N/A <sup>b</sup>	Figure S37
2b	reductive quenching of $^1\text{DCA}$ by <b>1-P</b>	N/A <sup>b</sup>	N/A <sup>b</sup>	Figure S36 Figure S38
3	electron transfer from <b>1</b> to $^1\text{DCA}$	$1.32 \cdot 10^{10}$	$1.46 \cdot 10^{10}$	Figure S33 Figure S34
3b	electron transfer from <b>1-P</b> to $^1\text{DCA}$	-	$1.54 \cdot 10^{10}$	Figure S35
4	recovery of $\text{DCA}^{*-}$ by electron transfer	-	-	-
4B	propagation pathway	-	-	section 4.8.3

a) The determination of rate constants of steps 1 and 2 is discussed in the main manuscript and in section 4.2.

b) No Stern-Volmer analysis possible due to competing inherent first- and second order decay pathways.

#### 4.4.1. Quenching of DCA by stilbene

##### Reductive quenching of $^1\text{DCA}$ by *cis*- and *trans*-stilbene

Further information concerning step 3 in Figure S32 is given here.

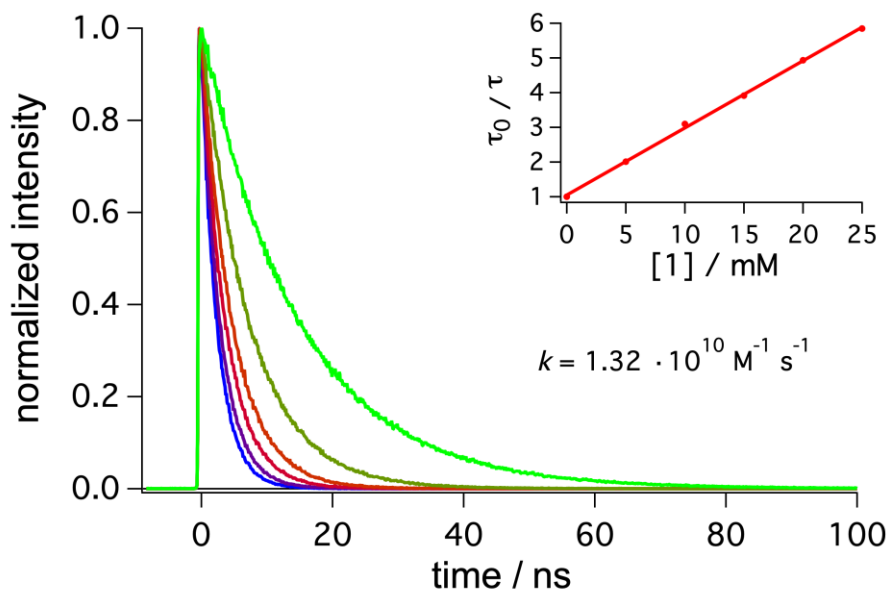


**Figure S33.** Singlet state quenching of DCA by *cis*-stilbene (1). DCA (10  $\mu\text{M}$ ) in de-aerated **acetonitrile** was excited at 405 nm. The emission decay was monitored at 435 nm in the absence (green) and in the presence of different concentrations of *cis*-stilbene (5, 10, 15, 20 and 25 mM). The inset in the upper right corner contains the resulting Stern-Volmer plot and the calculated quenching rate constant.

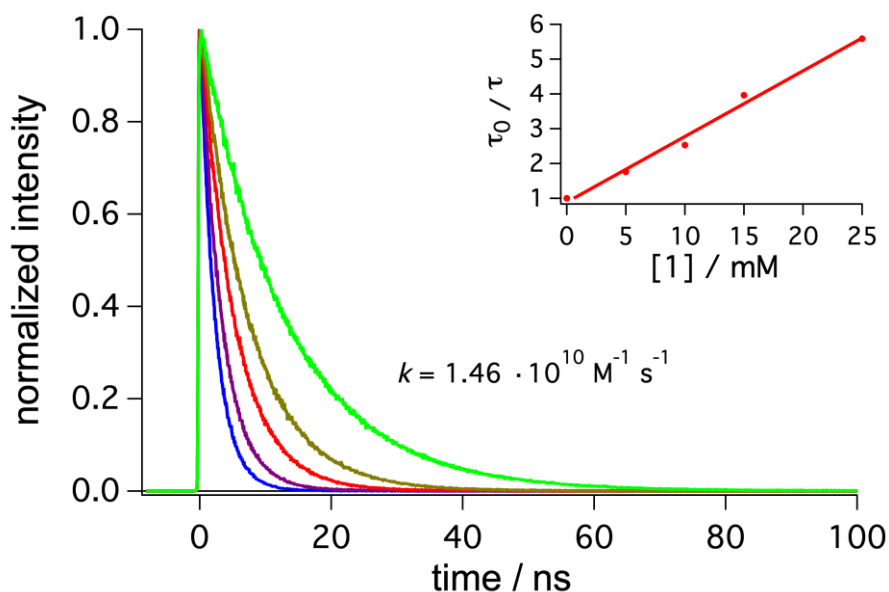


**Figure S34.** Singlet state quenching of DCA by *cis*-stilbene (1). DCA (50  $\mu\text{M}$ ) in de-aerated **dichloromethane** was excited at 405 nm. The emission decay was monitored at 435 nm in the absence (green) and in the presence of different concentrations of *cis*-stilbene (5, 10, 15 and 25 mM). The inset in the upper right corner contains the resulting Stern-Volmer plot and the calculated quenching rate constant.

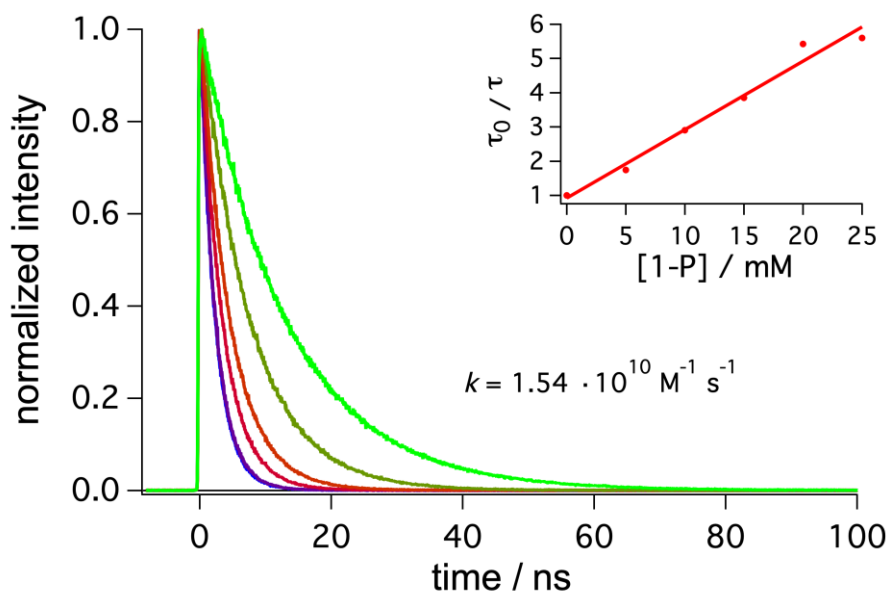


**Figure S35.** Singlet state quenching of DCA by *trans*-stilbene (**1-P**). DCA (50  $\mu\text{M}$ ) in de-aerated dichloromethane was excited at 405 nm. The emission decay was monitored at 435 nm in the absence (green) and in the presence of different concentrations of *trans*-stilbene (5, 10, 15, 20 and 25 mM). The inset in the upper right corner contains the resulting Stern-Volmer plot and the calculated quenching rate constant.

### **Reductive quenching of $^3\text{DCA}$ by *cis*- and *trans*-stilbene**

Further information concerning [step 2b](#) in Figure S32 is given here.

$^3\text{DCA}$  can decay either via a first order deactivation to the ground state or via a second order triplet-triplet annihilation upconversion process. Consequently, the  $^3\text{DCA}$  decay is more complex than a typical bimolecular quenching that can be analysed with a Stern-Volmer analysis. However, with natural lifetimes in the microsecond timescale (e.g. 165  $\mu\text{s}$  in dichloromethane, see section 4.3.1) any significant quenching of  $^3\text{DCA}$  by different substrates should be easily detectable, though exact quantification is not targeted here. With respect to the essentially unchanged traces upon addition of *cis*- and *trans*-stilbene, reductive quenching of  $^3\text{DCA}$  is unlikely as alternative pathway to triplet-triplet annihilation upconversion (Figure S36, Figure S37, Figure S38).

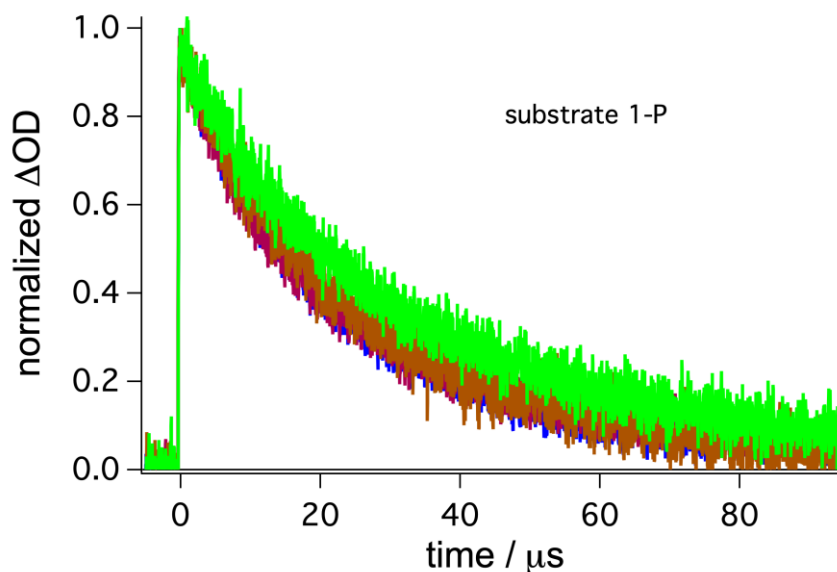


**Figure S36.** Triplet state decay of DCA in the presence of *trans*-stilbene (**1-P**).  $[\text{Os}(\text{bpy})_3](\text{PF}_6)_2$  ( $50 \mu\text{M}$ ) in de-aerated acetonitrile was excited at 532 nm in the presence of DCA ( $500 \mu\text{M}$ ). Decay of transient signals of  $^3\text{DCA}$  were monitored at 440 nm in the absence (green) and in the presence of different concentrations of *trans*-stilbene (10, 20, 30 mM).

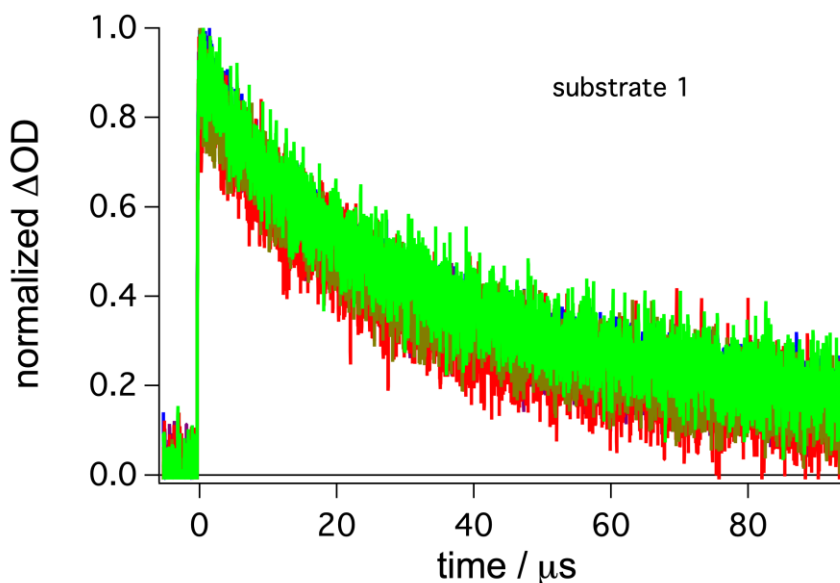


**Figure S37.** Triplet state decay of DCA in the presence of *cis*-stilbene (**1**).  $[\text{Os}(\text{bpy})_3](\text{PF}_6)_2$  ( $50 \mu\text{M}$ ) in de-aerated dichloromethane was excited at 532 nm in the presence of DCA ( $2 \text{ mM}$ ). Decay of transient signals of  $^3\text{DCA}$  were monitored at 730 nm in the absence (green) and in the presence of different concentrations of *cis*-stilbene (10, 20, 30, 40 mM).

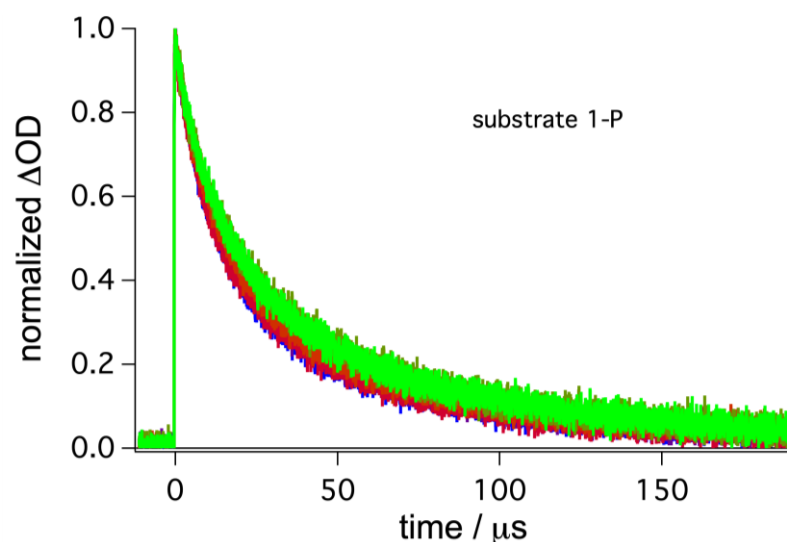


**Figure S38.** Triplet state decay of DCA in the presence of *trans*-stilbene (**1-P**).  $[\text{Os}(\text{bpy})_3](\text{PF}_6)_2$  ( $50 \mu\text{M}$ ) in de-aerated dichloromethane was excited at 532 nm in the presence of DCA (3 mM). Decay of transient signals of  $^3\text{DCA}$  were monitored at 810 nm in the absence (green) and in the presence of different concentrations of *trans*-stilbene (10, 20, 30, 50, 100 mM).

#### 4.4.2. Quenching of $[\text{Os}(\text{bpy})_3](\text{PF}_6)_2$ by stilbene

Further information concerning [step 1b](#) in Figure S32 is given here.

#### Reductive quenching of $^3[\text{Os}(\text{bpy})_3](\text{PF}_6)_2$ by *cis*- and *trans*-stilbene

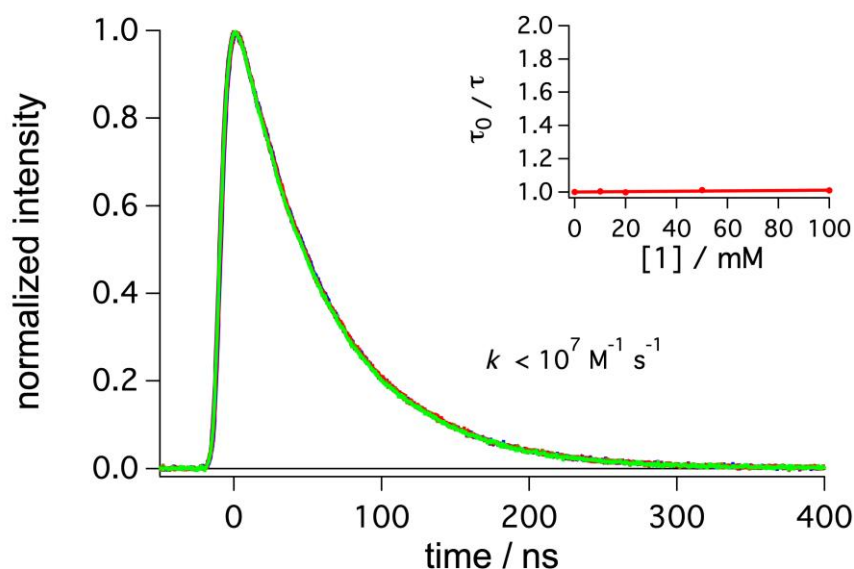


**Figure S39.** Triplet state decay of  $[\text{Os}(\text{bpy})_3](\text{PF}_6)_2$  in the presence of *cis*-stilbene (**1**).  $[\text{Os}(\text{bpy})_3](\text{PF}_6)_2$  ( $50 \mu\text{M}$ ) in de-aerated acetonitrile was excited at 532 nm. The emission decay was monitored at 700 nm in the absence (green) and in the presence of different concentrations of *cis*-stilbene (10, 20, 50 and 100 mM). The inset in the upper right corner contains the resulting Stern-Volmer plot and the calculated quenching rate constant.

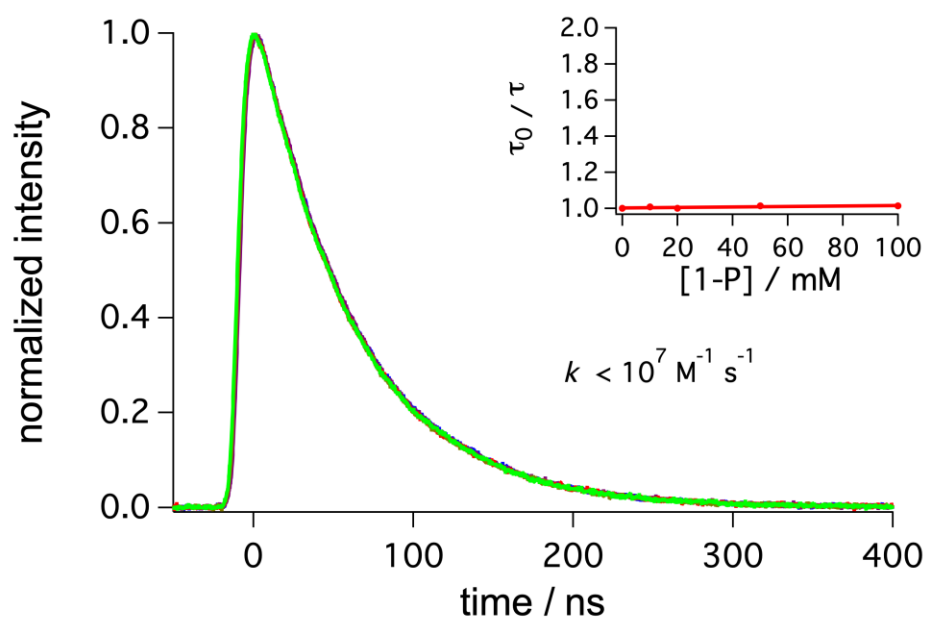


**Figure S40.** Triplet state decay of  $[\text{Os}(\text{bpy})_3](\text{PF}_6)_2$  in the presence of *trans*-stilbene (**1-P**).  $[\text{Os}(\text{bpy})_3](\text{PF}_6)_2$  (50  $\mu\text{M}$ ) in de-aerated acetonitrile was excited at 532 nm. The emission decay was monitored at 700 nm in the absence (green) and in the presence of different concentrations of *trans*-stilbene (10, 20, 50 and 100 mM). The inset in the upper right corner contains the resulting Stern-Volmer plot and the calculated quenching rate constant.

## 4.5. Mechanistic investigations of [2+2]-cycloaddition

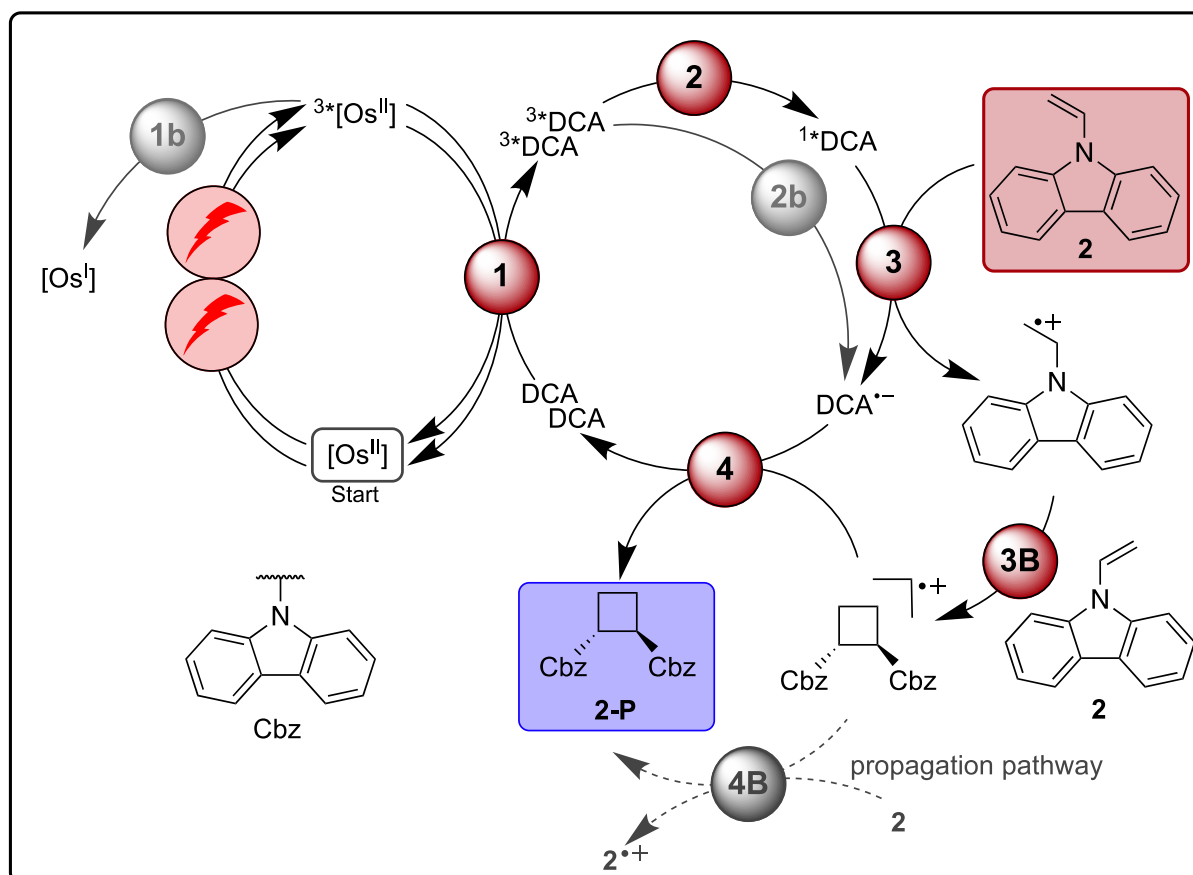


**Figure S41.** Possible mechanism for red light driven photoredox catalysis with  $[\text{Os}(\text{bpy})_3](\text{PF}_6)_2$  and DCA, as in Figure 4 of the main manuscript, but here including the additional side reaction steps 1b, 2b and 4B.

**Table S16.** Summary of relevant data for sTTA-UC in acetone for the [2+2]-cycloaddition of substrate **2**.<sup>a</sup>

step no.	description of step	$k_Q / \text{M}^{-1} \text{s}^{-1}$	Figure
		acetone	
1	TTET from $[\text{Os}(\text{bpy})_3]^{2+}$ to DCA	$4 \cdot 10^9$	Figure S18
1b	reductive quenching of $[\text{Os}(\text{bpy})_3]^{2+}$ by substrate <b>2</b>	$2.8 \cdot 10^7$	Figure S44
2	triplet-triplet annihilation between $^3\text{DCA}$	$6.4 \cdot 10^9$	Figure S21
2b	reductive quenching of $^1\text{DCA}$ by substrate <b>2</b>	N/A <sup>b</sup>	Figure S43
3	electron transfer from substrate <b>2</b> to $^1\text{DCA}$	$2.1 \cdot 10^{10}$	Figure S42
3B	trapping of radical intermediate by <b>2</b>	-	-
4	recovery of DCA by electron transfer from $\text{DCA}^{\bullet-}$	-	-
4B	propagation pathway	-	section 4.8.3

a) The determination of the rate constants for steps 1 and 2 is discussed in the main manuscript and in section 4.2. b) No Stern-Volmer analysis possible due to competing inherent first- and second order decay pathways.

#### 4.5.1. Quenching of DCA by vinylcarbazole (2)

##### Reductive quenching of $^1\text{DCA}$ by vinylcarbazole (2)

Further information concerning [step 3](#) in Figure S41 is given here.

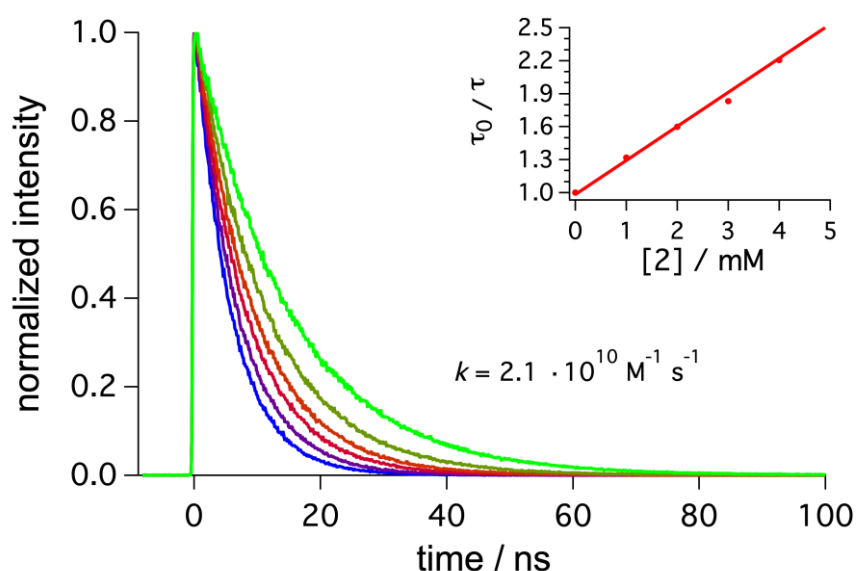


**Figure S42.** Singlet state quenching of DCA by substrate **2**. DCA (50  $\mu\text{M}$ ) in de-aerated acetone was excited at 405 nm. The emission decay was monitored at 435 nm in the absence (green) and in the presence of different concentrations of substrate **2** (5, 10, 15, 20 and 25 mM). The inset in the upper right corner contains the resulting Stern-Volmer plot and the calculated quenching rate constant.

##### Reductive quenching of $^3\text{DCA}$ by vinylcarbazole (2)

Further information concerning [step 2b](#) in Figure S41 is given here.

As discussed in more detail in section 4.4.1, for the quenching of  $^3\text{DCA}$  a Stern-Volmer analysis is not readily possible, but a qualitative analysis is realistic. Given the decay of  $^3\text{DCA}$  with a lifetime in the microsecond time range and the observation that this decay is essentially unchanged upon addition of vinylcarbazole **2**, reductive quenching of  $^3\text{DCA}$  is unlikely as alternative pathway to triplet-triplet annihilation upon conversion.

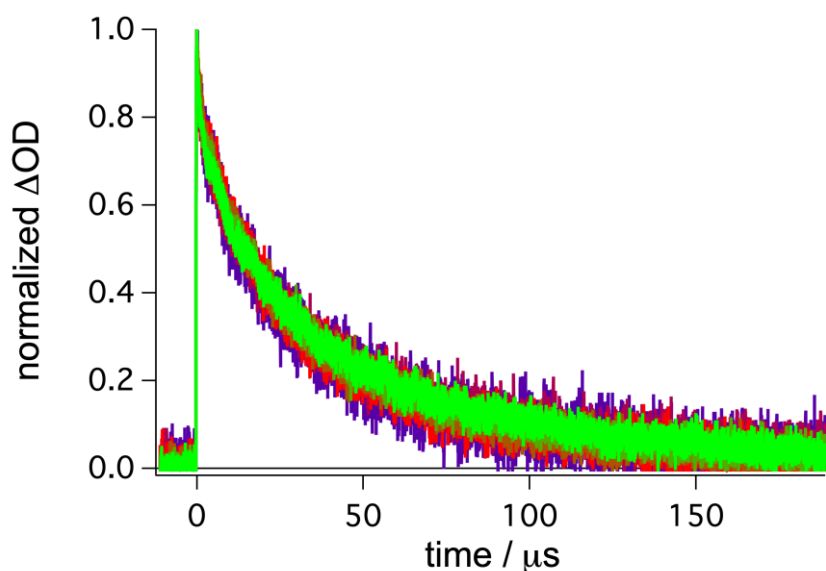


**Figure S43.** Triplet state decay of DCA in the presence of vinylcarbazole (**2**).  $[\text{Os}(\text{bpy})_3](\text{PF}_6)_2$  ( $50 \mu\text{M}$ ) in de-aerated acetone was excited at 532 nm in the presence of DCA ( $500 \mu\text{M}$ ). Decay of transient signals of  $^3\text{DCA}$  were monitored at 440 nm in the absence (green) and in the presence of different concentrations of vinylcarbazole **2** (25, 50, 75, 100, 150 mM).

#### 4.5.2. Quenching of $[\text{Os}(\text{bpy})_3](\text{PF}_6)_2$ by vinylcarbazole (**2**)

Further information concerning [step 1b](#) in Figure S41 is given here.

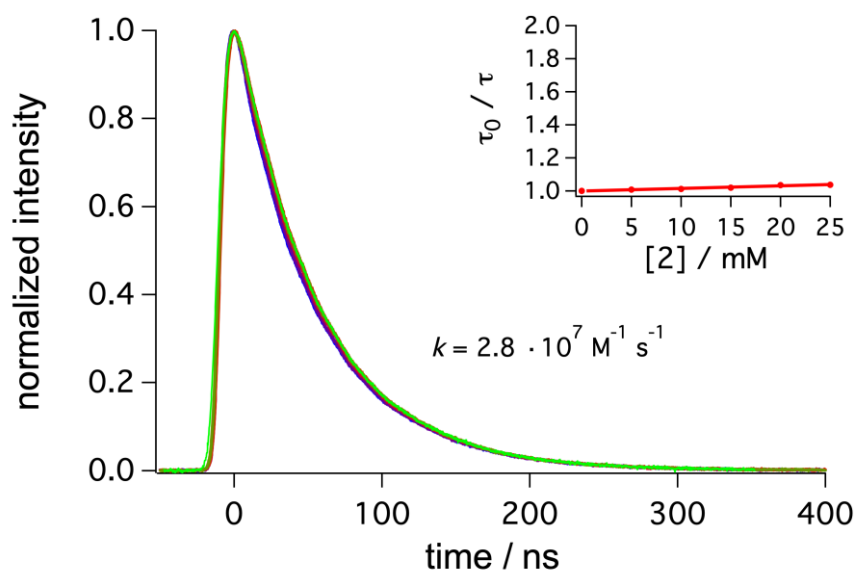


**Figure S44.** Triplet state decay of  $[\text{Os}(\text{bpy})_3](\text{PF}_6)_2$  in the presence of substrate **2**.  $[\text{Os}(\text{bpy})_3](\text{PF}_6)_2$  ( $50 \mu\text{M}$ ) in de-aerated acetone was excited at 532 nm. The emission decay was monitored at 720 nm in the absence (green) and in the presence of different concentrations of substrate **2** (5, 10, 15, 20 and 25 mM). The inset in the upper right corner contains the resulting Stern-Volmer plot and the calculated quenching rate constant.

## 4.6. Mechanistic investigations of Newman-Kwart rearrangement

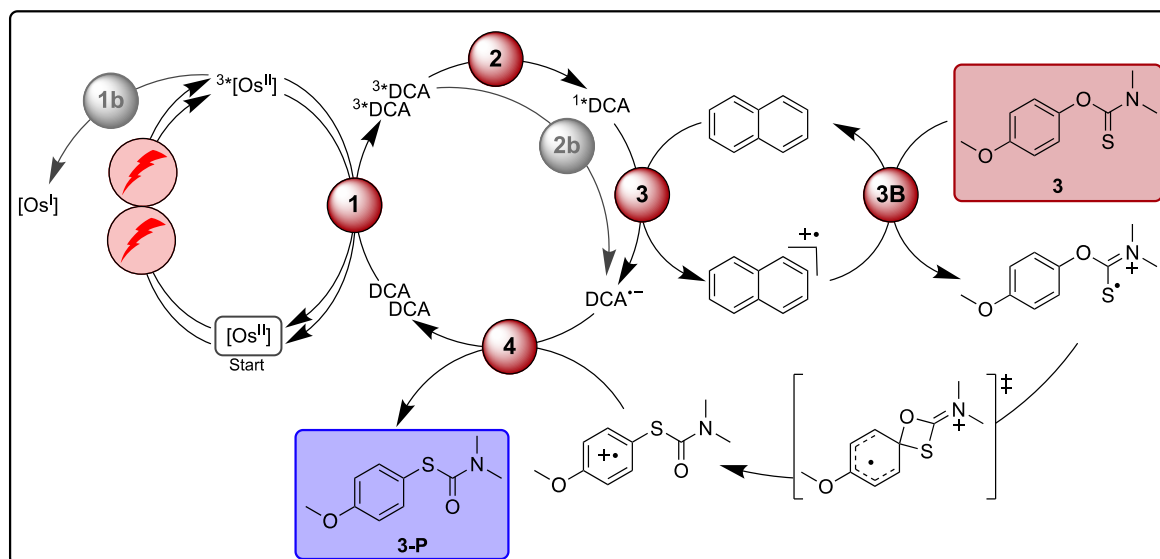


**Figure S45.** Possible mechanism for red light driven photoredox catalysis with  $[\text{Os}(\text{bpy})_3](\text{PF}_6)_2$  and DCA, as in Figure 5 of the main manuscript, but here including the additional side reaction steps 1b and 2b.

**Table S17.** Summary of relevant data for sTTA-UC in acetonitrile and dichloromethane for the Newman-Kwart rearrangement of substrate **3**.<sup>a</sup>

step no.	description of step	$k_Q / \text{M}^{-1} \cdot \text{s}^{-1}$		Figure
		MeCN	DCM	
1	TTET from $[\text{Os}(\text{bpy})_3]^{2+}$ to DCA	$4 \cdot 10^9$	$3 \cdot 10^9$	Figure S17 Figure S19
1b	reductive quenching of $[\text{Os}(\text{bpy})_3]^{2+}$ by substrate <b>3</b>	-	$4.5 \cdot 10^7$	Figure S52
1b	reductive quenching of $[\text{Os}(\text{bpy})_3]^{2+}$ by naphthalene	-	$< 10^7$	Figure S53
2	triplet-triplet annihilation between $^3\text{DCA}$	$6.9 \cdot 10^9$	$6.8 \cdot 10^9$	Figure S20 Figure S23
2b	reductive quenching of $^1\text{DCA}$ by substrate <b>3</b>	N/A <sup>b</sup>	N/A <sup>b</sup>	-
3	electron transfer from naphthalene to $^1\text{DCA}$	$1.5 \cdot 10^{10}$	$1.1 \cdot 10^{10}$	Figure S48 Figure S49
3b	electron transfer from substrate <b>3</b> to $^1\text{DCA}$	$1.5 \cdot 10^{10}$	$1.0 \cdot 10^{10}$	Figure S46 Figure S47
3b	electron transfer from biphenyl to $^1\text{DCA}$	$1.9 \cdot 10^9$	$< 10^8$	Figure S50 Figure S51
3B	electron transfer from naphthalene radical cation to substrate <b>3</b>	-	-	-
4	recovery of DCA by electron transfer from $\text{DCA}^{\bullet-}$	-	-	-

a) The determination of rate constants of steps 1 and 2 is discussed in the main manuscript and in section 4.2.

b) No Stern-Volmer analysis possible due to competing inherent first- and second order decay pathways.

#### 4.6.1. Quenching of DCA by substrate 3 or redox mediator

Further information concerning [step 3](#) in Figure S45 is given here.

##### Reductive quenching of $^1\text{DCA}$ by substrate 3

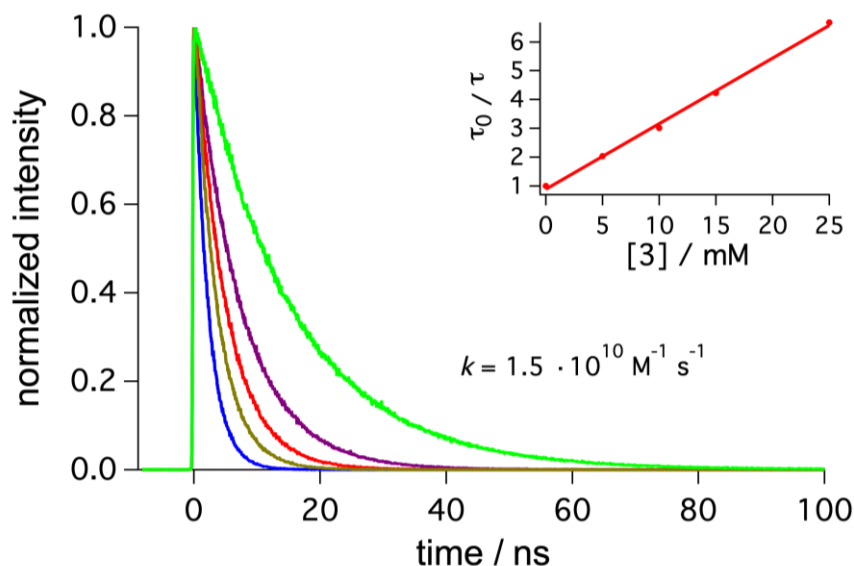


**Figure S46.** Singlet state quenching of DCA by substrate 3. DCA (50  $\mu\text{M}$ ) in de-aerated **acetonitrile** was excited at 405 nm. The emission decay was monitored at 435 nm in the absence (green) and in the presence of different concentrations of substrate 3 (5, 10, 15 and 25 mM). The inset in the upper right corner contains the resulting Stern-Volmer plot and the calculated quenching rate constant.

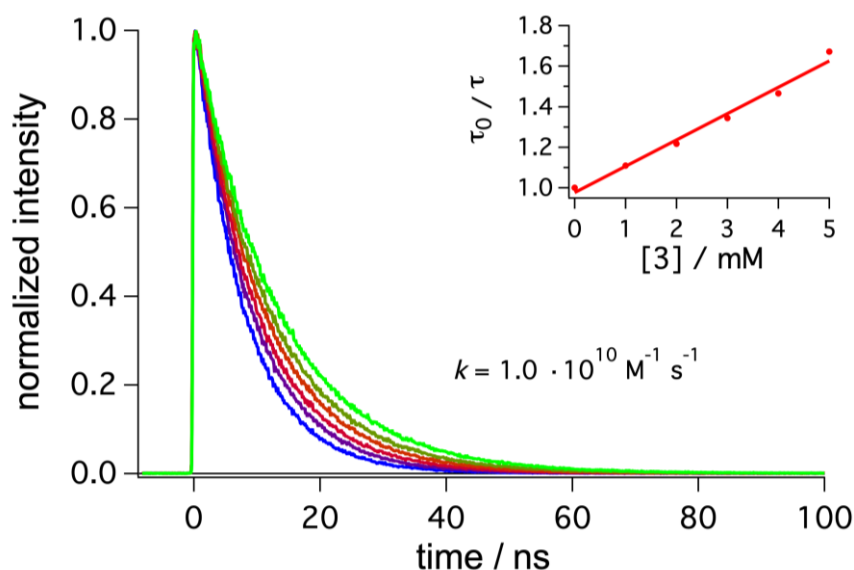


**Figure S47.** Singlet state quenching of DCA by substrate 3. DCA (50  $\mu\text{M}$ ) in de-aerated **dichloromethane** was excited at 405 nm. The emission decay was monitored at 435 nm in the absence (green) and in the presence of different concentrations of substrate 3 (1, 2, 3, 4 and 5 mM). The inset in the upper right corner contains the resulting Stern-Volmer plot and the calculated quenching rate constant.

### Reductive quenching of $^1\text{DCA}$ by redox mediator

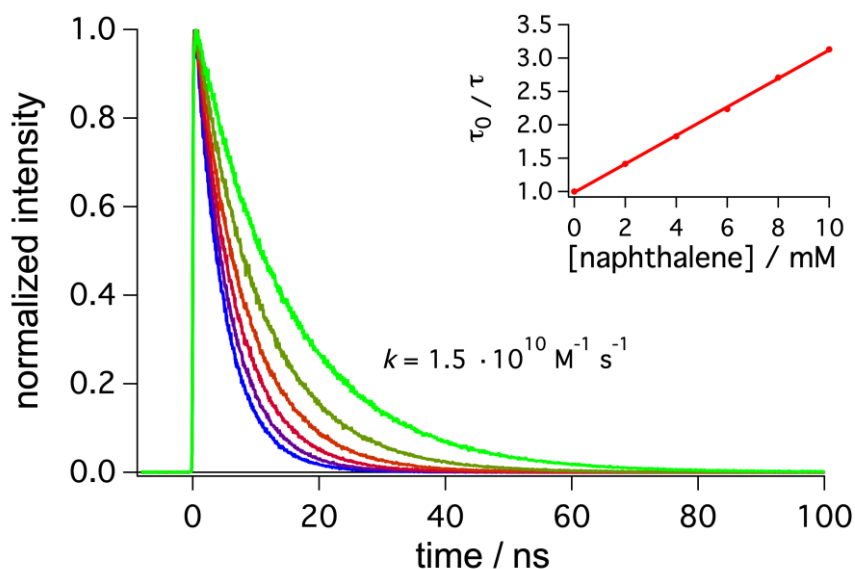


**Figure S48.** Singlet state quenching of DCA by naphthalene. DCA (15  $\mu\text{M}$ ) in de-aerated **acetonitrile** was excited at 405 nm. The emission decay was monitored at 435 nm in the absence (green) and in the presence of different concentrations of naphthalene (2, 4, 6, 8 and 10 mM). The inset in the upper right corner contains the resulting Stern-Volmer plot and the calculated quenching rate constant.

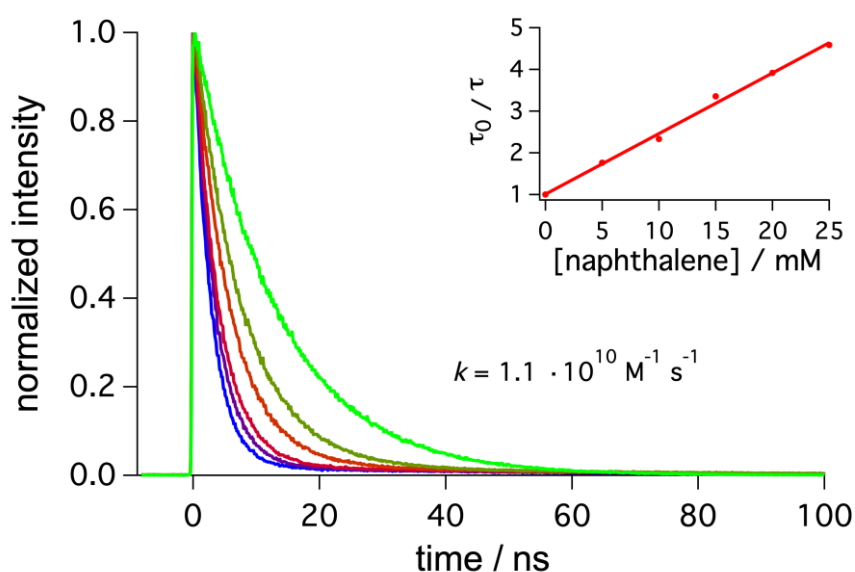


**Figure S49.** Singlet state quenching of DCA by naphthalene. DCA (50  $\mu\text{M}$ ) in de-aerated **dichloromethane** was excited at 405 nm. The emission decay was monitored at 435 nm in the absence (green) and in the presence of different concentrations of naphthalene (5, 10, 15, 20 and 25 mM). The inset in the upper right corner contains the resulting Stern-Volmer plot and the calculated quenching rate constant.

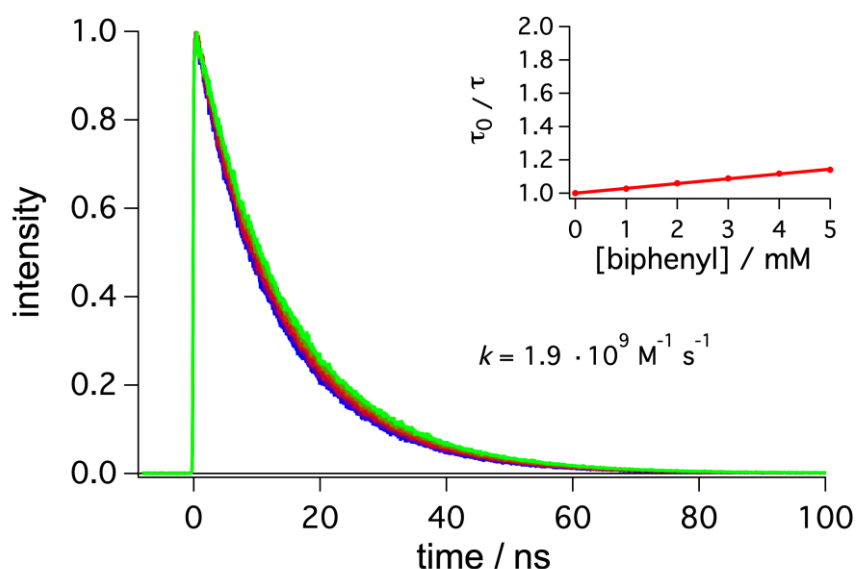


**Figure S50.** Singlet state quenching of DCA by biphenyl. DCA (50  $\mu\text{M}$ ) in de-aerated **acetonitrile** was excited at 405 nm. The emission decay was monitored at 435 nm in the absence (green) and in the presence of different concentrations of biphenyl (1, 2, 3, 4 and 5 mM). The inset in the upper right corner contains the resulting Stern-Volmer plot and the calculated quenching rate constant.

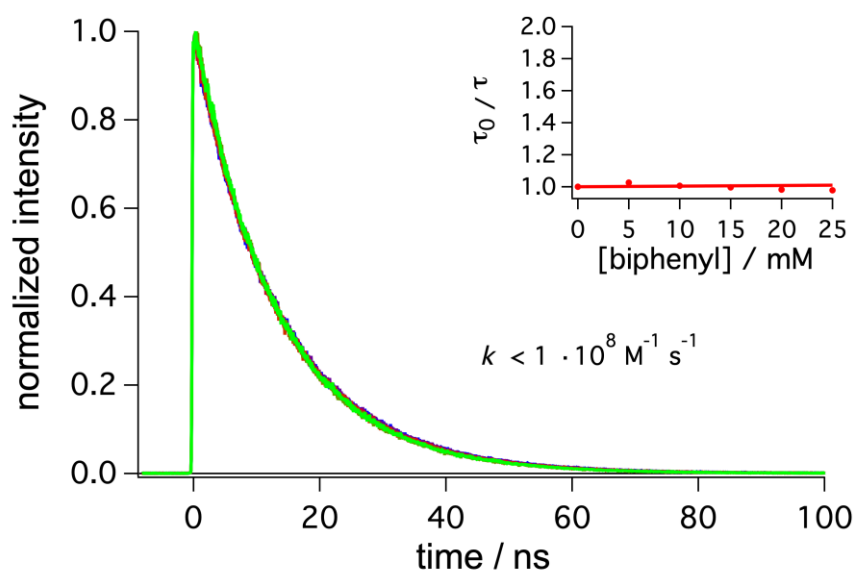


**Figure S51.** Singlet excited state decay of DCA in the presence of biphenyl. DCA (50  $\mu\text{M}$ ) in de-aerated **dichloromethane** was excited at 405 nm. The emission decay was monitored at 435 nm in the absence (green) and in the presence of different concentrations of biphenyl (5, 10, 15, 20 and 25 mM). The inset in the upper right corner contains the resulting Stern-Volmer plot and the calculated quenching rate constant.

#### 4.6.2. Quenching of $[\text{Os}(\text{bpy})_3](\text{PF}_6)_2$ by substrate **3** or redox mediator

Further information concerning [step 1b](#) in Figure S45 is given here.

##### Reductive quenching of $^3[\text{Os}(\text{bpy})_3]^{2+}$ by substrate **3**

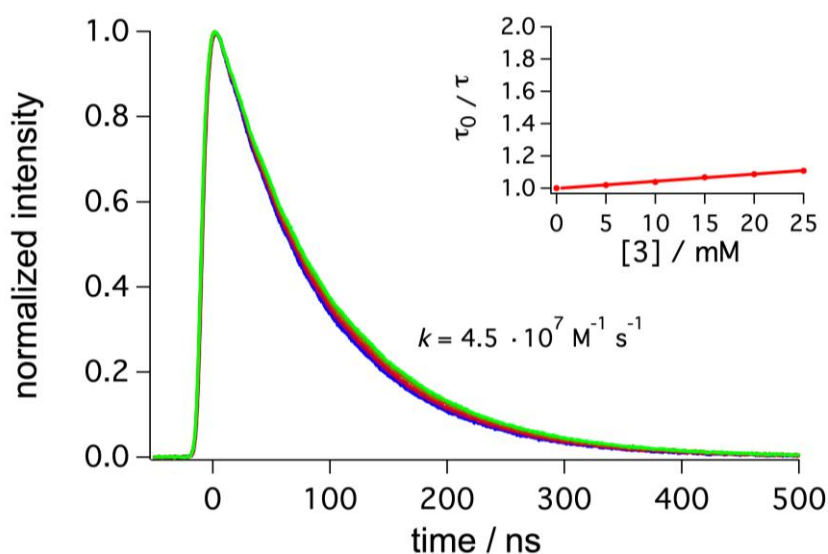


**Figure S52.** Triplet state quenching of  $[\text{Os}(\text{bpy})_3](\text{PF}_6)_2$  by substrate **3**.  $[\text{Os}(\text{bpy})_3](\text{PF}_6)_2$  ( $50 \mu\text{M}$ ) in de-aerated dichloromethane was excited at 532 nm. The emission decay was monitored at 700 nm in the absence (green) and in the presence of different concentrations of substrate **3** (5, 10, 15, 20 and 25 mM). The inset in the upper right corner contains the resulting Stern-Volmer plot and the calculated quenching rate constant.

##### Reductive quenching of $^3[\text{Os}(\text{bpy})_3]^{2+}$ by redox mediator

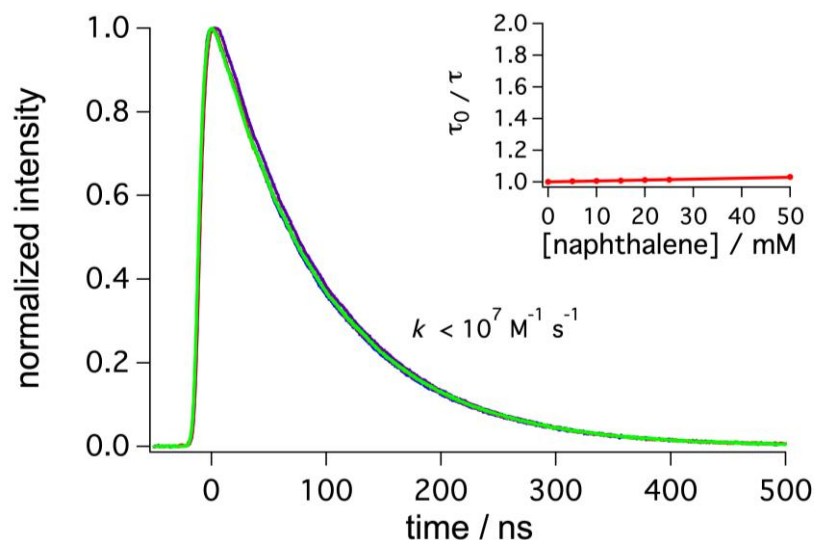


**Figure S53.** Triplet excited state decay of  $[\text{Os}(\text{bpy})_3](\text{PF}_6)_2$  in the presence of naphthalene.  $[\text{Os}(\text{bpy})_3](\text{PF}_6)_2$  ( $50 \mu\text{M}$ ) in de-aerated dichloromethane was excited at 532 nm. The emission decay was monitored at 700 nm in the absence (green) and in the presence of different concentrations of naphthalene (5, 10, 15, 20, 25 and 50 mM). The inset in the upper right corner contains the resulting Stern-Volmer plot and the calculated quenching rate constant.

## 4.7. Mechanistic investigations of ether-to-ester rearrangement

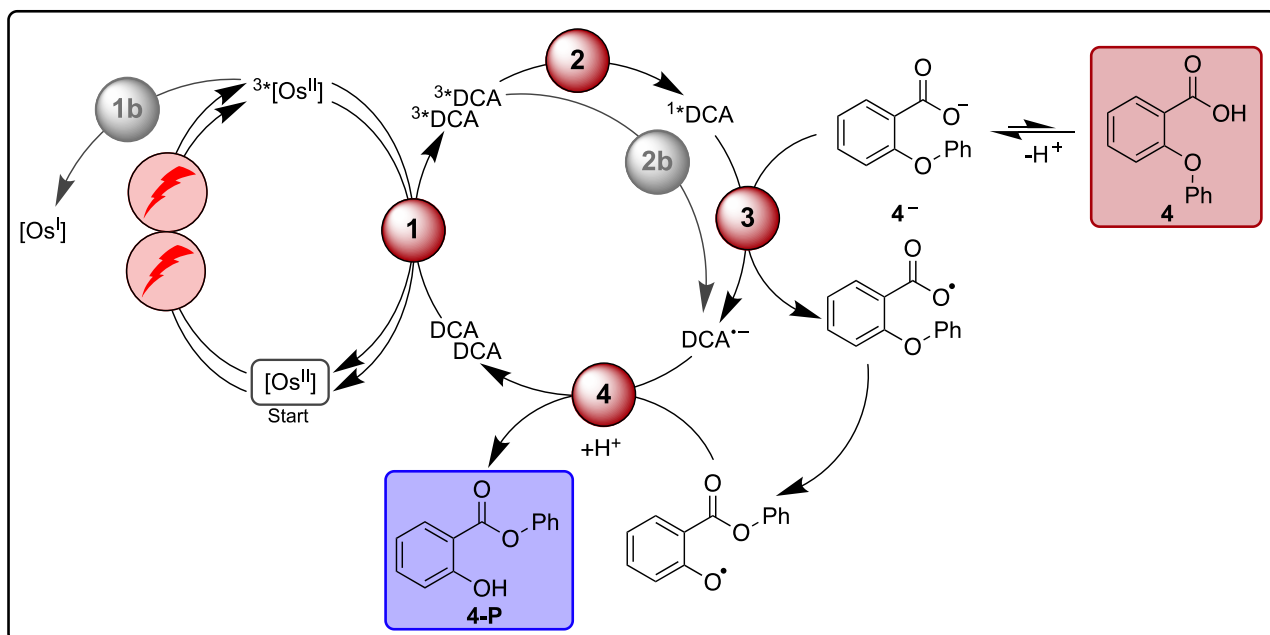


**Figure S54.** Possible mechanism for red light driven photoredox catalysis with  $[\text{Os}(\text{bpy})_3](\text{PF}_6)_2$  and DCA, as in Figure 6 of the main manuscript, but here including the additional side reaction steps 1b and 2b.

**Table S18.** Summary of relevant data for sTTA-UC in dichloromethane for the ether-to-ester rearrangement of substrate **4**.<sup>a</sup>

step no.	description of step	$k_Q / \text{M}^{-1} \cdot \text{s}^{-1}$ dichloromethane	Figure
1	TRET from $[\text{Os}(\text{bpy})_3]^{2+}$ to DCA	$3 \cdot 10^9$	Figure S19
1b	reductive quenching of $[\text{Os}(\text{bpy})_3]^{2+}$ by substrate <b>4</b> <sup>-</sup>	- <sup>b</sup>	Figure S59 Figure S58
1b	reductive quenching of $[\text{Os}(\text{bpy})_3]^{2+}$ by substrate <b>4</b>	$7.2 \cdot 10^6$	Figure S60
2	triplet-triplet annihilation between $^3\text{DCA}$	$6.8 \cdot 10^9$	Figure S23
2b	reductive quenching of $^1\text{DCA}$ by substrate <b>4</b> <sup>-</sup>	N/A <sup>c</sup>	-
2b	reductive quenching of $^1\text{DCA}$ by substrate <b>4</b>	N/A <sup>c</sup>	-
3	electron transfer from substrate <b>4</b> <sup>-</sup> to $^1\text{DCA}$	$5.0 \cdot 10^9$	Figure S53
3b	electron transfer from substrate <b>4</b> to $^1\text{DCA}$	$< 10^6$	Figure S56
3b	electron transfer from tMePy to $^1\text{DCA}$	$1.0 \cdot 10^8$	Figure S57
4	recovery of DCA by electron transfer from $\text{DCA}^{\bullet-}$	-	-

a) The determination of rate constants of steps 1 and 2 is discussed in the main manuscript and in section 4.2.

b) The anionic substrate and  $[\text{Os}(\text{bpy})_3]^{2+}$  result in concentration-independent quenching of the lifetime (possibly as a result of aggregation), therefore no Stern-Volmer analysis was made. c) No Stern-Volmer analysis possible due to competing inherent first- and second order decay pathways.

#### 4.7.1. Quenching of DCA by substrate 4 or 4<sup>-</sup>

Further information concerning [step 3](#) in Figure S54 is given here.

##### **Reductive quenching of <sup>1</sup>DCA by substrate 4, deprotonated substrate 4<sup>-</sup> or base**

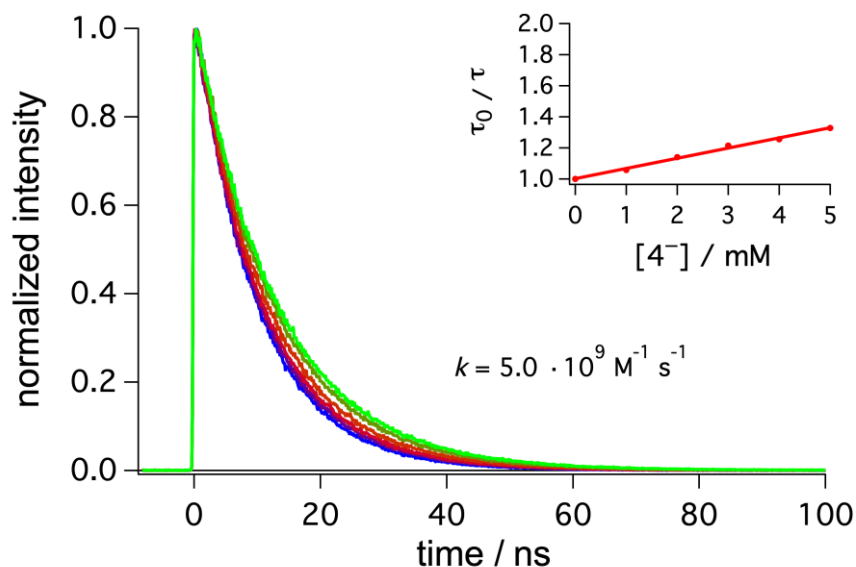


**Figure S55.** Singlet state quenching of DCA by substrate 4<sup>-</sup>. DCA (50  $\mu\text{M}$ ) in de-aerated dichloromethane was excited at 405 nm. The emission decay was monitored at 435 nm in the absence (green) and in the presence of different concentrations of substrate 4<sup>-</sup> (as TBA<sup>+</sup> salt, 1, 2, 3, 4 and 5 mM). The inset in the upper right corner contains the resulting Stern-Volmer plot and the calculated quenching rate constant.

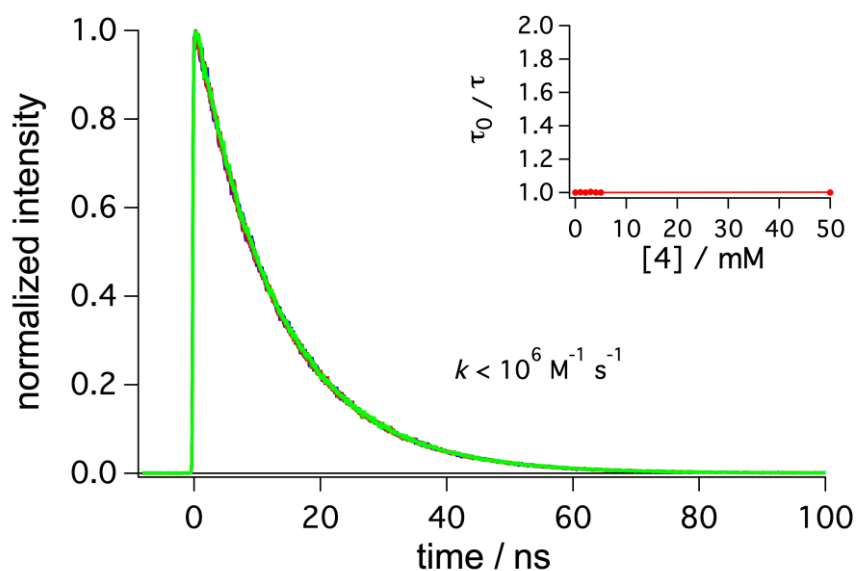


**Figure S56.** Singlet state decay of DCA in the presence of substrate 4. DCA (50  $\mu\text{M}$ ) in de-aerated dichloromethane was excited at 405 nm. The emission decay was monitored at 435 nm in the absence (green) and in the presence of different concentrations of substrate 4 (1, 2, 3, 4, 5 and 50 mM). The inset in the upper right corner contains the resulting Stern-Volmer plot and the calculated quenching rate constant.

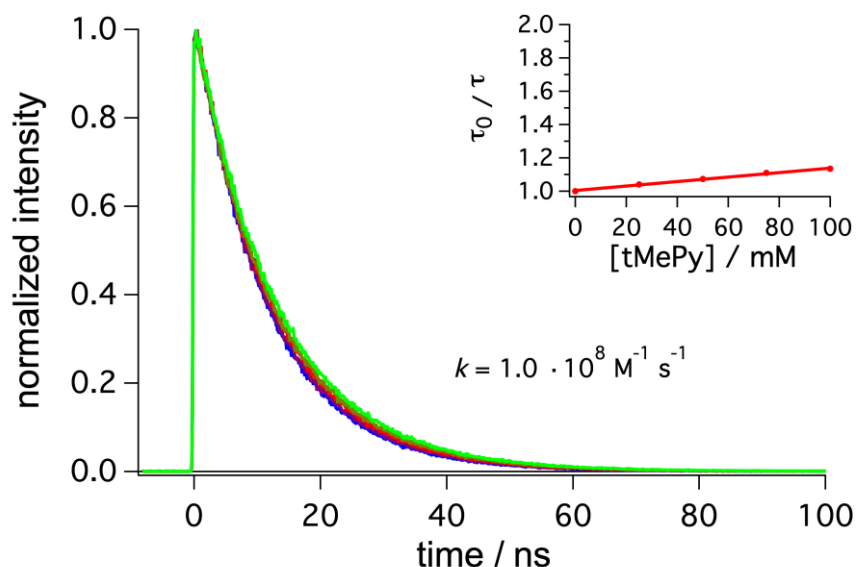


**Figure S57.** Singlet state quenching of DCA by tMePy. DCA (50  $\mu\text{M}$ ) in de-aerated dichloromethane was excited at 405 nm. The emission decay was monitored at 435 nm in the absence (green) and in the presence of different concentrations of tMePy (20, 40, 60, 80 and 100 mM). The inset in the upper right corner contains the resulting Stern-Volmer plot and the calculated quenching rate constant.

#### 4.7.2. Quenching of triplet-excited $[\text{Os}(\text{bpy})_3](\text{PF}_6)_2$ by substrate $4^-$ or $4^{\cdot-}$

Further information concerning [step 1b](#) in Figure S54 is given here.

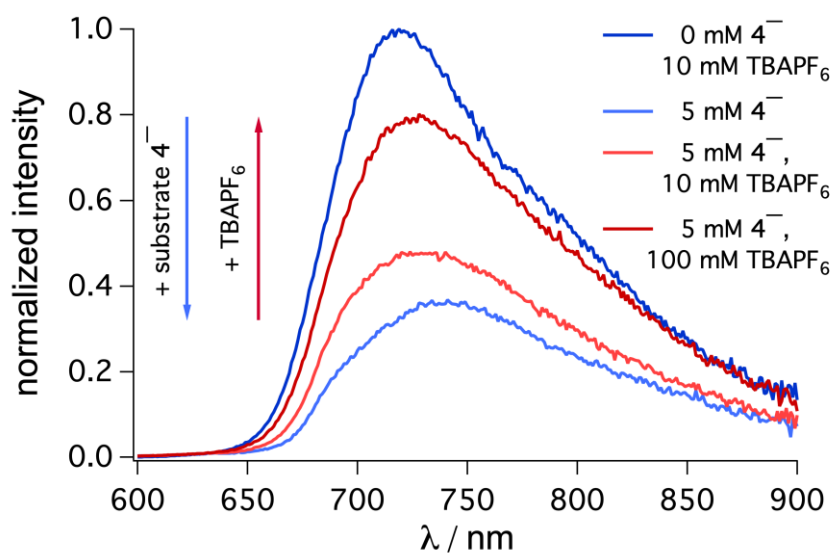


**Figure S58.** Triplet state quenching of  $[\text{Os}(\text{bpy})_3](\text{PF}_6)_2$  by substrate  $4^-$ .  $[\text{Os}(\text{bpy})_3](\text{PF}_6)_2$  (50  $\mu\text{M}$ ) in de-aerated dichloromethane was excited at 500 nm. The steady-state emission was monitored in the absence (dark blue) and in the presence of substrate  $4^-$  (5 mM, pale blue). Red traces illustrate the effect of adding TBAPF<sub>6</sub>.

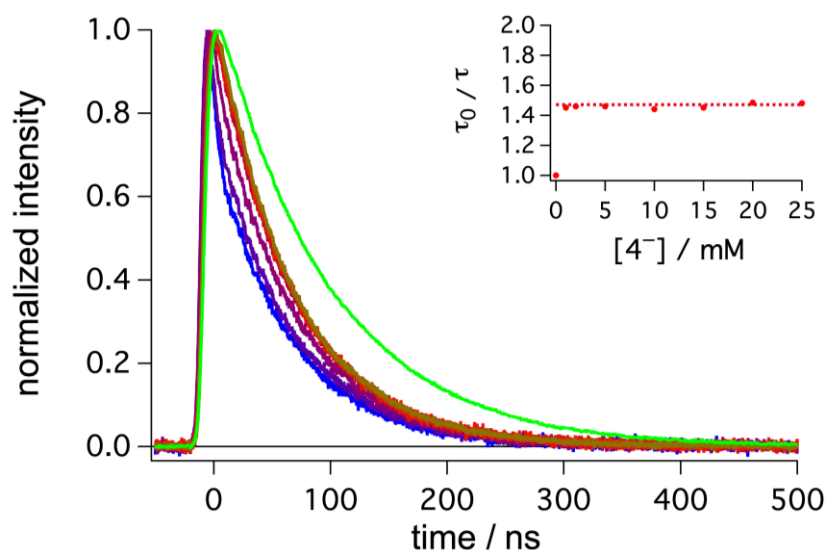


**Figure S59.** Triplet state decay of  $[\text{Os}(\text{bpy})_3](\text{PF}_6)_2$  in the presence of substrate  $4^-$ .  $[\text{Os}(\text{bpy})_3](\text{PF}_6)_2$  ( $50 \mu\text{M}$ ) in de-aerated dichloromethane was excited at 532 nm. The emission decay was monitored at 700 nm in the absence (green) and in the presence of different concentrations of substrate  $4^-$  (1, 2, 5, 10, 15, 20 and 25 mM). The inset in the upper right corner contains the resulting Stern-Volmer plot. No quenching constant was calculated, but the data suggest an essentially concentration-independent (static) quenching or a counter-ion induced change in the natural lifetime of  $[\text{Os}(\text{bpy})_3]^{2+}$ . At higher concentrations (above 10 mM) of substrate, a biexponential fit function was needed to account for a laser-limited (static) quenching contribution ( $\sim 6$  ns). These observations might due to aggregation in solution, in line with steady-state measurements in **Figure S58** and observations for other metal complexes.<sup>53–56</sup>

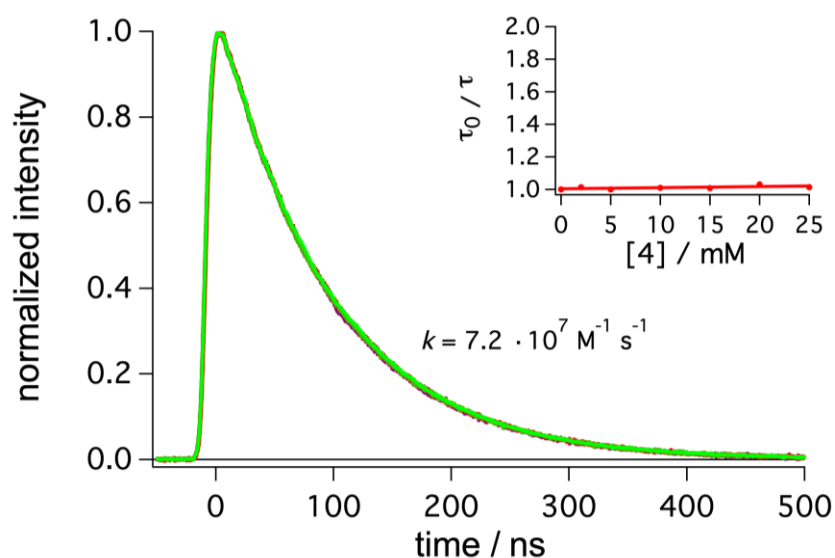


**Figure S60.** Triplet state decay of  $[\text{Os}(\text{bpy})_3](\text{PF}_6)_2$  in the presence of substrate **4**.  $[\text{Os}(\text{bpy})_3](\text{PF}_6)_2$  ( $50 \mu\text{M}$ ) in de-aerated dichloromethane was excited at 532 nm. The emission decay was monitored at 700 nm in the absence (green) and in the presence of different concentrations of substrate **4** (2, 5, 10, 15, 20 and 25 mM). The inset in the upper right corner contains the resulting Stern-Volmer plot and the calculated quenching rate constant.

## 4.8. Radical chain mechanism, salt effect and deactivation pathways

### 4.8.1. Exciplex formation

For excited state quenching of  $^1\text{DCA}$  several examples of (emissive) exciplexes have been reported in the literature.<sup>50,57–60</sup> The stabilisation of the excited state by exciplex formation and consequent emission at longer wavelengths represents a possible unproductive deactivation pathway that does not lead to the desired oxidative quenching of  $^1\text{DCA}$ . Typically excimer formation is more likely in apolar solvents, in which the radical ions formed upon electron transfer between individual excimer components are less well stabilized than in polar solvents.<sup>57,61,62</sup>

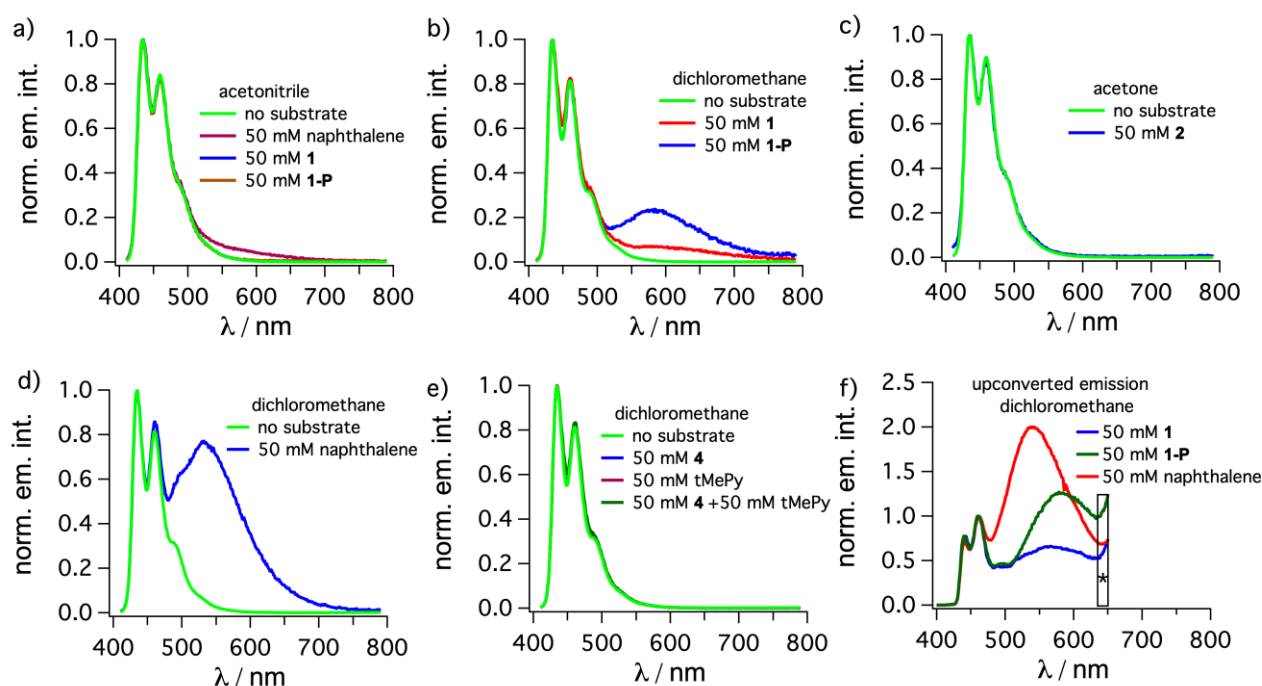


**Figure S61.** Normalized steady-state emission spectra of  $^1\text{DCA}$  in the absence and presence of different compounds. DCA (20  $\mu\text{M}$ ) was excited at 400 nm in the presence of (a) **1** (50 mM), **1-P** (50 mM) or naphthalene (50 mM) in acetonitrile, (b) **1** (50 mM) or **1-P** (50 mM) in dichloromethane, (c) **2** (50 mM) in acetone, (d) naphthalene (50 mM) in dichloromethane or **4** (50 mM), tMePy (50 mM) or **4** and tMePy (each 50 mM) in dichloromethane. The emission spectra without additives is given as green trace in all parts (a-e). Upconverted emission of  $[\text{Os}(\text{bpy})_3](\text{PF}_6)_2$  (20  $\mu\text{M}$ ) excited with a 705 nm cw laser in the presence of DCA (2 mM) and either **1**, **1-P** or naphthalene (50 mM in each case) was also detected in dichloromethane for all cases that showed clear excimer emission bands by direct excitation (see a-e). Towards 650 nm, the unquenched emission of  $^3[\text{Os}(\text{bpy})_3]^{2+}$  is marked with an asterisk. All emissions have been normalized to the highest emission peak of  $^1\text{DCA}$ .

Indeed, excitation of DCA at 400 nm in acetonitrile resulted in essentially identical emission spectra in the presence of substrate **1** and product **1-P** after normalization to the emission maximum (Figure S61a) while in

dichloromethane new excimer emission bands between 500 and 750 nm are visible (Figure S61b). In the case of substrate **2** in acetone and for substrate **4** (deprotonated by tMePy as well as for its protonated form) no excimer emission band was detected (Figure S61c and e). For naphthalene (which is the redox mediator for the conversion of substrate **3**) in dichloromethane a clear excimer emission band between 500 nm and 700 nm is detected.

Also under upconversion conditions, with [Os(bpy)<sub>3</sub>](PF<sub>6</sub>)<sub>2</sub> (20 μM) excited at 705 nm with a cw laser in the presence of DCA (2 mM) in dichloromethane and either **1** (50 mM), **1-P** (50 mM) or naphthalene (50 mM) added, excimer emission contributes to the emission spectra between 450 and 650 nm (Figure S61f).

These measurements indicate that for the isomerisation of *cis*-stilbene (**1**) exciplex formation (especially with the product *trans*-stilbene **1-P**) can lead to an alternative deactivation pathway. This is as well the case for the naphthalene-mediated Newman-Kwart rearrangement of substrate **3**. In line with these findings, a (weak) emission upon cw laser irradiation was visible over the complete time of irradiation in the photoredox catalysis experiments for these two reactions.

#### 4.8.2. Salt effect of TBAPF<sub>6</sub>

The presence of TBAPF<sub>6</sub> was found to be beneficial as additive for the light-driven reaction in dichloromethane. For the Newman-Kwart rearrangement of substrate **3** (Table S5,

Table S6) the addition of the salt was indispensable for productive reaction, while in its absence no reaction was observed at all. The ether-to-ester rearrangement of substrate **4** (Table S7, Table S8) was markedly faster in the presence of salt.

The lifetime of  $^1\text{DCA}$  is on the same time scale as the pulse duration of the excitation laser pulse ( $\sim 10$  ns) in our laser setup and the direct excited state decay of  $^1\text{DCA}$  cannot be detected with this setup, but long-lived intermediates resulting from quenching of  $^1\text{DCA}$  can be readily monitored. As a representative reaction partner, naphthalene was chosen as quencher, because this compound is known to give a comparatively high cage escape yield for electron-transfer photoproducts (at least in acetonitrile  $\sim 0.58$ ),<sup>63</sup> thereby possibly allowing the direct detection of new spectroscopic signals in transient UV-vis spectroscopy.

Interestingly, the spectroscopic signals detected 200 ns after the excitation of DCA (25  $\mu\text{M}$ ) in dichloromethane in the presence of 100 mM naphthalene significantly differ depending on the presence or absence of TBAPF<sub>6</sub> (Figure S62, middle). In the absence of the salt the spectroscopic features of  $^3\text{DCA}$  are clearly visible (with a new absorption band around 440 nm) while in the presence of TBAPF<sub>6</sub> the radical anion ( $\text{DCA}^{\bullet -}$ ) with absorption maxima around 640 nm and 705 nm is visible. Small spectroscopic differences between the reference and the measured spectra are attributed to solvents effects, as the reference spectra were recorded in acetonitrile. A similar analysis with other substrates (Table S19 under slightly modified conditions) revealed that in polar solvents such as acetonitrile (for **1** and **1-P**) and acetone (**2**) the radical anion is readily detectable, while in dichloromethane this is not the case for any of the substrates in the absence of TBAPF<sub>6</sub> as additive. Unfortunately, quantification is challenging, among other reasons due to more complex isomerisation of substrate **1** (involving different intermediates in more apolar solvents such as dichloromethane<sup>64,65</sup> compared to acetonitrile<sup>61</sup>). Interestingly, for *trans*-stilbene **1-P** (extinction coefficient of 69500  $\text{M}^{-1} \text{cm}^{-1}$  at 472 nm)<sup>66</sup> a weak signal of the radical cation or dimer radical cation intermediate can be detected in dichloromethane in the absence of salt. This observation implies that the resolution of our measurement is in this case not high enough to detect the radical anion of DCA (extinction coefficient of 8400  $\text{M}^{-1} \text{cm}^{-1}$  at 705 nm)<sup>67</sup>. This is in line with previous spectroscopic investigations in dichloromethane.<sup>17,65,68</sup> A comparison to the bleach of  $[\text{Ru}(\text{bpy})_3]^{2+}$  at 455 nm indicates that the cage escape yield of free ions is less than 10% in the absence of salt, based on the assumption that the spectroscopic features of  $\text{DCA}^{\bullet -}$  can be unambiguously identified for signal intensities above 5 m $\Delta\text{OD}$  (data summarized in Table S19, spectroscopic data not shown). Due to the unknown spectroscopic features of most of the investigated radical cations and possible alternative pathways (e.g. formation of  $^3\text{DCA}$ ) with additional overlapping signals, quantification for all substrates is not straightforward and below the scope of this investigation. Investigations of  $^1\text{DCA}$  quenching imply that the cage escape yields to form solvent-separated ions can differ significantly depending on the substrate.<sup>20,69</sup>

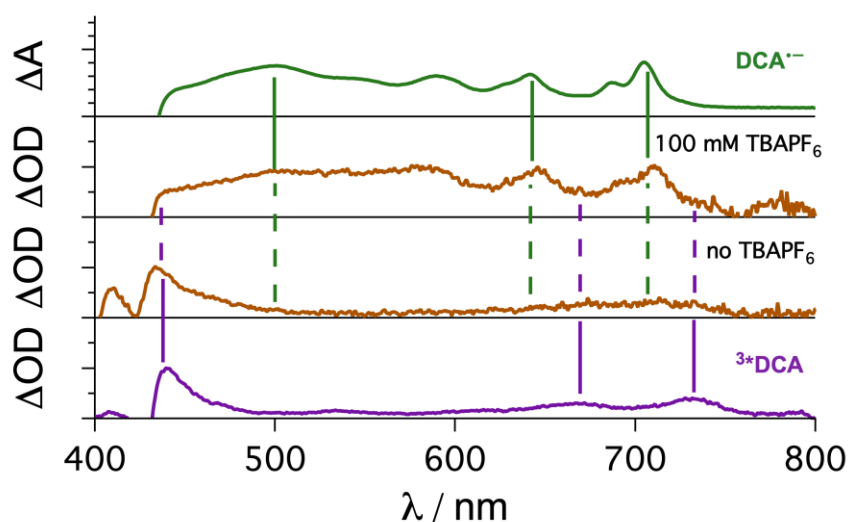


**Figure S62.** Spectral differences in transient absorption spectra included by addition of TBAPF<sub>6</sub>. DCA (25 μM) in de-aerated dichloromethane was excited at 435 nm in the presence of naphthalene (100 mM). Measurements occurred both in the presence as well as in the absence of 100 mM TBAPF<sub>6</sub> (middle panel) and the transient absorption spectra were recorded with a time delay of 200 ns after the laser pulses, time-integrated over 200 ns. The reference spectra of DCA<sup>•-</sup> (top) and <sup>3</sup>\*DCA (bottom) in acetonitrile are shown for comparison. Both reference spectra were reproduced from the literature.<sup>3</sup>

Overall, our measurements imply that there is a significant change in the reactivity for the excited state quenching step of <sup>1</sup>\*DCA in dichloromethane depending on the exact conditions and the additive. Investigations of different systems for the quenching of <sup>1</sup>\*DCA have previously shown that the addition of a salt can facilitate the dissociation of radical ion pairs to solvent separated ion pairs.<sup>70-72</sup> The formation of <sup>3</sup>\*DCA has been suggested in apolar solvents and can occur either via charge recombination pathway (from contact ion pairs),<sup>41,57,59,61,73</sup> or intersystem crossing (e.g. from exciplexes between DCA and quencher).<sup>50,59,74</sup> Therefore it seems reasonable to conclude that the addition of TBAPF<sub>6</sub> supports the charge separation to form solvent-separated ion pairs,<sup>17,68</sup> which is the first step towards substrate activation in the mechanisms proposed for our systems.

In principle also signals for the naphthalene radical cation should be detectable upon electron transfer to <sup>1</sup>\*DCA, in addition to the clearly detectable DCA<sup>•-</sup> in Figure S62. Unfortunately, the spectroscopic features of the naphthalene radical cation are broad and comparably weak, with a absorption band maximum around 580 nm and an extinction coefficient of ~5000 M<sup>-1</sup> cm<sup>-1</sup>.<sup>75</sup> Weak naphthalene radical cation absorption is presumably causing the slight spectroscopic differences between the reference spectra (Figure S62, top) of DCA<sup>•-</sup> and the spectra obtained by transient spectroscopy in the presence of TBAPF<sub>6</sub> (Figure S62, middle). Subsequent formation of new transient intermediates (e.g. dimer cation of naphthalenes)<sup>75</sup> complicate the identification of the bands caused by naphthalene-related species in this case.

**Table S19.** <sup>1</sup>DCA quenching and radical anion detection under different conditions.

quencher	solvent	Additive	DCA <sup>•-</sup> detectable? <sup>a</sup>	$\Phi_{\text{Ion}}$ <sup>b</sup>
<b>1</b>	acetonitrile	-	yes	0.13 <sup>66</sup>
<b>1</b>	dichloromethane	-	no	< 0.1
		TBAPF <sub>6</sub>	yes	-
<b>1-P</b>	acetonitrile	-	yes	0.21 <sup>66</sup>
<b>1P</b>	dichloromethane	-	no <sup>d</sup>	< 0.1
		TBAPF <sub>6</sub>	yes	-
<b>2</b>	acetone	-	yes	-
<b>3</b>	dichloromethane	-	no <sup>c</sup>	< 0.1
		TBAPF <sub>6</sub>	no <sup>c</sup>	< 0.1
		-	no <sup>c</sup>	< 0.1 <sup>e</sup>
<b>naphthalene</b>	dichloromethane	TBAPF <sub>6</sub>	yes	-
<b>4</b>	dichloromethane	TBAPF <sub>6</sub>	no	< 0.1
<b>4 + tMePy</b>	dichloromethane	-	no	< 0.1
		TBAPF <sub>6</sub>	no	< 0.1

a) The presence of DCA<sup>•-</sup> was determined based on transient absorption spectrum recorded 200 ns after the laser pulse (time integration 200 ns). Conditions: DCA (75  $\mu$ M), quencher (75 mM), additive (75 mM) in de-aerated solvent, excited at 437 nm. b) New values determined against [Ru(bpy)<sub>3</sub>]<sup>2+</sup>, further details are provided in the text. c) Formation of <sup>3</sup>DCA detected. d) *trans*-Stilbene radical cation detectable. e) In acetonitrile:  $\sim$ 0.58.<sup>20</sup>

#### 4.8.3. Photochemical quantum yield estimation and radical chain mechanism

The photochemical quantum yield can give insights into the mechanism of a light-driven reaction and provide insights about radical chain mechanisms.<sup>76</sup> Especially for oxidative substrate activation, radical chain mechanisms represent a viable reaction pathway and have to be considered.<sup>76,77</sup> For the isomerisation of *cis*- (**1**) to *trans*-stilbene (**1-P**) in acetonitrile, a radical chain mechanism has been reported earlier for high concentrations of substrate under conditions with low light intensities, while in apolar solvents such as benzene no propagation pathway was reported.<sup>9</sup> Furthermore, for the [2+2] cycloaddition reaction of vinylcarbazole (**2**) a radical chain propagation has been found earlier in a reaction sensitized by fluorenone in acetone under an Argon atmosphere ( $\phi_{\text{PC}} \sim 2.1$ ).<sup>78</sup>

The photochemical quantum yield  $\phi_{\text{PC}}$  is defined as the number of molecules formed divided by the number of photons absorbed (equation S7).

$$\phi_{PC} = \frac{\# \text{ product formed}}{\# \text{ photons absorbed}} = \frac{\text{amount of product}}{\text{photon flux} \cdot \text{time} \cdot \text{fraction of absorbed light}} = \frac{n}{PF \cdot t \cdot f} \quad (\text{S7})$$

$$PF = \frac{P}{E_{\lambda ex}} = P \cdot \frac{\lambda ex}{h \cdot c} \quad (\text{S8})$$

$$f = 1 - 10^{-A_{\lambda ex}} \quad (\text{S9})$$

The amount of product formed in the course of the light-driven reaction over a certain irradiation time is calculated using the known concentration of starting material and the reaction volume to obtain the overall amount of substance in solution. The amount of product (n) is then determined by quantitative NMR measurements against dioxane as internal standard. For quantum yields above 1, a propagation pathway is occurring, while for quantum yields (significantly) below 1 a radical chain mechanism is less likely.

The number of photons absorbed can be calculated from the known photon flux (PF, as photons per time) multiplied with the irradiation time. In our case, a cw laser setup was used and the laser power (P, in W or J/s) determined with a laser power meter was directly used together with the energy of the laser at the excitation wavelength ( $E_{\lambda ex}$ ) to calculate the photon flux per second (PF, equation S8). In combination with the time of irradiation (t), the number of photons emitted by the cw laser can be calculated. Multiplication with the fraction of absorbed light (f, equation S9), which is determined from the absorbance A at the excitation wavelength, measured by UV-vis absorption of diluted solutions, results in the number of photons absorbed by the photocatalyst.

### **Photochemical quantum yield for *cis-trans* isomerisation**

The results for the photochemical quantum yield determination by direct excitation with a blue cw laser for the isomerisation of *cis*- (**1**) to *trans*-stilbene (**1-P**) are summarized in Table S20 for different solvents. The data for the light-driven reaction with red light in the presence of sensitizer are given in Table S21.

Our determined photochemical quantum yields (Table S20) for a solution of 0.1 M *cis*-stilbene in acetonitrile with blue light irradiation are about one third of the reported literature value ( $\phi_{PC} \sim 0.32$  at a concentration of 0.05 M *cis*-stilbene).<sup>9</sup> This result implies that at this concentration no propagation pathway is present, while at higher concentrations of 0.3 M of stilbene a photochemical quantum yield of 2.7 was measured previously. In general a correlation between high concentration and high photochemical quantum yields (including a radical chain mechanism) have been proposed and one would therefore in principle expect a higher quantum yield for the case of 0.1 M **1** in comparison to the measurement at 0.05 M.<sup>9</sup> Furthermore, the light intensity has been suggested to have an influence on the photochemical quantum yield, and at higher light intensities lower quantum yields were determined for DCA,<sup>9</sup> as well as for other systems in which a radical chain mechanism was operative.<sup>79</sup> The main differences between our measurements and those reported in literature is probably the collimated and significantly more intense light source used in our investigation. Therefore, the photochemical quantum yield was also calculated for the reaction with red light irradiation in the presence of  $[\text{Os}(\text{bpy})_3]^{2+}$ . Unsurprisingly, the overall quantum yield ( $\sim 0.015$ ) was lower than the value determined by direct excitation with blue light ( $\sim 0.03$ ), but a similar value as for the triplet-

triplet annihilation upconversion quantum yield ( $\sim 0.0148$  in dichloromethane, see section 4.3.2) is obtained. This would suggest that each  $^1\text{DCA}$  populated results in a successful substrate turnover and subsequent product formation. The findings that the charge separation quantum yield after excited-state quenching of  $^1\text{DCA}$  is below unity (particularly in the absence of TBAPF<sub>6</sub>, section 4.8.2) and that *trans*-stilbene **1-P** is also capable to quench the excited state (offering an alternative unproductive pathway with respect to product formation) are remarkable. Even though the conditions used for spectroscopic measurements and the light-driven reactions might not be perfectly comparable, these findings indicate that the hypothesis that every  $^1\text{DCA}$  formed under upconversion conditions indeed leads to productive substrate turnover is not very plausible. Therefore, contributions to the product formation through a radical chain mechanism seems more likely as explanation for the similar upconversion quantum yield and photochemical *cis-trans* isomerisation quantum yield with red light.

**Table S20.** Summary of relevant data for the determination of the photochemical quantum yield for light-driven isomerisation of **1** with 405 nm cw laser irradiation.

solvent	$A_{405\text{nm}}^{\text{a}}$	f	P / mW	PF / $\mu\text{mol}\cdot\text{s}^{-1}$	t / s	absorbed photons / $\mu\text{mol}$	product / $\mu\text{mol}$	$\phi_{\text{PC}}$
MeCN	0.62	0.76	453	1.53	90	$\sim 105$	$\sim 14$	$\sim 0.13$
					180	$\sim 210$	$\sim 23$	$\sim 0.11$
DCM	$>3$	$\sim 1$	452	1.53	180	$\sim 275$	$\sim 8$	$\sim 0.03$
					360	$\sim 550$	$\sim 14$	$\sim 0.03$

Conditions: *cis*-stilbene (**1**, 100 mM), DCA (5 mol%), 405 nm cw laser irradiation. a) Absorbance in the NMR tube estimated based on the measured absorbance from diluted solutions taking the dilution factor and the smaller path length in the NMR tube into account.

**Table S21.** Summary of relevant data for the determination of the photochemical quantum yield for light-driven isomerisation of **1** in the presence of osmium sensitizer with 635 nm cw laser irradiation.

$[\text{Os}(\text{bpy})_3]^{2+}$	$A_{635\text{nm}}$	f	P / mW	PF / $\mu\text{mol}\cdot\text{s}^{-1}$	t / s	absorbed photons / $\mu\text{mol}$	product / $\mu\text{mol}$	$\phi_{\text{PC}}^{\text{a}}$
1 mol%	1.28	0.95	400	2.12	900	$\sim 1800$	$\sim 14$	$\sim 0.015$
					1800	$\sim 3600$	$\sim 23$	$\sim 0.013$
0.1 mol%	0.128	0.255	400	2.12	900	$\sim 490$	$\sim 4$	$\sim 0.017$
					1800	$\sim 980$	$\sim 9$	$\sim 0.019$

Conditions: *cis*-stilbene (**1**, 100 mM),  $[\text{Os}(\text{bpy})_3](\text{PF}_6)_2$ , DCA (5 mol%), 635 nm cw laser irradiation in dichloromethane-*d*<sub>2</sub> (0.6 mL). a) Calculated quantum yield multiplied with a factor of two to account for the need of two photons per catalytic turnover.

### Photochemical quantum yield for [2+2]-cycloaddition

The results for the photochemical quantum yield determination by direct excitation for the cycloaddition of substrate **2** are summarized in Table S22. In this case a 447 nm cw laser instead of the 405 nm cw laser was used to account for the background reactivity observed without 425 nm long-pass filter (see Table S3). The data for the red light-driven reaction in the presence of osmium sensitizer are given in Table S23.

A similar analysis as in the previous subsection for the *cis-trans* isomerisation is also possible in this case; the photochemical quantum yield ( $\sim 0.18$ ) determined by direct blue light excitation is below unity and deviates substantially from the literature value of 2.1.<sup>78</sup> A comparison of  $\phi_{PC}$  under conditions with red light irradiation (Table S23) results again in a smaller absolute quantum yield of  $\sim 0.0017$ . As in the previous example discussed above, this is on the same order of magnitude as the upconversion quantum yield in acetone ( $\sim 0.0013$ ). Therefore, with the same arguments discussed above are applicable, and contributions from a radical chain mechanism seem plausible for this reaction under red light irradiation despite the low apparent photochemical quantum yield.

**Table S22.** Summary of relevant data for the determination of the photochemical quantum yield for light-driven isomerisation of **2** with 447 nm cw laser irradiation.

$A_{447\text{nm}}^a$	f	P / mW	PF / $\mu\text{mol}\cdot\text{s}^{-1}$	t / s	absorbed photons / $\mu\text{mol}$	product / $\mu\text{mol}^b$	$\phi_{PC}$
0.30	0.5	501	1.87	90	$\sim 84$	$\sim 15$	$\sim 0.18$
				180	$\sim 168$	$\sim 24$	$\sim 0.14$

Conditions: substrate **2** (200 mM), DCA (2.5 mol%), 447 nm cw laser irradiation in acetone- $d_6$  (0.6 mL). a) Absorbance in the NMR tube estimated based on the measured absorbance from diluted solutions taking the dilution factor and the shorter path length in the NMR tube into account. b) Concentration divided by 2 to account for the need of one photon and two molecules of substrate to form one equivalent of product.

**Table S23.** Summary of relevant data for the determination of the photochemical quantum yield for light-driven isomerisation of **2** in the presence of sensitizer with 635 nm cw laser irradiation.

$A_{635\text{nm}}$	f	P / mW	PF / $\mu\text{mol}\cdot\text{s}^{-1}$	t / s	absorbed photons / $\mu\text{mol}$	product / $\mu\text{mol}$	$\phi_{PC}^a$
1.28	0.95	400	2.121	3600	$\sim 7230$	$\sim 6$	$\sim 0.0017$
				7200	$\sim 14460$	$\sim 10$	$\sim 0.0014$

Conditions: substrate **2** (200 mM),  $[\text{Os}(\text{bpy})_3](\text{PF}_6)_2$  (0.5 mol%), DCA (2.5 mol%), 635 nm cw laser irradiation. a) Calculated quantum yield multiplied by a factor of two to account for the need of two photons per catalytic turnover.

#### 4.8.4. Deactivation *via* electron transfer cascade pathway

For the isomerisation of substrate **1** and the dimerization of substrate **2** contributions from a radical chain mechanism are plausible (see section 4.8.3). The slow reaction progress for the rearrangements of substrate **3** and **4**, requiring irradiation times of several days under red light irradiation, seemed curious in comparison to the reasonably fast conversions observed for the same reactions under blue light irradiation (section 2.3.3 and 2.3.4). Salt effects or low cage escape yields might explain to some extent the need for long reaction times, but these two effects should be comparable under red and blue light irradiation. Recently, we were able to obtain mechanistic insights into the elementary steps after triplet-triplet annihilation upconversion using time-resolved laser spectroscopy,<sup>10</sup> and this might also provide useful insights in the present cases here, although the lower upconversion quantum yields and the lower cage escape yields in the present system might complicate the detection of transient intermediates.

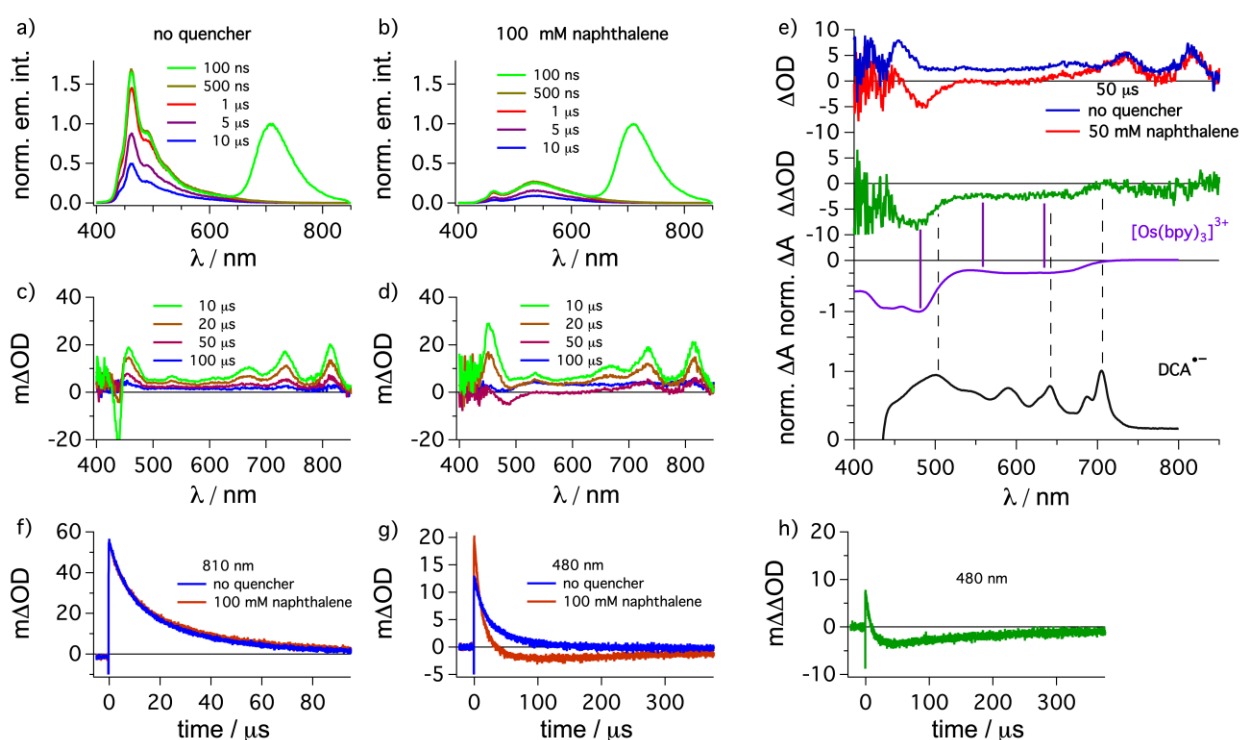


**Figure S63.** Time-resolved spectroscopy for upconversion system with and without naphthalene (called “quencher”) present.  $[\text{Os}(\text{bpy})_3](\text{PF}_6)_2$  (50  $\mu\text{M}$ ) in dichloromethane was excited at 532 nm in the presence DCA (5 mM) and  $\text{TBAPF}_6$  (100 mM) and the emission spectra (a) and transient absorption spectra (c) were recorded with different time delays after the laser pulse (as indicated in the figure, all time-integrated over 200 ns). Measurements under identical conditions in the presence of naphthalene (100 mM) are presented in (b) and (d). A comparison of the transient absorption spectra with a time-delay of 50  $\mu\text{s}$  after the laser pulse in the presence (red) and absence (blue) of naphthalene as well as the subtraction of these two waves (green) together with the spectroelectrochemically generated  $[\text{Os}(\text{bpy})_3]^{3+}$  (purple) and electrochemically generated  $\text{DCA}^{\bullet-}$  (black) is given in (e). In the lowest panels, the kinetic traces at 810 nm (f) and 480 nm (g) for the solutions described above in the presence (red) and absence (blue) of naphthalene are displayed together

with the difference-of-difference trace for the signal over time at 480 nm (h). A mathematical smoothing function was applied to enhance the quality of the data presented in (f) and (g).

As a representative model system, we investigated the DCA excited state quenching by naphthalene under triplet-triplet annihilation upconversion conditions. Investigation of the effect of the presence of naphthalene on our upconversion system consisting of  $[\text{Os}(\text{bpy})_3](\text{PF}_6)_2$  (50  $\mu\text{M}$ ), DCA (5 mM) and TBAPF<sub>6</sub> (100 mM) in dichloromethane was measured under pulsed 532 nm laser excitation (Figure S63). As expected, a delayed emission of  $^1\text{DCA}$  was observed in the absence of naphthalene (Figure S63a) while in the presence of naphthalene (100 mM) most of the upconverted emission of  $^1\text{DCA}$  was completely quenched and mainly the (weaker) excimer emission was detected between 450 and 650 nm (Figure S63b). At short delay times of 100 ns unquenched prompt emission of  $^3[\text{Os}(\text{bpy})_3]^{2+}$  is still detected in the presence and absence of naphthalene (see a and b). The transient absorption spectra recorded with different time delays after the laser pulse clearly show very dominant spectral features of  $^3\text{DCA}$  with maxima around  $\sim 440\text{-}450$  nm, 735 nm and 810 nm, irrespective of whether naphthalene is added or not (Figure S63c and d). As expectable for an additional elementary step following triplet-triplet annihilation upconversion, some differences become observable with longer delay times after the laser pulse, but the most prominent difference is a negative band with a maximum around 480 nm (Figure S63d, brown trace with a time-delay of 50  $\mu\text{s}$ ) that is not detected in the absence of naphthalene. In principle, spectroscopic features of  $\text{DCA}^{\bullet-}$  and oxidized naphthalene radical cation would be expected as positive new signals, while a negative signal indicates a ground state bleach or an (intense) emission band in that spectral range. Emission might in principle serve as an explanation here (with signals between 400 nm and 600 nm) and is indeed detectable in the absence of naphthalene (negative signal around 440 nm in Figure S63c). However, the emission intensity is rather low in the presence of naphthalene (this can be rationalized by the fact that almost all emission is quenched by naphthalene, as concluded above). An alternative explanation for the observable negative signal would be a ground state bleach, and indeed, the difference-of-difference spectrum obtained with a time delay of 50  $\mu\text{s}$  resembles very well the shape obtained for the Os(III) complex (obtained by electrochemical oxidation, purple trace in Figure S63e). Furthermore, the comparison of the kinetic traces at 810 nm (Figure S63f), where only contributions from  $^3\text{DCA}$  are present, and at 480 nm (Figure S63g), where  $^3\text{DCA}$  and  $[\text{Os}(\text{bpy})_3]^{3+}$  contribute to the overall signal, clearly shows that naphthalene addition makes a difference only at the latter wavelength. The subtraction of both traces at 480 nm (Figure S63h) indicates that  $[\text{Os}(\text{bpy})_3]^{3+}$  is present over several hundred microseconds. The more positive signal at 480 nm over the first  $\sim 10$   $\mu\text{s}$  after the laser pulse in the difference-of-difference trace is attributed to a decreased signal intensity in the absence of naphthalene, caused by the more intense upconverted emission contributing to the overall signal in comparison to the trace in the presence of naphthalene where the upconverted emission is quenched. The absence of any band corresponding to the naphthalene radical cation and the formation of  $[\text{Os}(\text{bpy})_3]^{3+}$  within the first 50  $\mu\text{s}$  after the laser pulse clearly indicates that an electron transfer cascade to yield  $[\text{Os}(\text{bpy})_3]^{3+}$  is a fast but unwanted deactivation pathway. Overall, the insights gained within this

spectroscopic investigation of the full triplet-triplet annihilation upconversion system in the presence of naphthalene point out that measurements of the system as a whole can provide a better understanding of (desired and undesired) reactions than separate measurements of the individual steps.

While the bleach in Figure S63e can be unambiguously attributed to  $[\text{Os}(\text{bpy})_3]^{3+}$  (as discussed above), the signal intensity of  $\text{DCA}^{\bullet-}$  is weak. A possible reason for this might be the overall low signal intensity and better spectral resolution around 500 nm in comparison to 700 nm, rendering the detection of the radical anion more difficult. Analogous investigations in acetonitrile or acetone (in which the upconversion quantum yields are much lower) have not been performed.

#### 4.8.5. Catalyst stability under long-term irradiation

For some of the reactions investigated herein, very long irradiation times are required (14 days for substrate **3**, 140 hours for substrate **4**). Consequently, the stability of the catalytic system comprised of  $[\text{Os}(\text{bpy})_3](\text{PF}_6)_2$  and DCA was probed by  $^1\text{H-NMR}$  spectroscopy following long-term irradiation (Figure S64).

Due to the low concentration of  $[\text{Os}(\text{bpy})_3](\text{PF}_6)_2$  (1 mol%), its proton resonances are weak compared to those of the other reaction components, yet the data in Figure S64 clearly shows that substantial portions of both  $[\text{Os}(\text{bpy})_3]^{2+}$  (green boxes in **Figure S64**) and the DCA annihilator remain intact (blue box in **Figure S64**), although some degradation of DCA seems to have occurred. Overall, this analysis indicates that our catalyst combination is largely stable over up to 14 days and sTTA-UC seems plausible even under long-term irradiation.

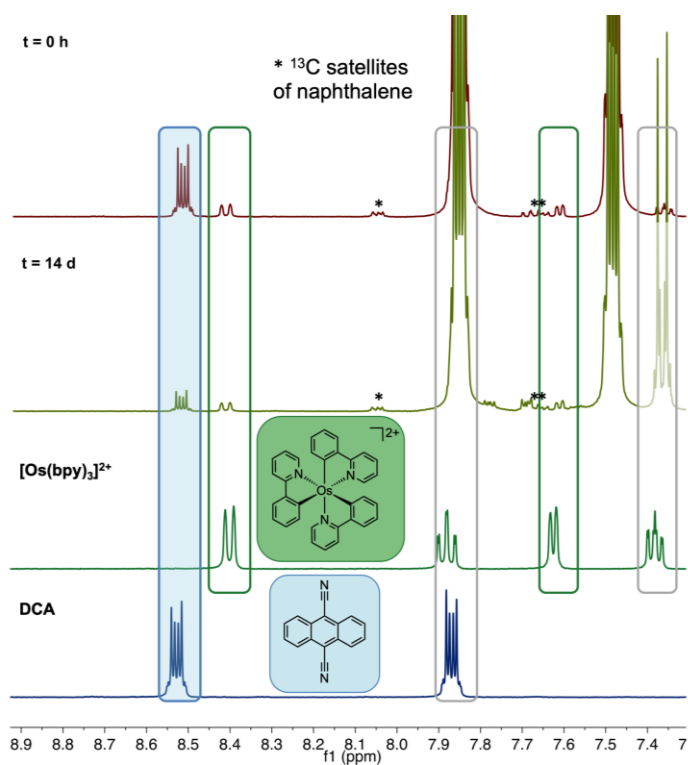


**Figure S64.** Extract of the  $^1\text{H-NMR}$  spectra monitoring the Newman-Kwart rearrangement of substrate **3** under 635 nm cw-laser irradiation, shown together with reference spectra of  $[\text{Os}(\text{bpy})_3](\text{PF}_6)_2$  and DCA in dichloromethane- $\text{d}_2$ . Reaction conditions for the light-driven reaction: 50 mM **3**, 1 mol%  $[\text{Os}(\text{bpy})_3](\text{PF}_6)_2$ , 10 mol% DCA, naphthalene (2 eq.) and  $\text{TBAPF}_6$  (1 eq.) in dichloromethane- $\text{d}_2$ . IS = internal standard (1,4-dioxane). Key proton resonances present in the reference as well as in the reaction mixture before and after irradiation are highlighted in green ( $[\text{Os}(\text{bpy})_3]^{2+}$ ) and blue (DCA). Grey framed parts indicate zones, in which proton resonances originating from different reaction components overlap with one another.

## 5. NMR data

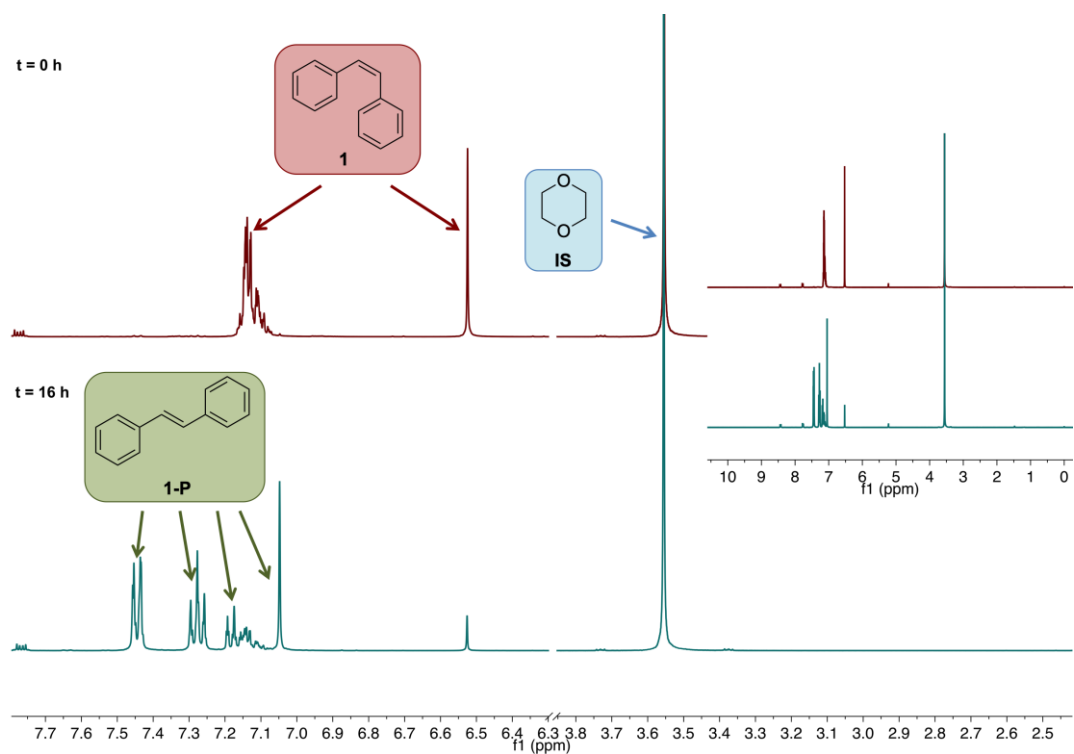


**Figure S65.** <sup>1</sup>H-NMR spectra monitoring isomerisation of substrate **1** over time using 635 nm cw-laser irradiation. Reaction conditions: 50 mM **1**, 0.1 mol% [Os(bpy)<sub>3</sub>](PF<sub>6</sub>)<sub>2</sub> and 5 mol% DCA in dichloromethane-d<sub>2</sub>. IS = internal standard (1,4-dioxane).

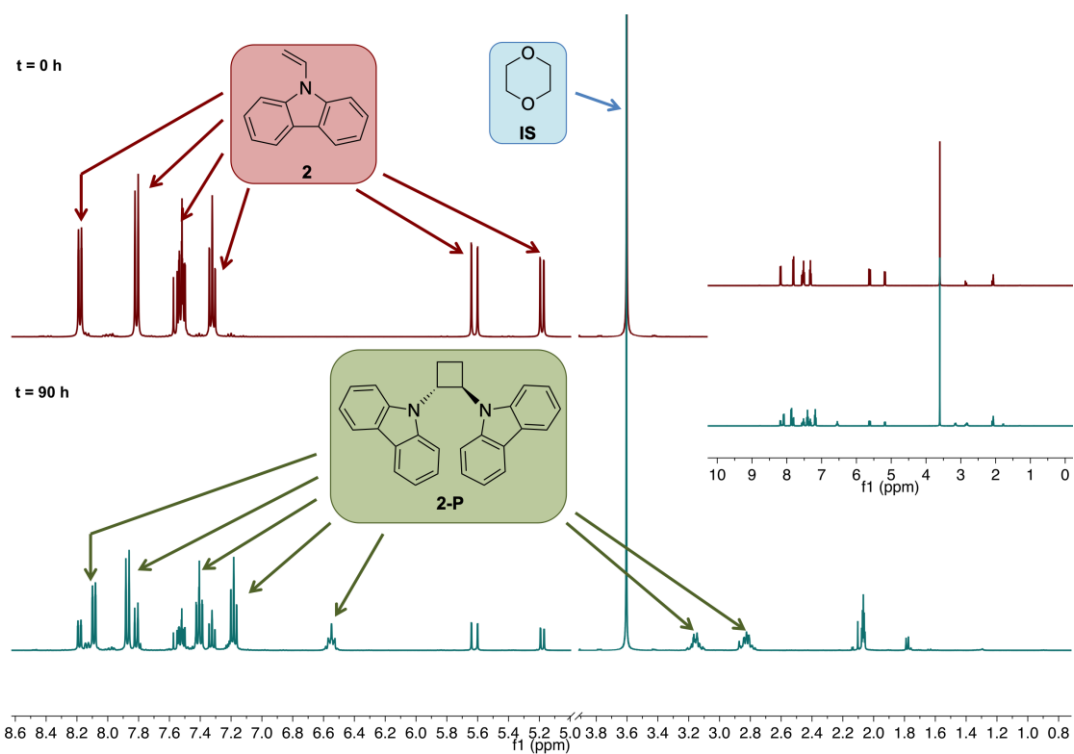


**Figure S66.** <sup>1</sup>H-NMR spectra monitoring cycloaddition of substrate **2** over time using 635 nm cw-laser irradiation. Reaction conditions: 200 mM **2**, 0.5 mol% [Os(bpy)<sub>3</sub>](PF<sub>6</sub>)<sub>2</sub> and 2.5 mol% DCA in acetone-d<sub>6</sub>. IS = internal standard (1,4-dioxane).

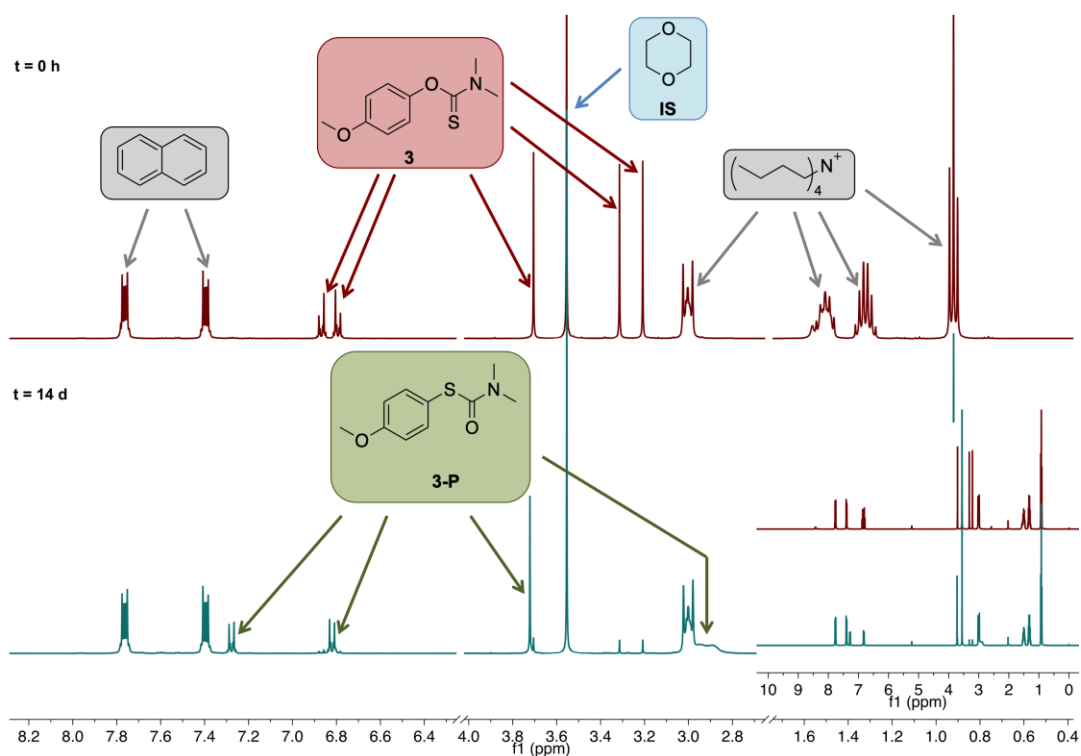


**Figure S67.**  $^1\text{H-NMR}$  spectra monitoring Newman-Kwart rearrangement of substrate **3** over time using 635 nm cw-laser irradiation. Reaction conditions: 50 mM **3**, 1 mol%  $[\text{Os}(\text{bpy})_3](\text{PF}_6)_2$ , 10 mol% DCA, naphthalene (2 eq.) and  $\text{TBAPF}_6$  (1 eq.) in dichloromethane- $d_2$ . IS = internal standard (1,4-dioxane).

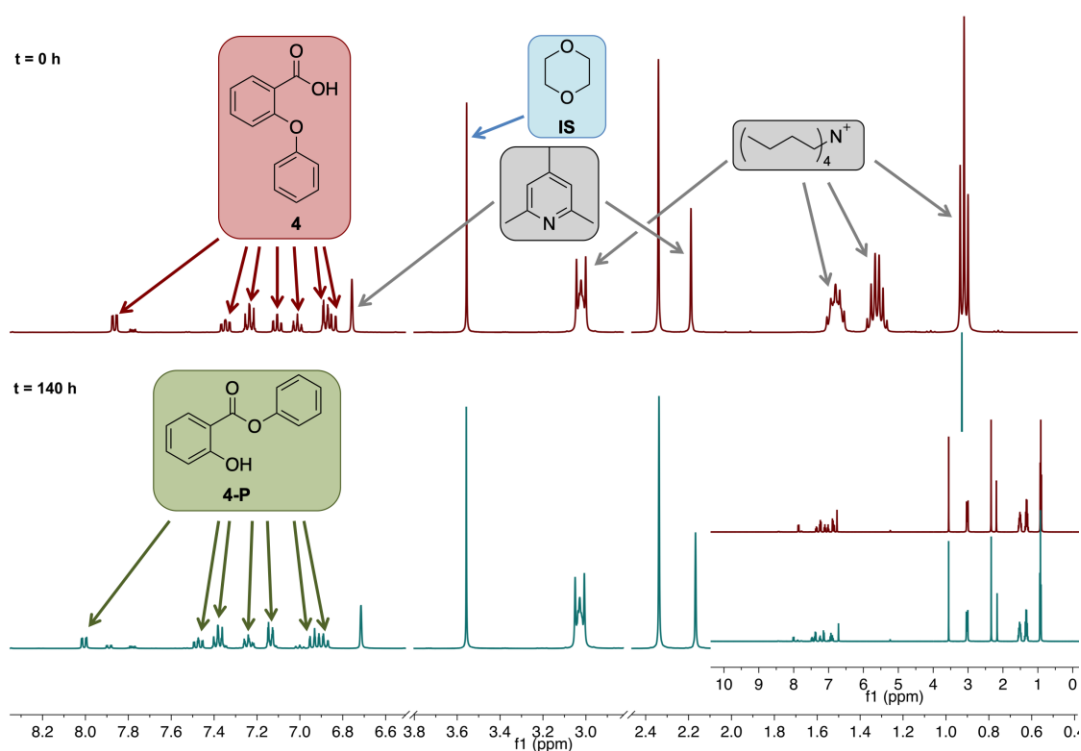


**Figure S68.**  $^1\text{H-NMR}$  spectra monitoring isomerisation of substrate **4** over time using 635 nm cw-laser irradiation. Reaction conditions: 100 mM **4**, 0.5 mol%  $[\text{Os}(\text{bpy})_3](\text{PF}_6)_2$ , 5 mol% DCA,  $\text{TBAPF}_6$  (1 eq.) and 2,4,6-trimethylpyridine (1 eq.) in dichloromethane- $d_2$ . IS = internal standard (1,4-dioxane).

## 6. References

- 1 Y. Wei, M. Zheng, L. Chen, X. Zhou and S. Liu, *Dalton Trans.*, 2019, **48**, 11763–11771.
- 2 H. E. Gottlieb, V. Kotlyar and A. Nudelman, *J. Org. Chem.*, 1997, **62**, 7512–7515.
- 3 F. Glaser and O. S. Wenger, *JACS Au*, 2022, **2**, 1488–1503.
- 4 F. Glaser, C. B. Larsen, C. Kerzig and O. S. Wenger, *Photochem. Photobiol. Sci.*, 2020, **19**, 1035–1041.
- 5 A. F. Roesel, M. Ugandi, N. T. T. Huyen, M. Májek, T. Broese, M. Roemelt and R. Francke, *J. Org. Chem.*, 2020, **85**, 8029–8044.
- 6 S.-F. Wang, X.-P. Cao and Y. Li, *Angew. Chem. Int. Ed.*, 2017, **56**, 13809–13813.
- 7 M. Riener and D. A. Nicewicz, *Chem. Sci.*, 2013, **4**, 2625.
- 8 H. Maeda, M. Yamamoto, H. Nakagawa and K. Mizuno, *Chinese Chem. Lett.*, 2010, **21**, 365–368.
- 9 F. D. Lewis, J. R. Petisce, J. D. Oxman and M. J. Nepras, *J. Am. Chem. Soc.*, 1985, **107**, 203–207.
- 10 F. Glaser, C. Kerzig and O. S. Wenger, *Chem. Sci.*, 2021, **12**, 9922–9933.
- 11 R. Pérez-Ruiz, *Top. Curr. Chem.*, 2022, **380**, 23.
- 12 B. Pfund, D. M. Steffen, M. R. Schreier, M.-S. Bertrams, C. Ye, K. Börjesson, O. S. Wenger and C. Kerzig, *J. Am. Chem. Soc.*, 2020, **142**, 10468–10476.
- 13 B. D. Ravetz, A. B. Pun, E. M. Churchill, D. N. Congreve, T. Rovis and L. M. Campos, *Nature*, 2019, **565**, 343–346.
- 14 A. Olesund, J. Johnsson, F. Edhborg, S. Ghasemi, K. Moth-Poulsen and B. Albinsson, *J. Am. Chem. Soc.*, 2022, **144**, 3706–3716.
- 15 F. Edhborg, A. Olesund and B. Albinsson, *Photochem. Photobiol. Sci.*, 2022, **21**, 1143–1158.
- 16 Y. Murakami and K. Kamada, *Phys. Chem. Chem. Phys.*, 2021, **23**, 18268–18282.
- 17 Y. Kuriyama, H. Sakuragi, K. Tokumaru, Y. Yoshida and S. Tagawa, *Bull. Chem. Soc. Jpn.*, 1993, **66**, 1852–1855.
- 18 K. Suzuki, A. Kobayashi, S. Kaneko, K. Takehira, T. Yoshihara, H. Ishida, Y. Shiina, S. Oishi and S. Tobita, *Phys. Chem. Chem. Phys.*, 2009, **11**, 9850–9860.
- 19 S. Hamai and F. Hirayama, *J. Phys. Chem.*, 1983, **87**, 83–89.
- 20 I. R. Gould, D. Ege, J. E. Moser and S. Farid, *J. Am. Chem. Soc.*, 1990, **112**, 4290–4301.
- 21 S. Hirayama, *J. Am. Chem. Soc.*, 1981, **103**, 2934–2938.
- 22 A. Rosspeintner, G. Angulo and E. Vauthey, *J. Am. Chem. Soc.*, 2014, **136**, 2026–2032.
- 23 M. A. Bergkamp, P. Gütllich, T. L. Netzel and N. Sutin, *J. Phys. Chem.*, 1983, **87**, 3877–3883.
- 24 B. Noble and R. D. Peacock, *Inorg. Chem.*, 1996, **35**, 1616–1620.
- 25 D. A. W. Ross, P. A. Scattergood, A. Babaei, A. Pertegás, H. J. Bolink and P. I. P. Elliott, *Dalton Trans.*, 2016, **45**, 7748–7757.
- 26 D. Liu, Y. Zhao, Z. Wang, K. Xu and J. Zhao, *Dalton Trans.*, 2018, **47**, 8619–8628.
- 27 S. A. E. Omar, P. A. Scattergood, L. K. McKenzie, C. Jones, N. J. Patmore, A. J. H. M. Meijer, J. A. Weinstein, C. R. Rice, H. E. Bryant and P. I. P. Elliott, *Inorg. Chem.*, 2018, **57**, 13201–13212.

- 28 M. Staffilani, P. Belser, F. Hartl, C. J. Kleverlaan and L. De Cola, *J. Phys. Chem. A*, 2002, **106**, 9242–9250.
- 29 T. Riis-Johannessen, N. Dupont, G. Canard, G. Bernardinelli, A. Hauser and C. Piguet, *Dalton Trans.*, 2008, **9226**, 3661.
- 30 L. A. Büldt, A. Prescimone, M. Neuburger and O. S. Wenger, *Eur. J. Inorg. Chem.*, 2015, **2015**, 4666–4677.
- 31 M. Montalti, A. Credi, L. Prodi and M. T. Gandolfi, *Handbook of Photochemistry*, CRC Press, Third Edit., 2006.
- 32 S. Welter, N. Salluce, A. Benetti, N. Rot, P. Belser, P. Sonar, A. C. Grimsdale, K. Mullen, M. Lutz, A. L. Spek and L. De Cola, *Inorg. Chem.*, 2005, **44**, 4706–4718.
- 33 R. E. Holmlin, J. A. Yao and J. K. Barton, *Inorg. Chem.*, 1999, **38**, 174–189.
- 34 J. B. Bilger, C. Kerzig, C. B. Larsen and O. S. Wenger, *J. Am. Chem. Soc.*, 2021, **143**, 1651–1663.
- 35 C. Wegeberg, D. Häussinger and O. S. Wenger, *J. Am. Chem. Soc.*, 2021, **143**, 15800–15811.
- 36 M. Padilla, F. Peccati, J. L. Bourdelande, X. Solans-Monfort, G. Guirado, M. Sodupe and J. Hernando, *Chem. Commun.*, 2017, **53**, 2126–2129.
- 37 J. C. Gonzalez-Gomez, N. P. Ramirez, T. Lana-Villarreal and P. Bonete, *Org. Biomol. Chem.*, 2017, **15**, 9680–9684.
- 38 E. Hasegawa, N. Izumiya, T. Fukuda, K. Nemoto, H. Iwamoto, S. Takizawa and S. Murata, *Tetrahedron*, 2016, **72**, 7805–7812.
- 39 M. Sakamoto, X. Cai, M. Hara, M. Fujitsuka and T. Majima, *J. Am. Chem. Soc.*, 2004, **126**, 9709–9714.
- 40 A. A. Abdel-Shafi and F. Wilkinson, *J. Phys. Chem. A*, 2000, **104**, 5747–5757.
- 41 K. Kikuchi, M. Hoshi, T. Niwa, Y. Takahashi and T. Miyashi, *J. Phys. Chem.*, 1991, **95**, 38–42.
- 42 A. P. Darmany, *Chem. Phys. Lett.*, 1984, **110**, 89–94.
- 43 S. M. Bachilo and R. B. Weisman, *J. Phys. Chem. A*, 2000, **104**, 7713–7714.
- 44 C. Kerzig and O. S. Wenger, *Chem. Sci.*, 2018, **9**, 6670–6678.
- 45 B. M. Wilke and F. N. Castellano, *J. Chem. Educ.*, 2013, **90**, 786–789.
- 46 A. Haefele, J. Blumhoff, R. S. Khnayzer and F. N. Castellano, *J. Phys. Chem. Lett.*, 2012, **3**, 299–303.
- 47 T. J. B. Zähringer, M.-S. Bertrams and C. Kerzig, *J. Mater. Chem. C*, 2022, **10**, 4568–4573.
- 48 C. Fan, L. Wei, T. Niu, M. Rao, G. Cheng, J. J. Chruma, W. Wu and C. Yang, *J. Am. Chem. Soc.*, 2019, **141**, 15070–15077.
- 49 Y. Zhou, F. N. Castellano, T. W. Schmidt and K. Hanson, *ACS Energy Lett.*, 2020, **5**, 2322–2326.
- 50 A. F. Olea, D. R. Worrall and F. Wilkinson, *Photochem. Photobiol. Sci.*, 2003, **2**, 212–217.
- 51 A. F. Olea, D. R. Worrall, F. Wilkinson, S. L. Williams and A. A. Abdel-Shafi, *Phys. Chem. Chem. Phys.*, 2002, **4**, 161–167.
- 52 J. N. Demas and D. G. Taylor, *Inorg. Chem.*, 1979, **18**, 3177–3179.

- 53 D. R. McMillin, J. R. Kirchoff and K. V. Goodwin, *Coord. Chem. Rev.*, 1985, **64**, 83–92.
- 54 R. M. Everly and D. R. McMillin, *Photochem. Photobiol.*, 1989, **50**, 711–716.
- 55 J. D. Earley, A. Zieleniewska, H. H. Ripberger, N. Y. Shin, M. S. Lazorski, Z. J. Mast, H. J. Sayre, J. K. McCusker, G. D. Scholes, R. R. Knowles, O. G. Reid and G. Rumbles, *Nat. Chem.*, 2022, **14**, 746–753.
- 56 E. P. Farney, S. J. Chapman, W. B. Swords, M. D. Torelli, R. J. Hamers and T. P. Yoon, *J. Am. Chem. Soc.*, 2019, **141**, 6385–6391.
- 57 Y. Takahashi, K. Wakamatsu, K. Kikuchi and T. Miyashi, *J. Phys. Org. Chem.*, 1990, **3**, 509–518.
- 58 R. C. Kanner and C. S. Foote, *J. Am. Chem. Soc.*, 1992, **114**, 678–681.
- 59 R. C. Kanner and C. S. Foote, *J. Am. Chem. Soc.*, 1992, **114**, 682–688.
- 60 K. Kikuchi, T. Niwa, Y. Takahashi, H. Ikeda, T. Miyashi and M. Hoshi, *Chem. Phys. Lett.*, 1990, **173**, 421–424.
- 61 F. D. Lewis and M. Kojima, *J. Am. Chem. Soc.*, 1988, **110**, 8664–8670.
- 62 J. Eriksen and C. S. Foote, *J. Phys. Chem.*, 1978, **82**, 2659–2662.
- 63 I. R. Gould and S. Farid, *J. Am. Chem. Soc.*, 1993, **115**, 4814–4822.
- 64 R. Akaba, H. Sakuragi and K. Tokumaru, *Chem. Phys. Lett.*, 1990, **174**, 80–84.
- 65 B. W. Zhang, Y. Kuriyama, Y. Cao and K. Tokumaru, *Bull. Chem. Soc. Jpn.*, 1993, **66**, 1859–1862.
- 66 F. D. Lewis, R. E. Dykstra, I. R. Gould and S. Farid, *J. Phys. Chem.*, 1988, **92**, 7042–7043.
- 67 S. U. Pedersen, T. B. Christensen, T. Thomasen and K. Daasbjerg, *J. Electroanal. Chem.*, 1998, **454**, 123–143.
- 68 Y. Kuriyama, T. Arai, H. Sakuragi and K. Tokumaru, *Chem. Lett.*, 1992, **21**, 879–882.
- 69 E. Vauthey, C. Högemann and X. Allonas, *J. Phys. Chem. A*, 1998, **102**, 7362–7369.
- 70 K. Mizuno, N. Ichinose and Y. Otsuji, *Chem. Lett.*, 1985, **14**, 455–458.
- 71 K. Gollnick and G. Wellnhofer, *J. Photochem. Photobiol. A Chem.*, 1993, **74**, 137–145.
- 72 E. Hasegawa, T. Mukai and K. Yanagi, *J. Org. Chem.*, 1989, **54**, 2053–2058.
- 73 T. B. Truong and J. Santamaria, *J. Chem. Soc. Perkin Trans. 2*, 1987, 1–5.
- 74 N. Orbach, J. Novros and M. Ottolenghi, *J. Phys. Chem.*, 1973, **77**, 2831–2836.
- 75 M. Rasmusson, E. Åkesson, L. Ebersson and V. Sundström, *J. Phys. Chem. B*, 2001, **105**, 2027–2035.
- 76 M. A. Cismesia and T. P. Yoon, *Chem. Sci.*, 2015, **6**, 5426–5434.
- 77 L. Pitzer, F. Sandfort, F. Strieth-Kalthoff and F. Glorius, *J. Am. Chem. Soc.*, 2017, **139**, 13652–13655.
- 78 R. A. Crellin, M. C. Lambert and A. Ledwith, *J. Chem. Soc. D Chem. Commun.*, 1970, 682.
- 79 B. Reiß, Q. Hu, E. Riedle and H. A. Wagenknecht, *ChemPhotoChem*, 2021, **5**, 1009–1019.